UNIVERSITÀ
DEGLI STUDI
FIRENZE

Università degli Studi di Firenze
Dipartimento di Ingegneria dell'Informazione (DINFO)
Corso di Dottorato in Ingegneria dell'Informazione
Curriculum: Automatica, Ottimizzazione e Sistemi Complessi

Nonlinear dynamics on networks: deterministic and stochastic approaches

Candidate
Sara Nicoletti

Supervisors
Prof. Duccio Fanelli

Prof. Giorgio Battistelli

Prof. Luigi Chisci

Prof. Giacomo Innocenti

PhD Coordinator
Prof. Fabio Schoen

ciclo xxxiii, 2017-2020

Università degli Studi di Firenze, Dipartimento di Ingegneria dell'Informazione (DINFO).

Al mio nonno, perché avrei voluto che mi vedesse diventare grande.

Contents

Chapter 1

Introduction

Networks constitute the backbone of complex systems, i.e. systems composed of many elements interacting with each other. Network science is an interdisciplinary research field that has been attracting the interest of many scientists in the last years. From the human brain [19, 105] to community interactions [75], ecology [52] to biological processes [88], a lot of physical phenomena occurring in nature can be described through complex systems, as collective dynamics which emerge at the macroscopic level from the interactions of microscopical constituents [53, 97].

Phenomena belonging to all the different fields cited above, and many others, are strictly related to the structure of the underlying networks. Indeed, the brain consists of many interconnected neurons, ecosystems are made of interacting species, social systems are constructed over interactions among individuals, just to mention a few examples.

In general, complex networks can be described as organized structures composed of a large number of units, individuals, components or agents, interconnected through intricated patterns of interactions. Over the years, scientific research has been focused on the individual components of a complex system and their interactions. Two papers proved fundamental in network science: the first one, by Duncan Watts and Steven Strogatz, was about small-world networks [185], and the second one, on scale-free networks, written by Albert-László Barabási and Réka Albert [25]. These works draw attention to the non-trivial underlying networks of real-world complex systems, being them very different from the simplest structures of lattices or random graphs; indeed, large scale networks are tipically characterized by

complex topologies and heterogeneous architectures. At the same time, some structural properties are universal and common to networks originating from different (biological, social or man-made) complex systems. Their structures play a crucial role also in the dynamics of complex systems, acting on the emergence of collective behaviours.
In this respect, the potential implications of networks for the questions concerning the dynamical processes hosted on top of them, attracted a lot of attention. Resilience of networks, their synchronization properties, consensus formation, disease spreading, represent some examples taken from different contexts for the applicability of concepts of dynamical models hosted on complex networks.

Dynamical processes on networks can be described by identifying each node of the network with a single element, or a group of elements, of the system, such as for example peoples, animals, or chemical species. Such models require to introduce the notion of a corresponding variable σ_i for each node i, characterizing its dynamical state. Considering a specific dynamical process on a network, the knowledge of the state variable of all nodes defines the microscopic state of the entire system, whose configuration at time t is described by the vector variable $x(t) = (x_1(t), x_2(t), \ldots, x_N(t))$, where N stands for the number of nodes constituting the network. The evolution of the system is described by the dynamics of the configuration $\sigma(t)$ in the phase space, defined by all the possible configurations x that the system can assume. Due to the large number of variables and the stochastic nature of most phenomena, it is often impossible to focus on the microscopic dynamics of such systems, so the description is tipically based on the so-called master equation. In this approach, the investigated variable is the probability $P(x,t)$ to find the system at time t in a given configuration x and the master equation represents an evolution probability equation for $P(x,t)$.

Noise is a key ingredient in the dynamical description of many real-world phenomena [80, 182]. Stochastic perturbations can derive from an external noise, due for example to thermal fluctuations, or can stem from an endogeneous noise, reflecting the inherent discreteness of the scrutinized medium [26, 38, 56, 127, 182]. In the first case, noise manifests as an external contribution while, in the second one, it is intrinsically related to the system. The dynamics can derive from simple interactions between adjacent nodes, like diffusion or other linear processes, or also involve a local reaction on the single nodes. For instance, for reaction-diffusion processes the elements

interact depending on specific self-reactions and diffuse across the spatial medium defined by the network [19, 136, 139, 152, 178]. Turing patterns represent the most celebrated example of collective phenomena emerging in reaction-diffusion models for chemical species [178], but applications can also be found in ecology [96] or for epidemic spreading [137].

A lot of dynamical systems are well described by classical networks [24, 116, 147], however it can happen that the basic interactions in many other cases involve more than two nodes at the same time [27, 113], as for instance in the case of brain networks [162], protein interaction networks [68], ecological communities [85] and co-authorship networks [158]. These systems necessitate to be described by a structure accounting for multi-body interactions, like hypergraphs [29, 67, 81]. In mathematics, a hypergraph is a graph in which a "generalised" edge can join any number of vertices, at variance with an ordinary graph where an edge connects exactly two vertices. The research on high-order structures is attracting a lot of interest in the scientific community, from social contagion model [57] to the study of synchronization [109, 132], passing through random walk models [40] and diffusion [71], being them a useful tool to go beyond the limit of binary interactions of classical network models.

In this thesis we focus on studying dynamical models on networks and, in the last part, dynamical models on hypergraphs, with a particular focus on reaction-diffusion processes. When each node represents a dynamical system, usually nothing can be a priori said on collective behaviors once the nodes are coupled together [173]. Examples are represented by chaotic systems that synchronize to the same solution [160], or by stationary inhomogeneous patterns emerging from diffusing species [19]. Particular attention is devoted to the role of the noise and its ability to eventually guarantee an amplification process for systems defined on networks with specific topologies, like non-normal networks [70, 188].

Most of the work is also dedicated to network generation. For reaction-diffusion models, dynamics depends on the Laplacian matrix and its spectrum [1, 146, 179]. Our contribution aims at providing a novel procedure to generate networks with any desired Laplacian spectrum, in the general challenging context of network design.

Chapter 2 is an introductory chapter, where we first recall some basic

concepts about graphs. We further focus on reaction-diffusion processes hosted on networks, entering into the detail of the equations and investigating the role of the Laplacian matrix to assess the stability of such systems at a deterministic level. The role of stochastic contributions is also presented together with the formalism of master and Fokker-Planck equations. In the last section of the chapter, we also introduce the formalism of hypergraphs and the definition of the associated Laplacian matrix.

In Chapter 3 we consider the first dynamical model of this thesis, which describes the activity of neurons arranged on a simple network made of three nodes located at the vertices of a triangular loop. The model is a simplified version of the Wilson-Cowan model [165, 186] for neurons in the brain and consists of a two-species model of the excitatory-inhibitory type. The complexity of the model is reduced to just one reaction parameter, one coupling constant and one parameter that sets the asymmetry of the loop. The phenomenon of stochastic quasicycles is investigated as consequence of the interplay between endogeneous noise and non-normality of the system. We show that, by increasing the strength of the internode coupling, one moves the system towards the Hopf bifurcation and the amplitude of the stochastic oscillations is consequently magnified. Non-normality is a key ingredient to guarantee the amplification effects on noise-assisted oscillations: when the system is constrained to evolve with a constant rate of deterministic damping for the perturbations, the amplification correlates with the degree of non-normal reactivity. The role of non-normality is also studied from a thermodynamic point of view: we show that nonconservative forces push the system out of equilibrium, and the stationary value of the entropy increases with the reactivity index.

We carry on the study of non-normality in Chapter 4 where a stochastic reaction-diffusion model on network is considered. On each patch of the network, two species are assumed to interact following a non-normal reaction scheme. When the interaction unit is replicated on a directed linear lattice, noise gets amplified via a self-consistent process, related to the degenerate spectrum of the embedding support. The same phenomenon holds when the system is bound to explore a quasi-degenerate network, in the sense that the eigenvalues of the Laplacian operator accumulate in a compact region of the complex plane. Non-normality and quasi-degenerate spectrum may, therefore, amplify the inherent stochasticity and consequently alter the perception of stability, as quantified via conventional deterministic methods.

The concept of system stability is of paramount importance as it relates to resilience, the ability of a system to oppose to external perturbations. It is then crucial to investigate on possible strategies to enforce stability in a desired system. In many cases of interest, the spectrum of the underlying graph Laplacian sets the system stability and ultimately shapes the matter or information flow. This motivates devising suitable strategies, with rigorous mathematical foundation, to generate Laplacians that possess prescribed spectra. In Chapter 5, we show that a weighted Laplacian can be constructed so as to exactly realize a desired complex spectrum. In a special case, we are able to write analytical expressions for the entries of the Laplacian matrix and consequently speculate on the conditions to have positive non diagonal elements in such matrix. The networks obtained with the presented procedure are fully connected, so we present two sparsification procedures to remove unessential links. The generation method is tested for two examples of coupled oscillators, i.e. the Stuart-Landau and the Kuramoto models.

Unlike the previous chapters where we focused on networks, in Chapter 6 we consider high-order interactions studying hypergraphs and dynamical systems defined on top of them. To analyze the stability of the associated homogeneous equilibria we use the master stability function approach with applications to reaction-diffusion systems and synchronization models. We will show that the role of the localization property of the Laplace operator is fundamental in emerging of collective behavior. We also investigate the localization property aiming to expand this analysis in a more formal way. The idea is to perform a numerical analysis to predict this eigenvector property. In this respect, the paper [92] proves fundamental: localization properties of random networks can be predicted by the perturbation theory. In a very similar way, we apply the perturbation theory [95,167] to the Laplacian matrix defined for hypergraphs and, as a preliminar result, we obtain an approximation for the Laplacian eigenvalues reproducing qualitatively well the original ones.

Chapter 2

Dynamics on complex networks

2.1 Complex networks

A complex network is, from a mathematical point of view, a graph. In graph theory [147,179], a *graph* is a structure made of a set of objects in which pairs of objects are related. The objects are called *nodes*, or vertices, and each of the related pairs of vertices is called *link*, or edge. Network theory is the study of graphs as a representation of relations between discrete objects; it has applications in many disciplines including engineering, biology, sociology and many others. Network science [5,34] has proved successful in describing many real-world systems [24, 116, 147], which, despite inherent differences, share common structural features. Real systems are represented as a set of nodes connected by links characterized by different weights accounting for the strength of the connections. In these cases the networks are called *weighted* and *signed*, if the weights can also assume negative values. The edges of a network may be directed or undirected depending on the symmetry of the relation between connected nodes; if at least one edge is directed, the network is consequently called *directed*, otherwise, if every edge is undirected, it is called *undirected*.

A network is completely defined by the *adjacency matrix* $\mathbf{A} \in \mathbb{R}^{N \times N}$, where N is the number of nodes constituting the network. Suppose to label the nodes with an index $i = 1, \ldots, N$. The generic entry A_{ij} is equal to the weight of the link from node j to node i, and is zero if the connection does not exist. For unweighted networks, the entries of $\mathbf{A}$ are only zeros and ones, and this matrix is called *binary*. In general, the adjacency matrix of

a network is asymmetric, except for undirected networks whose adjacency matrices are symmetric.

Given a graph, one can define the *Laplacian matrix*

$$L_{ij} = A_{ij} - k_i^{in}\delta_{ij} \tag{2.1}$$

where A_{ij} denotes the entries of the adjacency matrix of the graph and $k_i^{in} := \sum_j A_{ij}$ the ingoing connectivity of generic node i, that is the number of incoming edge in node i; δ_{ij} stands for the usual Kronecker δ. For graphs with non-negative weights, the Laplacian matrix is always characterized by $N-1$ eigenvalues with negative real part and one null eigenvalue, associated to a basis of N (possibly generalized) eigenvectors, which encode the network structure. The Laplacian matrix can be interpreted as a matrix representation of a particular case of the Laplace operator (its name is due to this similarity). Suppose to consider a heat distribution across a graph described by a vector variable ϕ, where ϕ_i is the heat at vertex i. If two nodes i and j are connected, the heat transferred between them is proportional to $\phi_i - \phi_j$; otherwise, no heat is transferred. For heat capacity c, this is described by the Newton's law

$$\begin{aligned}\frac{d\phi_i}{dt} &= -c\sum_j A_{ij}(\phi_i - \phi_j) = -c\sum_j A_{ij}\phi_i + c\sum_j A_{ij}\phi_j \\ &= -c\big(k_i^{out}\phi_i - \sum_j A_{ij}\phi_j\big) = -c\sum_j \big(\delta_{ij}k_i^{out} - A_{ij}\big)\phi_j = \sum_j L_{ij}\phi_{ij}.\end{aligned} \tag{2.2}$$

Notice that this equation takes the same form of the heat equation where the matrix L is replacing the Laplacian operator ∇^2.

In general, a diffusion process defined on a network can be described by an equation of the form

$$\dot{x}_i = \sum_j L_{ij}x_j \tag{2.3}$$

where the Laplacian matrix L_{ij} is defined above. The diffusion process refers to the flow of a substance from regions of high concentration to regions of low concentration; in the case of a discrete support, the system evolves toward an asymptotic state called synchronization [12, 163] or consensus [58], corresponding to an N dimensional vector with all entries equal to $\frac{1}{N}\sum_i x_i(0)$. This vector corresponds to the normalized right eigenvector of L associated to 0.

The graphs may have different properties depending on the characteristic of the corresponding interactions; we can have complete graphs where each pair of nodes is joined by a link, or connected graphs where each pair of nodes is connected by a path, just to cite a few. Lattices are the simplest graphs we can mention, being made of regular geometrical structures periodically repeated, like for example the crystalline material. It is also worth mentioning *random graphs* and the Erdös-Rényi model [66] to build this kind of network. A random graph is obtained by starting with a set of N isolated vertices and adding successive links between them at random. In general, random graphs may be described by a probability distribution or by a random process which generates them. For instance, in [125] use has been made of these networks to model ecosystems. One of the most studied class of networks are *scale-free networks* whose degree distribution follows a power law, that is the fraction p_k of nodes having k connections to other nodes goes for large values of k as $p_k \sim k^{-\gamma}$. Many networks describing real world phenomena have been reported to be scale-free, like the World Wide Web [69], the interactions in biological cells [4] and others, where the value of γ tipically ranges from 2 to 3. There are many different ways to build a network with a power-law degree distribution but the most famous model is the Barabási-Albert model [25], based on the preferential attachment method. Scale-free networks and random graphs will be used in what follows as a benchmark for our analysis.
Another class of paradigmatic networks is the so-called *small-world networks*. In [185], Watts and Strogatz proposed a random graph generation model that produces graphs with small-world properties, including short average path lengths and high clustering. Small-world networks have been found in many different fields, for example biology, sociology and business [3, 145, 183].

2.2 Reaction-diffusion processes on networks

Many examples of real-world phenomena can be described by reaction-diffusion processes on networks, from the spreading of infectious diseases [9, 100] to traffic behavior in technological systems [157], passing through metapopulation models [49]. Reaction-diffusion systems are tipically described by an equation of the form

$$\dot{x_i} = f_i(x_i) + D \sum_j L_{ij} x_j \tag{2.4}$$

where f_i is a generic nonlinear function accounting for the local reactions on each node i, the elements L_{ij} stand for the entries of the Laplacian matrix associated to the network and D represents the diffusion constant. Thus, equation (2.4) comprises a reaction term and a diffusive term; often local dynamics are combined with diffusive processes to describe the evolution of interacting species [19, 136].

In the continuum limit, where the spatial support is replaced by a continuous space region, the most known phenomena arising from the interplay between local dynamics and diffusive coupling is the formation of self-organizing patterns called *Turing patterns*. These appeared for the first time in 1952 in the seminal paper of Alan Turing [178] and have been theoretically analyzed and experimentally confirmed for chemical, biological and ecological systems later. They are also supposed to be connected to morphogenesis in biology [91] and to animal coats and skin pigmentation [129, 136]. At variance with the idea of diffusion as a stabilizing and homogenizing process, Alan Turing proposed the concept that a locally stable system under small perturbations can become unstable when a diffusion-like spatial coupling is introduced. In other words, if the examined system tends to a linearly stable uniform steady state in absence of diffusion, then spatially non-homogeneous patterns can result from diffusion-driven instability under certain conditions. This is the so-called phenomenon of Turing instability.

Collective behaviors consisting of spontaneously emerging spatio-temporal patterns can emerge also in systems defined on networks, hence on discrete systems. For the first time in 1971, Othmer and Scriven observed this phenomenon trying to describe multi-cellular morphogenesis [152], where they hypothesized that the differentiation between cells could be induced by the diffusion of the morphogens on the network of inter-cellular connections. A more recent work by Nakao and Mikhailov [139] focused on nonlinear patterns emerging in large random networks, in particular on an activator-inhibitor network system, where the combined effect of local reaction and network diffusion leads to a spontaneous differentiation of the network nodes into activator-rich and activator-low groups. A generalization of this model is proposed by Asllani, Di Patti and Fanelli [20] considering also finite size fluctuations. Here, it is proven that, due to the stochastic effects, self-organized patterns emerge also outside the region of deterministic Turing instability.

2.3 Equilibria stability in deterministic systems

In this section we introduce some concepts useful to analyze the stability of a reaction-diffusion system defined on a network. Let us consider a network made up of an arbitrary number N of nodes and suppose that the dynamical variable x_i is an m-dimensional vector. Suppose also that the function f_i is identical for each node of the network. The equation can thus be written as

$$\dot{\mathbf{x}}_i = \mathbf{f}(\mathbf{x_i}) + D\sum_{j=1}^{N} L_{ij}\mathbf{x_j} \tag{2.5}$$

Such system always admits homogeneous equilibrium of the form $\mathbf{x}_i = \mathbf{x}^*$ for any i, which can be either a (stationary) fixed point or a (time-dependent) limit cycle. To investigate the stability of this kind of equilibria we suppose to perturb the homogeneous state with a non-uniform small perturbation $\delta\mathbf{x_i}$, thus we consider the perturbed state $\mathbf{x}^* + \delta\mathbf{x_i}$. The Taylor expansion of (2.5) gives

$$\delta\dot{\mathbf{x}}_i = \partial_{\mathbf{x}}\mathbf{f}(\mathbf{x}^*)\delta\mathbf{x_i} + D\sum_{j=1}^{N} L_{ij}\delta\mathbf{x}_j = \sum_{j=1}^{N} J_{ij}\delta\mathbf{x}_j \tag{2.6}$$

where use has been made of the Laplacian property $\sum_j L_{ij} = 0$. The matrix $\partial_{\mathbf{x}}\mathbf{f}(\mathbf{x}^*)$ is an $m \times m$ dimensional matrix of derivatives and $J \in \mathbb{R}^{mN\times mN}$ is the *Jacobian matrix*. To facilitate the calculations and reduce the dimension of the problem, in the case of a diagonalizable Laplacian matrix , we can expand the perturbation vector on the basis of its eigenvectors. The expansion of the state vector $\delta\mathbf{x_i}$ on such basis represents an analogy with the Fourier series expansion, that one would obtain replacing the network with a regular lattice: the eigenvalues and eigenvectors of the network Laplacian can be identified with the Fourier wavelengths and modes for a continuous support. Then, we diagonalize the Laplacian matrix

$$\sum_j L_{ij}\phi_j^{(\alpha)} = \Lambda^{(\alpha)}\phi_i^{(\alpha)} \tag{2.7}$$

and express the perturbation on this basis

$$\delta\mathbf{x_i}(t) = \sum_{\alpha=1}^{N} \mathbf{c}_\alpha(t)\phi_i^{(\alpha)} \tag{2.8}$$

where $\mathbf{c}_\alpha \in \mathbb{R}^m$. Inserting the expression (2.8) in (2.6), we get

$$\sum_{\alpha=1}^{N} \dot{\mathbf{c}}_\alpha(t)\phi_i^{(\alpha)} = \partial_{\mathbf{x}}\mathbf{f}(\mathbf{x}^*) \sum_{\alpha=1}^{N} \mathbf{c}_\alpha(t)\phi_i^{(\alpha)} + D\sum_{\alpha=1}^{N} \Lambda^{(\alpha)}\mathbf{c}_\alpha(t)\phi_i^{(\alpha)} \tag{2.9}$$

which, due to the linear independence of the eigenvectors, reduces to a set of N decoupled m-dimensional systems

$$\dot{\mathbf{c}}_\alpha(t) = \mathbf{J}_\alpha \mathbf{c}_\alpha(t) \tag{2.10}$$

where the $m \times m$ matrix $\mathbf{J}_\alpha = \partial_{\mathbf{x}}\mathbf{f}(\mathbf{x}^*) + D\Lambda^{(\alpha)}$ is the α-th diagonal block of the Jacobian with respect to the eigenvector basis.

If the homogeneous solution $\mathbf{x}^*$ is a fixed point, the Jacobian is constant in time and the solution of (2.10) is simply

$$\mathbf{c}_\alpha(t) = \mathbf{c}_\alpha(0)\exp^{\mathbf{J}_\alpha t}. \tag{2.11}$$

Imposing that the determinant of the matrix $\mathbf{J}_\alpha - \lambda^{(\alpha)}\mathbf{I}_m$ is zero guarantees to have a non-trivial solution of the system (2.10). This condition also gives the expressions of the eigenvalues $\lambda^{(\alpha)}$ of the block matrix $\mathbf{J}_\alpha$; the maximum eigenvalue corresponds to the largest Lyapunov exponent of (2.10) and is also denoted as Master Stability Function [98, 159].

Otherwise, if the homogeneous solution is a limit cycle, the Jacobian is periodic in time, that is $\mathbf{J}_\alpha(t+T) = \mathbf{J}_\alpha(t)$, and we must refer to the Floquet theory [44, 86, 123]. In this way, the temporal dependence of the perturbation $\delta\mathbf{x}_i$ is expressed by the exponential function $\exp^{\mu_k^{(\alpha)}t}$, where $\mu_k^{(\alpha)}$ are the Floquet exponents defined by $\mu_k^{(\alpha)} = \log\left(\rho_k^{(\alpha)}\right)/T$ and $\rho_k^{(\alpha)}$ are the eigenvalues of the constant matrix $\mathbf{B}$ such that $\det(\mathbf{B}) = exp[\int_0^T \mathrm{tr}(\mathbf{J}_\alpha(t))\,dt]$. In both cases, to investigate the stability of the examined system, it is convenient to exploit the tools of *dispersion relation*, i.e. the relation between the maximum real part of $\lambda^{(\alpha)}$ or $\mu^{(\alpha)}$ and the Laplacian eigenvalues. This is the generalization of the dispersion relation defined on a continuous support. We can conclude that the system is stable if the exponents $\lambda^{(\alpha)}$ or $\mu^{(\alpha)}$ are negative for every α; otherwise, if even just one of them has a positive real part, then the perturbation grows along the direction associated to the corresponding eigenvector, and consequently the system displays a behavior distant from the equilibrium.

In the case of a non-diagonalizable Jacobian matrix, the solution of (2.6) can still be written in a closed analytical form using the *generalized eigenvectors*. In this case, as we will show in Chapter 4, the perturbation is

characterized by some multiplicative polynomials in t. These terms may promote the short-time amplification of the norm of the perturbation and consequently bring the system out of the equilibrium [133, 149].

The Laplacian spectrum and the dispersion relation will be the key ingredients of our analysis in the next chapters. As previously mentioned, many complex real-world phenomena are well described by dynamical network models. For many of such systems, dynamics depend on the graph Laplacian and its spectrum [126, 140]. Thus, controlling the spectrum is one of the most interesting challenges in spectral graph theory. Recently, an analytical procedure to realize any real desired spectrum on a positively weighted network was presented by Forrow, Woodhouse and Dunkel [74]. The Laplacians obtained in this way are, by construction, symmetric. In [148] we propose a generalization of this method to the case of directed networks, designing an arbitrary complex Laplacian spectrum. This will be the subject of Chapter 5.

2.4 Finite size corrections on dynamical systems

Stochasticity plays a fundamental role in the dynamical description of many real-world phenomena [80, 182]. We can recognize two kinds of noise; an external noise, due for example to thermal fluctuations, that does not depend on the system, and conversely an endogeneous noise, intrinsically related to the system. In this respect, we mention the effects due to the finite size system, that can be neglected only in the assumptions of an infinite volume.

In Chapter 3 we will focus on such corrections studying an excitatory-inhibitory model for neural dynamics. A deterministic description is in fact insufficient to study some complex phenomena that take place in the brain and stochastic contributions must be considered. The key ingredient in the analysis of such systems is the *master equation* [80]. In this section we want to recall some fundamental concepts that will be useful in the following.

Let us consider a network consisting of N nodes, each being labelled with an index i varying from 1 to N. Suppose to have several, chemical or physical, components arranged on this network, so we introduce the notation

$$\mathbf{X} = (\mathbf{x}_1, \mathbf{x}, \dots) \tag{2.12}$$

where $\mathbf{x}_i$ denotes a vector whose components $x_{i,a}$ are the numbers of agents of species X_a in cell, or node, i. Suppose that each cell has volume V_i. Using the language of chemical reactions, we can represent the interactions between the components of the system in this generic formulation

$$\sum_a N_a^A X_a \underset{k_A^-}{\overset{k_A^+}{\rightleftharpoons}} \sum_a M_a^A X_a \tag{2.13}$$

where the coefficient N_a^A is the number of molecules, or species, involved on the left and M_a^A is the number involved on the right. This description is not limited to the chemical field, because many classes of systems evolve in time thanks to the interactions between members of some population: think for example to population systems which die, give birth, mate and consume each other, or to systems of epidemics in which diseases are transmitted from individual to individual by contact. For convenience, we introduce the vector notation $\mathbf{N}^A = (N_1^A, N_2^A, \dots)$, $\mathbf{M}^A = (M_1^A, M_2^A, \dots)$ and we define $\mathbf{r}^A = \mathbf{M}^A - \mathbf{N}^A$; it is evident that, if the reaction A proceeds one step in the forward direction

$$\mathbf{x}_i \to \mathbf{x}_i + \mathbf{r}^A \tag{2.14}$$

otherwise, if it proceeds in the backward direction

$$\mathbf{x}_i \to \mathbf{x}_i - \mathbf{r}^A. \tag{2.15}$$

The rate constants are defined by

$$t_A^+(\mathbf{x}_i) = k_A^+ \prod_a \frac{x_{i,a}!}{(x_{i,a} - N_a^A)!} \tag{2.16}$$

$$t_A^-(\mathbf{x}_i) = k_A^- \prod_a \frac{x_{i,a}!}{(x_{i,a} - M_a^A)!} \tag{2.17}$$

which are respectively proportional to the number of ways of choosing the combination $\mathbf{N}^A$ or $\mathbf{M}^A$ from $\mathbf{x}_i$ molecules. The vector $\mathbf{X}$ must be read as a stochastic variable characterized by a time-dependent probability distribution $P(\mathbf{X}_i, t)$. We then introduce the notation

$$P(\mathbf{X}_i, t) \equiv P(\mathbf{x}_1, \mathbf{x}_2, \dots, t). \tag{2.18}$$

In general, the Master equation can be written as

$$\partial_t P(\mathbf{X},t) = \sum_i \sum_A \{[t_A^-(\mathbf{x}_i + \mathbf{r}^A)P(\mathbf{x}_i + \mathbf{r}^A, t) - t_A^+(\mathbf{x}_i)P(\mathbf{x}_i,t)] + [t_A^+(\mathbf{x}_i - \mathbf{r}^A)P(\mathbf{x}_i - \mathbf{r}^A, t) - t_A^-(\mathbf{x}_i)P(\mathbf{x}_i,t)]\}. \quad (2.19)$$

Master equations are tipically not solvable, so one can resort to stochastic simulations to numerically solve (2.19), for example the Gillespie algorithm. Otherwise, if the assumption of (finite) large volumes V_i holds, the Kramers-Moyal expansion allows to obtain a valid approximation of (2.19). Without entering into the details, the resulting approximated equation reads as

$$\partial_t P(\mathbf{X},t) = -\sum_i \sum_a \partial_a [A_a(\mathbf{x}_i)P(\mathbf{x}_i,t)] + \frac{1}{2}\sum_i \sum_{a,b} \partial_a \partial_b [B_{ab}(\mathbf{x}_i)P(\mathbf{x}_i,t)] \quad (2.20)$$

where

$$A_a(\mathbf{x}_i) = \sum_A r_a^A [t_A^+(\mathbf{x}_i - t_A^-(\mathbf{x}_i))] \quad (2.21)$$

$$B_{ab}(\mathbf{x}_i) = \sum_A r_a^A r_b^A [t_A^+(\mathbf{x}_i) + t_A^-(\mathbf{x}_i)]. \quad (2.22)$$

Eq.(2.20) is the so-called *Fokker-Plank equation* associated to (2.19), with the usual drift and diffusion terms [89]. Due to the strong nonlinearity of this equation with respect to the variables $\mathbf{x}_i$, it is often convenient to consider its associated *Langevin equation*. At variance with the Fokker-Plank equation that describes the evolution of the probability, the Langevin equation focuses on the realization of a single stochastic process.

As mentioned before, in Chapter 3 we will consider an excitatory-inhibitory model for neurons in the brain, formulated in terms of a birth-death stochastic process. For this model we will specifically write master equation, Fokker-Planck equation and consequently Langevin equations.

2.5 Higher-order networks: hypergraphs

A lot of dynamical systems are well described by classical networks, however it can happen that the basic interaction in many other cases involves more than two nodes at the same time [27, 113]. These systems necessitate to be described by a structure accounting for multi-body interactions, like hypergraphs. In mathematics, a hypergraph is a graph in which a "generalised"

edge can join any number of vertices, at variance with an ordinary graph where an edge connects exactly two vertices.

In this section we introduce the hypergraph formalism that will be useful in the following.

Let us consider a hypergraph $\mathcal{H}(V, E)$, where $V = \{v_1, \dots, v_n\}$ denotes the set of n nodes and $E = \{E_1, \dots, E_m\}$ the set of m hyperedges, that is for all $\alpha = 1, \dots, m$: $E_i \subset V$, i.e. an unordered collections of vertices. Note that if $E_\alpha = \{u, v\}$, i.e. $|E_\alpha| = 2$, then the hyperedge is actually a "standard" edge denoting a binary interaction among u and v. If all hyperedges have size 2 then the hypergraph is actually a network. If a hyperedge contains all its subsets, then we recover a simplicial complex.

We can define the *incidence matrix of the hypergraph* [1], $e_{i\alpha}$, carrying the information about how nodes are shared among edges (see middle panel Fig. 2.1), more precisely

$$e_{i\alpha} = \begin{cases} 1 & v_i \in E_\alpha \\ 0 & \text{otherwise}\,. \end{cases} \tag{2.23}$$

With such matrix one can construct the $n \times n$ adjacency matrix of the hypergraph, $\mathbf{A} = ee^T$, whose entry A_{ij} represents the number of hyper edges containing both nodes i and j. Note that often the adjacency matrix is defined by setting to 0 the main diagonal. Let us also define the $m \times m$ hyperedges matrix $\mathbf{C} = e^T e$, whose entry $C_{\alpha\beta}$ counts the number of nodes in $E_\alpha \cap E_\beta$.

The adjacency matrix allows to define a Laplace matrix [104, 132], whose entries are given by $k_i\delta_{ij} - A_{ij}$, where $k_i = \sum_j A_{ij}$ denotes the number of edges incident with node i. This matrix generalises the (combinatorial) Laplace matrix for networks, however it doesn't take in full account the higher-order structures encoded by the hypergraph, notably the sizes of the incident hyperedges are neglected.

To overcome this issue, authors of [40] have studied a random walk process defined on a generic hypergraph using a new (random walk) Laplace matrix; it is worth mentioning that the transition rates of the associated process, linearly correlate with the size of the involved hyperedges, stated differently exchanges are favoured among nodes belonging to the same and

[1] We will adopt the convention of using roman indexes for nodes and greek ones for edges.

large hyperedge, describing in this way the tightness of the high-order interaction among "close nodes". More precisely,

$$L_{ij}^{rw} = \delta_{ij} - \frac{k_{ij}^H}{\sum_{\ell \neq i} k_{i\ell}^H} ,$$

where the entries of $\mathbf{K}^H$ are given by

$$k_{ij}^H = \sum_{\alpha} (C_{\alpha\alpha} - 1) e_{i\alpha} e_{j\alpha} = (e\hat{C}e^T)_{ij} - A_{ij} \quad \forall i \neq j \ , \ k_{ii}^H = 0 \, , \tag{2.24}$$

and $\hat{C}$ is a matrix whose diagonal coincides with that of C and it is zero otherwise.

From this random walk Laplace operator one can straightforwardly derive the (combinatorial) Laplace matrix,

$$\mathbf{L}^H = \mathbf{D} - \mathbf{K}^H \, , \tag{2.25}$$

where the matrix $\mathbf{D}$ contains on the diagonal the values $k_i^H = \sum_{\ell \neq i} A_{i\ell}$ and zeros otherwise. It is clear from its very definition that $\mathbf{K}^H$ takes into account both the number and the size of the hyperedges incident with the nodes. It can also be noted that $\mathbf{K}^H$ can be considered as a *weighted adjacency matrix* whose weights have been self-consistently defined to account for the higher-order structures encoded in the hypergraph (see right panel of Fig. 2.1). It is worth emphasising that the dynamics defined on this weighted network is equivalent [46] to the dynamics on the hypergraph; this allows us to exploit the existing tools available for networks to the hypergraph framework, in particular the equations determining the evolution of the system state will depend on a $n \times n$ matrix, being n the number of nodes, making the resulting analysis simpler than the one for the simplicial complexes, because the latter require the use of tensors (see Section 6.2).

Given a hypergraph one can construct the *projected network*, that is the network obtained by mapping the nodes belonging to a hyperedge into a clique of suitable size (see left panel Fig. 2.1). If the hypergraph contains only simple hyperedges, then this projection is invertible and given a network one can construct a unique hypergraph whose projection is the former given network [40]. Let us observe that the projected network keeps track of the many body interactions only through the cliques, i.e. relying on binary ones. Let us conclude this section by remarking that the operator (2.25) admits $(1, \ldots, 1)^T$ as eigenvector associated to the zero eigenvalue. The existence

of such homogeneous solution will open the way to study (in)stability questions for dynamical systems where high-orders interactions, modelled using hypergraphs, are present. Such phenomena, strongly depend on the spectral properties of suitable operators, e.g. the Laplace matrix or coupling matrix. We postpone the study of the dynamics and we describe in Chapter 6 some main properties of the hypergraph spectra.

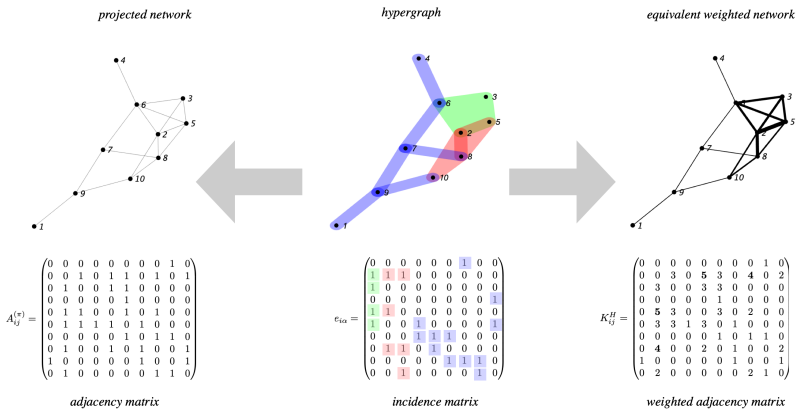

Figure 2.1: **Hypergraph and networks**. In the middle panel, a hypergraph is displayed. Hyperedges are coloured according to their size (blue for size 2, red for size 3 and green for size 4). The hypergraph's characteristics are encoded in the incidence matrix $e_{i\alpha}$. Here the information on how nodes are shared among hyperedges is stored. For ease of visualisation, we coloured the entries of $e_{i\alpha}$ by using the same colour-code that was used to highlight the size of the hyperedges. From the hypergraph, we can construct the projected network, specified by the adjacency matrix $A_{ij}^{(\pi)}$ (left panel), where nodes belonging to the same hyperedge form a complete clique of the suitable size. Alternatively, one can construct the equivalent weighted network (right panel) where the links of the cliques of the projected network are now weighted according to the entries of matrix K^H. The link (25) belongs to a hyperedge of size 3 and to another one of size 4. It is therefore the most important of the collection and because of this it receives the largest weight, $k_{25}^H = 5$. Observe also the link (28): it belongs to two hyperedges of size 3 and it is assigned a weight $k_{28}^H = 4$, larger than the one associated to the links that insist on the hyperedge of size 4.

Chapter 3

Non-normal amplification effects on complex systems

3.1 Non-normal dynamics in networked systems

As already mentioned in the previous section, noise is known to have significant effects on many different systems, changing the behavior predicted by a deterministic approach.

In this section, we examine what happens when stochastic contributions are combined with non-normal dynamics, as characterized below. Non-normality was studied for the first time in the context of hydrodynamics [177]. In [142] it was applied to the field of discrete structures by Neubert and Caswell proving that non-normal ecosystems manifest a high fragility to external perturbations. The non-normality properties have been solely studied by the ecologists' community for a long period with the only exceptions represented by the works of Murphy and Miller [134], and Hennequin et al. [94] in neuronal dynamics. However, non-normality is a recurring characteristic in real world networks, as described in [21]. In this paper the authors present a detailed study of a large dataset of networks belonging to various fields, proving that non-normality is a common property of empirical complex networks.

To explain the results of this chapter, we need at first to introduce the concept of non-normal system.

Consider the linear system

$$\dot{\mathbf{x}} = \mathbf{A}\mathbf{x}, \tag{3.1}$$

where $\mathbf{A}$ is a stable asymmetric matrix [176], namely its *spectral abscissa* is negative, $\alpha(\mathbf{A})$, where $\alpha(\mathbf{A}) = sup\,\mathrm{Re}(\sigma(\mathbf{A}))$ and $\sigma(\mathbf{A})$ denotes the spectrum of the matrix $\mathbf{A}$. By definition, $\mathbf{A}$ is non-normal if it satisfies $\mathbf{A}\mathbf{A}^T \neq \mathbf{A}^T\mathbf{A}$. Here, we call non-normal a network whose adjacency matrix $\mathbf{A}$ is non-normal [17]. It is thus clear that $\mathbf{A}$ needs to be asymmetric to be non-normal or, equivalently, the network needs to be directed to be non-normal.

The stability of the fixed point of (3.1) is determined by the eigenvalues of the matrix $\mathbf{A}$: if all the eigenvalues are real and negative, the perturbed system converges back to the fixed point. Thus, the spectrum of $\mathbf{A}$ gives information on the asymptotic behavior of the system. In situations when the supporting network is non-normal, however, more complex patterns may emerge, because the spectrum of the characteristic matrix $\mathbf{A}$ does not account for the short-time behavior of the system. If $\mathbf{A}$ is non-normal [176], it can happen that the *numerical abscissa*, namely $\omega(\mathbf{A}) = sup(\sigma(H(\mathbf{A})))$ is positive, $\omega(\mathbf{A}) > 0$, being $H(\mathbf{A}) = (\mathbf{A} + \mathbf{A}^*)/2$ the Hermitian part of $\mathbf{A}$. When this condition is satisfied, the system displays a transient growth before converging to zero or, in other words, the stable linear system can briefly evolve away from its stable point.

This phenomenon can be illustrated and measured by the norm of the state vector $\mathbf{x}$ as shown in Fig.3.1 [18]. The investigation of the local stability of any dynamical system with sufficiently smooth dynamics can be traced back to the study of a linear system of the type (3.1), by linearizing the dynamics around the fixed point. In this case, the above discussions are valid by replacing the matrix $\mathbf{A}$ with the Jacobian matrix $\mathbf{J}$ associated to the system.

In case nonlinear terms were present such transient phase could bring the system far away from the equilibrium, and thus non-normality can definitely reshape the dynamical behaviour of nonlinear systems [17]. For nonlinear systems, the typical transient due to the non-normality can be enforced even when a moderate perturbation is imposed, taking the system out of the basin of attraction of equilibrium [17, 19]. This especially holds when stochastic effects are taken into account, in fact noise can continuously bring the system far from the equilibrium, combined with the non-normality.

For the sake of completeness, we mention another methodological tool useful to debate on this topic: the *pseudo-spectrum*. The pseudo-spectrum

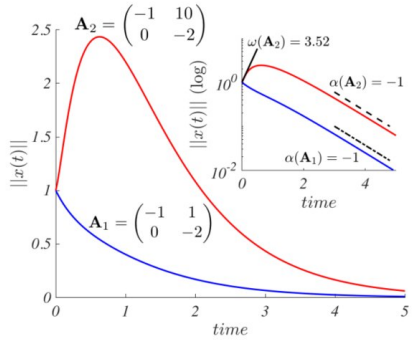

Figure 3.1: Time evolution of the norm of the solution of the linear ODE (3.1) for two transition matrices. The red curve corresponds to a non-normal matrix $\omega(\mathbf{A_2}) = 3.52$ while the blue curve to a normal one $\omega(\mathbf{A_1}) = -0.79$. The comparison between the two curves highlights the temporal growth of the norm for the non-normal system. In the inset the norm of the solution is reported in logarithmic scale to emphasise the short time behaviour described by the numerical abscissa (the straight black line has slope 3.52) and the long time related to the spectral abscissa (the dashed and dot dashed straight lines have slope -1). This figure is extracted from [18].

is defined for all $\epsilon > 0$ as $\sigma_\epsilon(\mathbf{A}) = \sigma(\mathbf{A} + \mathbf{E})$, for any perturbation $\|\mathbf{E}\| \leq \epsilon$. We remember that a complex number z is an eigenvalue of $\mathbf{A}$ if a bounded inverse of $\|z\mathbf{I} - \mathbf{A}\|$ does not exist. The pseudo-spectrum defines regions of the complex plane where $\|(z\mathbf{I} - \mathbf{A})^{-1}\|$ is larger than a prescribed positive number ϵ^{-1}. Practically, the pseudospectrum defines regions where eigenvalues of a matrix can be found because of a small perturbation, $\mathbf{A} + \mathbf{\Delta A}$, with $\|\Delta\mathbf{A}\| < \epsilon$. In case of normal matrices, these perturbations involve small variations of the spectrum, otherwise they become more important in the case of non-normal matrices. In what follows we will not enter into the detail of this tool; the interested reader can examine in depth the analysis in [176].

3.2 Non-normal amplification of stochastic quasicycles

We have seen that the norm of the solutions of a non-normal system may display a short time growth, even when the system is stable, when a perturbation is injected [17, 21, 143, 144]. The ability of a non-normal system to stimulate an initial rise of the associated norm, combined with the presence of stochastic contributions, could eventually yield a pronounced amplification process [31, 63, 94].

In this section, we focus on this peculiar aspect of non-normal systems, considering a variant of the model presented in [70]. In this work the authors consider the dynamics of excitatory and inhibitory populations arranged on a directed lattice. They showed that giant stochastic oscillations, with tunable frequencies, can be obtained, by replicating a minimal model for a quasicycle along a unidirectional chain. Endogenous noise enhances a coherent amplification across the array by instigating robust correlations among adjacent interacting populations. Resorting to the linear noise approximation, it is shown that the observed phenomenon reflects the non-normal character of the imposed interaction scheme. Quasicycles are regular oscillations in the concentration of the interacting species, due to the finite size corrections and demographic fluctuations, as specified in Section 2.4, and they disappear when the number of agents is infinite. The oscillations are tipically small in size, their amplitude being set by the strength of the imposed noise source, that is the inverse of the square root of the system size. Moreover, the power spectrum of the signal is generally broad. The results presented in [70] thus allow to circumvent these limitation. Here, we will inspect the dynamics of excitatory and inhibitory populations as in [70], organized in a loop, with varying coupling strength and degree of asymmetry. By forcing the system to evolve in a region of parameters where the homogeneous fixed point is stable, while freezing the (negative real part of the) largest eigenvalue to a constant amount, one can drive a sensible increase in the amplitude of the stochastic quasicycles by acting on the reactivity index, a measure that quantify the amount of non-normality. It is consequently speculated that triangular loops of the type here analyzed might define the minimal modules for self-sustained stochastic amplification in nature.

Feed-forward networks with triangular architecture are often assumed in neuroscience as fundamental storage and computational units [82, 124]. In

this respects, our conclusions point at the crucial role that might be exerted by the non-normal nature of neuronal connectivity in the functional dynamics of cortical networks, in agreement with [94]. The system being examined works as a veritable out-equilibrium thermal device under stationary conditions. The asymptotic entropy associated to steady operation increases with non-normality, hinting to a novel ingredient to be included in the microscopic foundation of out-of-equilibrium thermodynamics. The three-node setting explored here defines the minimal nontrivial (beyond simplistic binary connections) closed-loop which can sustain stochastic amplification, following consecutive iterations across the loop itself. Loops with more nodes display analogous dynamical features, but analytical inspection proves cumbersome, due to the progressive increase in the number of interacting populations.

The chapter is organized as follows: in the next section we will introduce the stochastic model to be probed. We will then turn to discussing its deterministic limit and studying the stability of the homogeneous fixed point in the relevant parameters plane. We will also characterize the degree of non-normal reactivity of the model, as witnessed by the numerical abscissa. The stochastic contribution is then analyzed, in Section 3.2.3, under the linear noise approximation: the amplitude of the quasi-cycle will be quantified and we will show that it positively correlate with the degree of reactivity displayed by the system. In Section 3.2.4, a thermodynamic interpretation is built and the concept of non-normal reactivity discussed with reference to this generalized framework.

3.2.1 Stochastic model

Consider the scheme depicted in Figure 4.1. Two populations of agents are made to mutually interact via a non linear excitatory and inhibitory circuit [187], reminiscent of the celebrated Wilson-Cowan model for neuronal dynamics [55, 141, 165, 184]. The agents are dislocated on three different patches (nodes) defining the edges of triangular loop. The coupling among adjacent nodes is controlled by two parameters: D sets the strength of the interaction, while $\epsilon \in [1/2, 1]$ stands for the degree of imposed asymmetry. The model is formulated as a simple birth and death process, as we shall detail in the following. As such, it accounts for demographic stochasticity, an inevitable source of disturbance which originates from the granularity of the inspected medium.

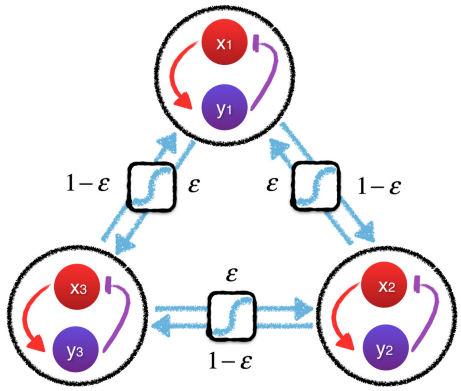

Figure 3.2: The scheme of the model is illustrated. Two populations, labeled respectively X and Y, are distributed on three distinct nodes of a triangular loop and therein interact via an activator-inhibitor cycle. The nodes of the collection are coupled together, through a nonlinear sigmoidal function. D controls the strength of the inter-node interaction, while $\epsilon \in [1/21]$ sets the degree of the coupling asymmetry.

Denote by X_i (resp. Y_i), one individual of the excitatory (resp. inhibitory) species, on node i ($i \in \{1, \cdots, \Omega = 3\}$). Label with n_{x_i} and n_{y_i} the number of, respectively, excitatory and inhibitory elements on node i . Furthermore, assume V_i to identify the volume of the $i-$th node. Then, the stochastic model is fully specified by the following chemical equations:

$$\begin{aligned} X_i &\xrightarrow{1} \emptyset \\ Y_i &\xrightarrow{1} \emptyset \\ \emptyset &\xrightarrow{f(s_{x_i})} X_i \\ \emptyset &\xrightarrow{f(s_{y_i})} Y_i \end{aligned} \tag{3.2}$$

where $f(\cdot) = \frac{1}{1+e^{-(\cdot)}}$ is a sigmoidal function which mimics the process of neuronal activation. Networks of excitatory and inhibitory neurons represent, in fact, the primary computational units in the brain cortex. Notably, inhibitory and excitatory loops, triggered by self-regulated threshold activation, are also found in genetic and metabolic cycles. Irrespectively of

the specific domain of pertinence, and in light of its inherent simplicity, the above stochastic framework can be readily adapted to all those settings where inhibition-excitation reaction schemes are at play.

The arguments of the sigmoid function read:

$$s_{x_i} = -r\left(\frac{n_{y_i}}{V_i} - \frac{1}{2}\right) + D\sum_{j=1}^{\Omega}\Gamma_{ij}\left(\frac{n_{x_j}}{V_j} - \frac{n_{y_j}}{V_j}\right) \tag{3.3}$$

$$s_{y_i} = +r\left(\frac{n_{x_i}}{V_i} - \frac{1}{2}\right) + D\sum_{j=1}^{\Omega}\Gamma_{ij}\left(\frac{n_{x_j}}{V_j} - \frac{n_{y_j}}{V_j}\right), \tag{3.4}$$

where Γ_{ij} are the entries of the Laplacian matrix. The spatial arrangement epitomized in Figure 4.1 yields the following adjacency matrix $\mathcal{A}$

$$\mathcal{A} = \begin{bmatrix} 0 & \epsilon & 1-\epsilon \\ 1-\epsilon & 0 & \epsilon \\ \epsilon & 1-\epsilon & 0 \end{bmatrix}$$

namely, $A_{ij} \neq 0$ if there is a link from j to i of weight ϵ or $1-\epsilon$. Then one can readily write $\Gamma_{ij} = \mathcal{A}_{ij} - k_i^{(in)}\delta_{ij}$, where $k_i^{(in)} = \sum_l \mathcal{A}_{il}$ denotes the strength (hereafter also referred to as to connectivity) of node i. In extended form

$$\Gamma = \begin{bmatrix} -1 & \epsilon & 1-\epsilon \\ 1-\epsilon & -1 & \epsilon \\ \epsilon & 1-\epsilon & -1 \end{bmatrix}. \tag{3.5}$$

The state of the system is completely described by the vector $\mathbf{n} = (n_{x_1}, n_{y_1}, ..., n_{x_\Omega}, n_{y_\Omega})$. Label with $P(\mathbf{n}, t)$ the probability for the system to be in the state $\mathbf{n}$ at time t. Under the Markov hypothesis, the chemical equations (3.2) are equivalent to a master equation for $P(\mathbf{n}, t)$:

$$\frac{\partial P}{\partial t}(\mathbf{n}, t) = \sum_{\mathbf{n}' \neq \mathbf{n}} T(\mathbf{n}|\mathbf{n}')P(\mathbf{n}', t) - T(\mathbf{n}'|\mathbf{n})P(\mathbf{n}, t) \tag{3.6}$$

The nonvanishing transition rates $T(\mathbf{n}'|\mathbf{n})$ from state $\mathbf{n}$ to state $\mathbf{n}'$, compatible with the former, are (let us observe that for the sake of clarity we only mention the changed variable in the new state)

$$T(n_{x_i} - 1|\mathbf{n}) = \frac{n_{x_i}}{V_i} \tag{3.7}$$

$$T(n_{y_i} - 1|\mathbf{n}) = \frac{n_{y_i}}{V_i} \tag{3.8}$$

and

$$T(n_{x_i} + 1|\mathbf{n}) = f\left(s_{x_i}\right) \tag{3.9}$$

$$T(n_{y_i} + 1|\mathbf{n}) = f\left(s_{y_i}\right) \tag{3.10}$$

To proceed with the analysis, we assume V_1 to be large and $\gamma_i = \frac{V_i}{V1} = \mathcal{O}(1)\ \forall i$, and seek for an approximate form of the master equation via a standard Kramers-Moyal expansion [80]. The ensuing calculations are analogous to those reported in [70] and for this reason omitted in the following. To illustrate the result of the analysis we define the macroscopic time $\tau = \frac{t}{V_1}$ and introduce the vector

$$\mathbf{z} = (x_1, y_1, \ldots, x_\Omega, y_\Omega) \tag{3.11}$$

where $x_i = \frac{n_{x_i}}{V_i}$, $y_i = \frac{n_{y_i}}{V_i}$ are the concentrations of the species on the node i, with $i = 1, 2, 3$. Notice that in our approach V_i is an unspecified macroscopic parameter fixing the volume of node i and, accordingly, the amplitude of the fluctuations due to demographic noise [see (3.15) and (3.16)]. Then, the master equation can be approximated as a Fokker-Planck equation

$$\frac{\partial P}{\partial \tau} = -\sum_{i=1}^{2\Omega} \frac{\partial}{\partial z_i} A_i P + \sum_{i=1}^{2\Omega} \frac{1}{2V_1} \frac{\partial^2}{\partial z_i^2} B_i P \tag{3.12}$$

with

$$\mathbf{A} = \begin{pmatrix} \ldots \\ \ldots \\ \frac{1}{\gamma_i}\left(T\left(n_{x_i} + 1|\mathbf{n}\right) - T\left(n_{x_i} - 1|\mathbf{n}\right)\right) \\ \frac{1}{\gamma_i}\left(T\left(n_{y_i} + 1|\mathbf{n}\right) - T\left(n_{y_i} - 1|\mathbf{n}\right)\right) \\ \ldots \\ \ldots \end{pmatrix} \tag{3.13}$$

and

$$\mathbf{B} = \begin{pmatrix} \ldots \\ \ldots \\ \frac{1}{\gamma_i^2}\left(T\left(n_{x_i} + 1|\mathbf{n}\right) + T\left(n_{x_i} - 1|\mathbf{n}\right)\right) \\ \frac{1}{\gamma_i^2}\left(T\left(n_{y_i} + 1|\mathbf{n}\right) + T\left(n_{y_i} - 1|\mathbf{n}\right)\right) \\ \ldots \\ \ldots \end{pmatrix}. \tag{3.14}$$

The Fokker-Planck equation (3.12) is equivalent to the following nonlinear Langevin equations for the stochastic concentrations of the involved species:

$$\frac{d}{d\tau}x_i = \frac{1}{\gamma_i}\left[f\left(s_{x_i}\right) - x_i\right] + \frac{1}{\sqrt{V_1}}\frac{1}{\gamma_i}\sqrt{x_i + f\left(s_{x_i}\right)}\lambda_i^{(1)} \tag{3.15}$$

$$\frac{d}{d\tau}y_i = \frac{1}{\gamma_i}\left[f\left(s_{y_i}\right) - y_i)\right] + \frac{1}{\sqrt{V_1}}\frac{1}{\gamma_i}\sqrt{y_i + f\left(s_{y_i}\right)}\lambda_i^{(2)} \tag{3.16}$$

where $< \lambda_i^{(l)}(\tau) >= 0$ and $< \lambda_i^{(l)}(\tau)\,\lambda_j^{(m)}(\tau) >= \delta_{ij}\delta_{lm}\delta\left(\tau - \tau'\right)$.

3.2.2 Deterministic limit

In the limit $V_1 \to +\infty$, one readily obtains the following deterministic equations

$$\dot{x}_i = \frac{1}{\gamma_i}\left[f(s_{x_i}) - x_i\right] \tag{3.17}$$

$$\dot{y}_i = \frac{1}{\gamma_i}[f(s_{y_i}) - y_i] \tag{3.18}$$

where the dot stands for the derivative with respect to the macroscopic time τ. Equations ((3.17)-(3.18)) are complemented by the self-consistent conditions:

$$s_{x_i} = -r\left(y_i - \frac{1}{2}\right) + D\sum_{j=1}^{\Omega}\Gamma_{ij}(x_j - y_j) \tag{3.19}$$

$$s_{y_i} = r\left(x_i - \frac{1}{2}\right) + D\sum_{j=1}^{\Omega}\Gamma_{ij}(x_j - y_j) \tag{3.20}$$

System ((3.17)-(3.18)) admits a homogeneous fixed point $x_i = y_i = \frac{1}{2}$, $\forall i$. To assess its stability, we proceed by linearizing the dynamics around the aforementioned equilibrium. To this end we set $x_i = \frac{1}{2} + \delta x_i$, $y_i = \frac{1}{2} + \delta y_i$ and expand in power of the perturbation amounts. By arresting the expansion to the first order, one obtains the following system of linear equations:

$$\begin{cases} \delta\dot{x}_i = \frac{1}{\gamma_i}\left[-\delta x_i - \frac{r}{4}\delta y_i + \frac{D}{4}\sum_{j=1}^{\Omega}\Gamma_{ij}(\delta x_j - \delta y_j)\right] \\ \delta\dot{y}_i = \frac{1}{\gamma_i}\left[-\delta y_i - \frac{r}{4}\delta x_i + \frac{D}{4}\sum_{j=1}^{\Omega}\Gamma_{ij}(\delta x_j - \delta y_j)\right] \end{cases}$$

which can be cast in matrix form as

$$\frac{d}{d\tau}\delta\mathbf{z} = J\delta\mathbf{z} \tag{3.21}$$

where $\delta\mathbf{z} = (\delta x_1, \delta y_1, \ldots, \delta x_\Omega, \delta y_\Omega)$ and the Jacobian matrix is given by

$$J = \begin{bmatrix} L_i & M_i & N_i \\ N_i & L_i & M_i \\ M_i & N_i & L_i \end{bmatrix} \tag{3.22}$$

being

$$L_i = \frac{1}{\gamma_i}L = \frac{1}{\gamma_i}\begin{bmatrix} -1-\frac{D}{4} & -\frac{r}{4}+\frac{D}{4} \\ \frac{r}{4}-\frac{D}{4} & -1+\frac{D}{4} \end{bmatrix} \tag{3.23}$$

$$M_i = \frac{1}{\gamma_i}M = \frac{1}{\gamma_i}\begin{bmatrix} \frac{D\epsilon}{4} & -\frac{D\epsilon}{4} \\ \frac{D\epsilon}{4} & -\frac{D\epsilon}{4} \end{bmatrix} \tag{3.24}$$

$$N_i = \frac{1}{\gamma_i}N = \frac{1}{\gamma_i}\begin{bmatrix} \frac{D(1-\epsilon)}{4} & -\frac{D(1-\epsilon)}{4} \\ \frac{D(1-\epsilon)}{4} & -\frac{D(1-\epsilon)}{4} \end{bmatrix} \tag{3.25}$$

To compute the eigenvalues of the Jacobian, and eventually elaborate on the stability of the equilibrium solution, we introduce the eigenvectors $\boldsymbol{\phi}^{(\alpha)}$ of the Laplacian matrix:

$$\Gamma\boldsymbol{\phi}^{(\beta)} = \Lambda^{(\beta)}\boldsymbol{\phi}^{(\beta)} \quad \beta = 1, ..., \Omega \tag{3.26}$$

where $\Lambda^{(\beta)}$ are the associated eigenvalues. Assuming the eigenvectors to form a complete basis, we can then decompose the perturbation on such a basis which corresponds to setting:

$$\delta x_i = \sum_{\alpha=1}^{\Omega} c_\beta \exp\left(\frac{\lambda}{\gamma_i}\tau\right)\phi_i^{(\beta)} \tag{3.27}$$

$$\delta y_i = \sum_{\alpha=1}^{\Omega} b_\beta \exp\left(\frac{\lambda}{\gamma_i}\tau\right)\phi_i^{(\beta)} \tag{3.28}$$

where $c_\alpha, b_\alpha, \lambda_\alpha$ are constants and λ_i sets the rate of the exponential growth (or damping), as obtained under the linear approximation. Inserting the above ansatz into the governing equation and performing the calculation, one readily gets:

$$\begin{pmatrix} \lambda+1-\frac{D}{4}\Lambda^{(\beta)} & \frac{r}{4}+\frac{D}{4}\Lambda^{(\beta)} \\ -\frac{r}{4}-\frac{D}{4}\Lambda^{(\beta)} & \lambda+1+\frac{D}{4}\Lambda^{(\beta)} \end{pmatrix}\begin{pmatrix} c_\beta \\ b_\beta \end{pmatrix} = 0 \tag{3.29}$$

A non trivial solution of the above system exists, provided the determinant of the associated matrix is identically equal to zero, or stated it differently, if the rates λ_α solve the quadratic equation

$$\lambda^2 + 2\lambda + 1 + \frac{r}{16}(r + 2D\Lambda^{(\beta)}) = 0 \tag{3.30}$$

that yields the closed formulae

$$\lambda = -1 \pm \sqrt{-\frac{r}{16}(r + 2D\Lambda^{(\beta)})} \quad \beta = 1, ..., \Omega \tag{3.31}$$

The eigenvalues of Laplacian Γ, specified in (3.5) reads $\Lambda^{(1)} = 0$, $\Lambda^{(2,3)} = -\frac{3}{2} \pm i\frac{\sqrt{3}}{2}(1 - 2\varepsilon)$. Hence, it is immediate to get:

$$\lambda_{1,2} = -1 \pm \frac{r}{4}i = -1 \pm i\omega_0 \tag{3.32}$$

The second eigenvalue $\Lambda^{(2)}$ yields

$$\lambda_{3,4} = -1 \pm \frac{1}{2}\sqrt{\chi} \tag{3.33}$$

and $\Lambda^{(3)}$

$$\lambda_{5,6} = -1 \pm \frac{1}{2}\sqrt{\bar{\chi}} \tag{3.34}$$

with

$$\chi = \frac{r}{4}\left[3D - r + \sqrt{3}Di(1 - 2\epsilon)\right], \tag{3.35}$$

and where $\bar{\chi}$ stands for the complex conjugate of χ. Separating the real and imaginary parts returns

$$\lambda_{3,4} = -1 \pm \frac{1}{2}\sqrt{\frac{|\chi| + \mathrm{Re}\{\chi\}}{2}} \pm i\,\mathrm{sgn}(Im\chi)\omega_1 \tag{3.36}$$

$$\lambda_{5,6} = -1 \pm \frac{1}{2}\sqrt{\frac{|\chi| + \mathrm{Re}\{\chi\}}{2}} \pm i\,\mathrm{sgn}(Im\bar{\chi})\omega_1 \tag{3.37}$$

where

$$\nu_1 = \frac{1}{2}\sqrt{\frac{|\chi| - \mathrm{Re}\{\chi\}}{2}}. \tag{3.38}$$

We also define α as the supremum of the real part of the spectrum of $\mathcal{J}$, in formulae:

$$\alpha = \sup_k \mathrm{Re}\,(\lambda_k) = -1 + \frac{1}{2}\sqrt{\frac{|\chi| + \mathrm{Re}\{\chi\}}{2}} \tag{3.39}$$

A straightforward calculation allows one to isolate the domain in the plane (ϵ, D) where the homogeneous fixed point proves stable. The stability is enforced by setting $D < D_c$ where the critical strength of interactions is explicitly given as a function of the imposed degree of asymmetry by

$$D_c(\epsilon) = \frac{-12 + \sqrt{144 + (4r^2 + 64)3\left(\epsilon - \frac{1}{2}\right)^2}}{\frac{3}{2}r\left(\epsilon - \frac{1}{2}\right)^2}; \tag{3.40}$$

This is a decreasing function of ϵ, suggesting that asymmetry anticipates the onset of the instability. Furthermore, D_c displays a minimum in r, and the critical value D_c diverges for $r \to 0$. It is therefore possible to select arbitrarily large values of D, provided that r is sufficiently small, while still constraining the system in the region of stable homogeneous fixed point.

The set of computed eigenvalues exhibits two distinct imaginary contributions, for $\varepsilon \neq \frac{1}{2}$, and $D < D_c$: $\omega_0 = r/4$, as introduced in equation (3.32), and ν_1 associated to the remaining set of eigenvalues, which reads

$$\nu_1 = \frac{1}{4}\sqrt{\frac{r[(3D - r)^2 + 3D^2(1 - 2\epsilon)^2] - r(3D - r)}{2}}. \tag{3.41}$$

Interestingly, the frequency ν_1 can be both smaller or bigger than ν_0: indeed it is possible to show that $\nu_1 > \nu_0$ if $D > D^* = 4r/(1 - 2\epsilon)^2$. If $D = D^*$, $\nu_0 = \nu_1$. In the limiting condition of a symmetric cycle, $\varepsilon = \frac{1}{2}$, the Laplacian displays a real spectrum. More specifically, $\chi = \frac{r}{4}(3D - r)$ is real. Thus, $\lambda_{3,4} = \lambda_{5,6} = -1 \pm \frac{1}{2}\sqrt{\frac{r}{4}(3D - r)}$. In this case, $D_c = \frac{r}{3} + \frac{16}{3r}$. For, $D < \hat{D} = \frac{r}{3}$, the system is stable and two frequencies are active, ν_0 and $\nu_1 = \frac{1}{2}\sqrt{\left|\frac{r}{4}(3D - r)\right|}$. Conversely, for $r/3 < D < D_c$ the system is stable but the frequency ν_1 disappears. For any choice of ϵ, at $D = D_c(\epsilon)$, two complex conjugate eigenvalues cross the vertical imaginary axis, signaling a Hopf bifurcation and the consequent inception of a limit cycle. In the following, we shall operate in the region of the plane (ϵ, D) where the system is predicted to stably converge to a homogeneous equilibrium, obtained by replicating on each one of the collection the trivial fixed point $(1/2, 1/2)$.

The fate of any imposed perturbation is eventually set by the spectrum $\sigma(\mathcal{J})$ of the Jacobian matrix $\mathcal{J}$, the matrix that governs the linear dynamics of the system around the examined equilibrium. Perturbations fade away when $\alpha < 0$ – for our specific case study, this amounts to setting $D < D_c$ – and the system converges back to its deputed equilibrium. A transient growth of the perturbation can however be seen, at short times, if $\mathcal{J}$ is *non*

normal and *reactive*. A matrix is said non-normal, if it does not commute with its adjoint [176]. Asymmetry, as reflecting a non trivial balance between intrinsic dynamics and enforced non local couplings, is thus a necessary condition for non-normality to emerge. Since, in our case, $\mathcal{J}$ is real, taking the adjoint is identical to considering the transpose of the matrix. In formulae, $\mathcal{J}$ is non-normal, provided $[\mathcal{J}, \mathcal{J}^T] \equiv \mathcal{J}\mathcal{J}^T - \mathcal{J}^T\mathcal{J} \neq 0$, where the apex T identifies the traspose operation. It is immediate to conclude that matrix $\mathcal{J}$, as defined in (3.22), is non-normal, for each choice of the involved parameters.

A straightforward manipulation [17,176] yields the following equation for the evolution of the norm of the perturbation $\|\delta\mathbf{z}\|$:

$$\frac{d\|\delta\mathbf{z}\|}{dt} = \frac{\delta\mathbf{z}^T\mathcal{H}(\mathcal{J})\delta\mathbf{z}}{\|\delta\mathbf{z}\|} \tag{3.42}$$

where $\mathcal{H}(\mathcal{J}) = \frac{\mathcal{J}+\mathcal{J}^T}{2}$ stands for Hermitian part of $\mathcal{J}$. The evolution of the perturbation, at short times, is intimately related to the so called *numerical abscissa*, $w = \sup\sigma\left(\mathcal{H}(\mathcal{J})\right)$. If $w > 0$, the system is termed *reactive*, and perturbation may display an initial, transient growth. In this paper, we are interested in shedding light on the interplay between reactivity, i.e. the inherent ability of the system to yield a short time enhancement of a deterministic perturbation, and the stochastic contribution stemming from demographic fluctuations. As we shall see, the amplification of quasi-cycles, self-sustained oscillations driven by granularity, correlates with the degree of reactive non-normality, as displayed by the system in its linearized version. To proceed in the analysis, we set to compute the eigenvalues of $\mathcal{H}(\mathcal{J})$, the Hermitian part of $\mathcal{J}$, and get the following closed expression for the reactivity index w:

$$w(J) = -1 + \frac{D}{4}\sqrt{3(\epsilon^2 - \epsilon + 1)}. \tag{3.43}$$

Hence, $w(J) > 0$ when $D > D_{react}(\epsilon) = \frac{4}{\sqrt{3(\epsilon^2-\epsilon+1)}}$. Notice that $D_{react}(\epsilon)$, the lower bound in D which sets the onset of a reactive response, is independent of r, and solely function of ϵ.

The above results are summarized in Figure 3.3, were the boundaries of stability are depicted in the reference plan (D, ϵ), for a fixed, although representative, value of r. The upper dashed line stands for D_c as given in equation (3.40). The lower dashed line refers instead to $D_{react}(\epsilon)$ and marks the boundary of the domain where matrix $\mathcal{J}$ is found to be reactive. Level

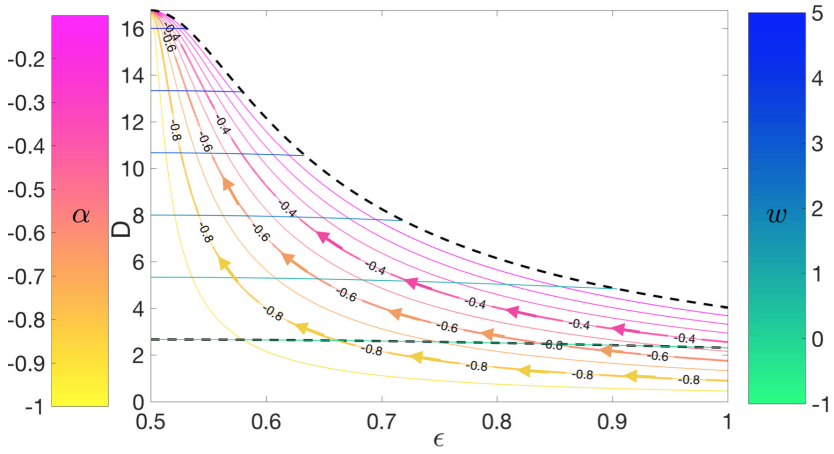

Figure 3.3: The domain of stability of the homogeneous equilibrium is depicted in the reference plane (ϵ, D) and for $r = 10$. The upper dashed curve stands for the Hopf bifurcation. Above the lower dashed curve the non-normal Jacobian matrix $\mathcal{J}$ is found to be reactive. Iso-α and iso-$w(J)$ curves are traced and colored with relevant codes which reflect their associated level, as specified in the bars on either side.

sets traced at constant values of α (see the color bar depicted on the left) and $w(J)$ (refer to the color bar reported on the right) foliate the scanned portion of the plane. Moving along iso-α lines implies freezing the rate of exponential damping of the perturbation to a constant value, or, stated it differently, visiting the subset of points that are, to some extent, equidistant from the frontier of the Hopf bifurcation. When crawling on iso-α lines, instead, one forces constantly the (largest) rate of short time growth, as seeded by reactive non-normality. While it is straightforward to obtain a closed analytical expression for iso-$w(J)$ curves, upon trivial inversion of equation (3.43), the calculation that yields an explicit representation of iso-α lines proves trickier. Label with $\bar{\alpha} < 0$ the selected iso-α. Then, after a cumbersome derivation, one gets the following expression for D, as function of both $\bar{\alpha}$ and ϵ

$$D_{iso-\alpha}(\epsilon) = \frac{-12(\bar{\alpha}+1)^2 r + \sqrt{144(\bar{\alpha}+1)^4 r^2 + [64(\bar{\alpha}+1)^4 + 4(\bar{\alpha}+1)^2 r^2]\frac{3}{4}r^2(2\epsilon-1)^2}}{\frac{3}{8}r^2(2\epsilon-1)^2} \tag{3.44}$$

which is employed for tracing the iso-α lines displayed in Figure 3.3. Starting from this setting, we shall hereafter elaborate on the role of non-normality in a stochastic framework. To anticipate our findings, we will prove that the amplitude of noise-driven oscillations grows with the degree of reactivity.

3.2.3 Linear noise approximation

To quantify the role of stochastic fluctuations around the deterministic equilibrium, we shall operate under the linear noise approximation. In concrete, we rewrite the stochastic densities x_i and y_i, for all nodes of the collection, as the sum of two distinct contributions: the deterministic fixed point, on the one side, and a stochastic perturbation, on the other. This latter is assumed to be modulated by a scaling factor $1/\sqrt{V_i}$, which follows the central limit theorem. In formula, we postulate:

$$x_i = \frac{1}{2} + \frac{\xi_i}{\sqrt{V_i}} \tag{3.45}$$

$$y_i = \frac{1}{2} + \frac{\eta_i}{\sqrt{V_i}}, \tag{3.46}$$

and introduce

$$\boldsymbol{\zeta} = (\xi_1, \eta_1, \ldots, \xi_\Omega, \eta_\Omega) \tag{3.47}$$

to label the vector of fluctuations. Inserting the above ansatz in the governing master equation and performing the expansion at the first order in $1/\sqrt{V_1}$ (see [70] for details about the technical steps involved in the calculations), one eventually gets the following set of linear Langevin equations:

$$\frac{d}{d\tau}\zeta_i = (\mathcal{J}\boldsymbol{\zeta})_i + \lambda_i \tag{3.48}$$

where $\boldsymbol{\lambda}$ stands for a Gaussian noise that satisfies the following conditions

$$< \boldsymbol{\lambda} >= 0, \tag{3.49}$$

$$< \lambda_i(\tau)\lambda_j(\tau') >= \mathcal{B}_{ij}\delta(\tau - \tau'), \tag{3.50}$$

The diffusion matrix $\mathcal{B}_{ij}$ is defined by its diagonal elements

$$\mathcal{B}_i = \left(\frac{1}{\gamma_1}, \frac{1}{\gamma_1}, \ldots, \frac{1}{\gamma_\Omega}, \frac{1}{\gamma_\Omega}\right). \tag{3.51}$$

When the volumes are equal, the diffusion matrix simply reduces to $\mathcal{B}_{ij} = \delta_{ij}$.

The above Langevin equations (3.48) admits an equivalent formulation in terms of an associated Fokker-Planck equation which can be formally cast in the form:

$$\frac{\partial}{\partial\tau}\Pi = -\sum_{i=1}^{2\Omega}\frac{\partial}{\partial\zeta_i}(\mathcal{J}\boldsymbol{\zeta})_i\Pi + \frac{1}{2}\frac{\partial^2}{\partial\zeta_i^2}\mathcal{B}_i\Pi. \tag{3.52}$$

This latter describes the evolution of the probability distribution $\Pi(\boldsymbol{\zeta}, \tau)$ of the fluctuations.

The solution at any time of the above Fokker-Planck equation is a multivariate normal distribution

$$\Pi(\boldsymbol{\zeta}, \tau) = \frac{1}{\sqrt{(2\pi)^n|\mathcal{C}|}}\exp\left\{\left\{-\frac{1}{2}\left(\boldsymbol{\zeta} - < \boldsymbol{\zeta} >\right)^T\mathcal{C}^{-1}\left(\boldsymbol{\zeta} - < \boldsymbol{\zeta} >\right)\right\}\right\} \tag{3.53}$$

where $|\mathcal{C}|$ is the determinant of the correlation matrix. The sought probability distribution $\Pi(\boldsymbol{\zeta}, \tau)$ is hence completely characterized in terms of the first and second moments of the fluctuations, $< \zeta_i >$ and $< \zeta_l\zeta_m >$. These latter quantities obey the following differential equations [70]:

$$\frac{d}{d\tau} < \zeta_i >= (\mathcal{J}\boldsymbol{\zeta})_i \tag{3.54}$$

$$\frac{d}{d\tau} < \zeta_l^2 >= 2 < (\mathcal{J}\boldsymbol{\zeta})_l\zeta_l > + \mathcal{B}_l = 2\sum_{j=1}^{2\Omega}\mathcal{J}_{lj} < \zeta_l\zeta_j > + \mathcal{B}_l \tag{3.55}$$

$$\frac{d}{d\tau} < \zeta_l\zeta_m >=< (\mathcal{J}\boldsymbol{\zeta})_l\zeta_m > + < (\mathcal{J}\boldsymbol{\zeta})_m\zeta_l >= \sum_{j=1}^{2\Omega}\mathcal{J}_{lj} < \zeta_m\zeta_j > + \mathcal{J}_{mj} < \zeta_l\zeta_j > . \tag{3.56}$$

The stationary moments can be analytically computed by setting to zero the time derivatives on the left hand side of (3.54) and solving the system that is consequently obtained. The first moments, at equilibrium, are immediately found to be identically equal to zero. Determining the second

moments implies dealing with a linear system, which can be drastically simplified, by invoking translation invariance across the loop. In particular, $< \zeta_i^2 >$ take two distinct values, respectively reflecting the typical amplitude of the fluctuations, as displayed by excitators and inhibitors.

In Figure 4.2 $< ||\boldsymbol{\zeta}||^2 > /3 = \sum_{i=1}^{3}(\xi_i^2 + \eta_i^2)/3$, the stationary norm of fluctuations on one node of the collection, is plotted against the reactivity index w, moving on (different) iso-α lines. Solid lines stand for the analytical calculations, as follows from (3.54), while the symbols refers the the homologous quantities computed from direct simulation of the non linear Langevin equations (3.15), via the Euler-Maruyama algorithm [64]. The satisfying agreement between theory and simulations testify on the adequacy of the linear noise approximation. The positive correlation between $< ||\boldsymbol{\zeta}||^2 > /3$ and w, suggests that non-normality controls the amplitude of emerging quasicycles. The effect becomes more pronounced when $\omega > 0$, i.e. when the reactivity of the non-normal Jacobian drives a self-consistent growth for the norm of the injected stochastic perturbation. Notice that w is found to increase when crawling the iso-α curves, from right to left, in the plane (ϵ, D): it is remarkable that the progressive gain in reactivity is triggered by a steady reduction in ϵ, which implies forcing the system symmetric, at odd with intuition. Despite the fact that we have here chosen to display the cumulative contribution, the norm of both the activators and inhibitors species is found to grow, with the reactivity index w. Moreover, the ensuing amplification can be made more conspicuous by differentiating the volumes V_i, across the loop.

To further characterize the amplification of the stochastic cycles, against w, at fixed α, we compute the power spectrum of the fluctuations around the deterministic fixed point. To this end we apply the temporal Fourier transform on both sides of (3.48) and obtain the following equation

$$-i\omega\tilde{\zeta}_i(\omega) = (\mathcal{J}\tilde{\zeta})_i + \tilde{\lambda}_i, \tag{3.57}$$

where $\tilde{\zeta}$ stands for the Fourier transform of ζ. Then, define the matrix $\Phi_{ij} = -i\omega\delta_{ij} - \mathcal{J}_{ij}$. The solution of (3.57) can be written as

$$\tilde{\zeta} = \Phi^{-1}\tilde{\boldsymbol{\lambda}}. \tag{3.58}$$

The power spectrum density matrix (PSDM) is consequently defined by the elements

$$\mathcal{P}_{ij}(\omega) = < \tilde{\zeta}_i(\omega)\tilde{\zeta}_j^*(\omega) > \tag{3.59}$$

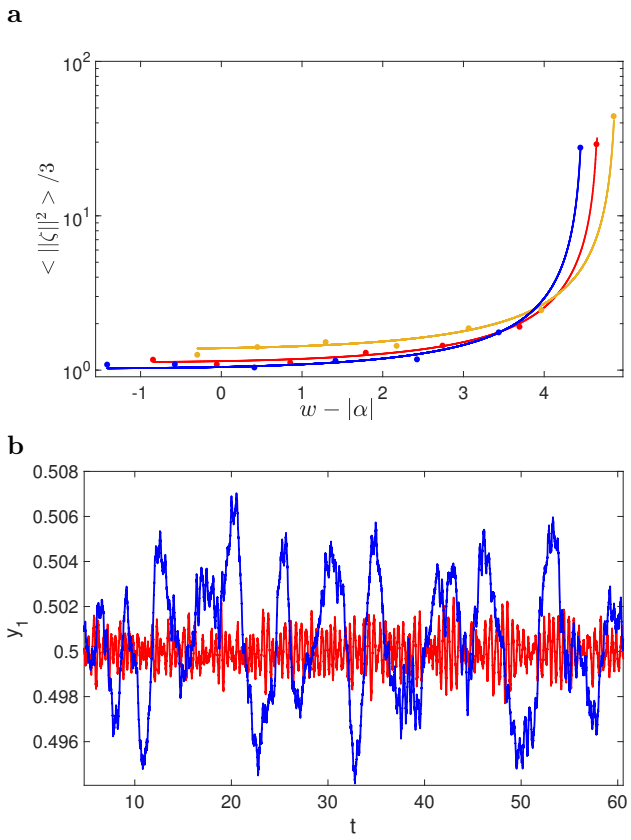

Figure 3.4: Panel (a): the asymptotic norm of the fluctuations $< ||\boldsymbol{\zeta}||^2 > /3 = \sum_{i=1}^{3}(\xi_i^2 + \eta_i^2)/3$, as displayed on each individual node, is plotted versus $w(J) - |\alpha|$, moving on iso-lines $\bar{\alpha}$. Different curves refer to different choices of $\bar{\alpha}$ $(= -0.8, -0.6, -0.4$, from bottom to top). Solid lines stands for the analytical solution after equations (3.54). Symbols are obtained from direct simulations of the non linear Langevin equations (3.15), averaging over $M = 300$ independent realizations. Here, $V_1 = V_2 = V_3 = 10^6$ and $r = 50$: Panel (b): stochastic trajectories are displayed, relative to the inhibitors on the first node, i.e. species y_1, for different values of the numerical abscissa. The red (small amplitude) trajectory is obtained for $w(J) = -0.24(\epsilon = 1)$, while the blue (large amplitude) trajectory refers to $w(J) = 5.18(\epsilon = 0.506)$. Here $r = 50$ and $V_1 = V_2 = V_3 = 10^6$.

A straightforward calculation yields

$$\mathcal{P}_{ij}(\omega) = \left(\Phi^{-1}(\omega)\mathcal{B}(\Phi^{-1})^{\dagger}(\omega)\right)_{ij}, \tag{3.60}$$

whose diagonal elements represent the power spectra of the signals. In Figure 3.5, three different power spectra, relative to the inhibitory species, are represented for distinct choices of the reactivity parameter w. When w is made to increase, while keeping α fixed, the power spectrum shifts towards the left, as prescribed by the formula for ω_1, which sets the position of the peak. In agreement with the above, the peak gains in potency when the degree of reactivity is augmented. Moving along iso-α is essential to prevent spurious contributions that might set in when the system is pushed towards the edge of the Hopf bifurcation. A gain of the quasicycles amplitude, is in fact observed when ϵ is kept constant and D modulated in the range from 0 to $D_c(\epsilon)$, as demonstrated in Figure 3.6. Although interesting per se, this phenomenon is, to a large extent, dictated by the progressive reduction in the value of α, which is enforced by making D to approach its critical value D_c. Disentangling this latter contribution from the contextual raise in reactivity is arduous, and this is ultimately the reason why we have chosen to foliate the relevant parameters space in curves characterized by a constant damping factor α. Similar conclusion holds when monitoring the power spectra of fluctuations relative to the excitatory species.

The above analysis suggests that the conversion of a stochastic input into regular oscillations is more efficient, in terms of amplification gain, when the reactivity of the system gets more pronounced. This observation provides an alternative angle to interpret the mechanism of noise-driven amplification, as originally discussed in [70]. In fact, it can be proven that the Jacobian matrix that rules the self-consistent amplification as displayed in [70] is non-normal: its inherent reactivity grows with the coupling strength among adjacent nodes, i.e. with the parameter that boosts the exponential magnification of fluctuations along the unidirectional chain. In the setting explored in [70], the analogue of the damping factor α is always constant and, as such, independent on the strength of the imposed coupling. This is at variance with the current implementation, where excitatory and inhibitory species are arranged on a triangular loop and iso-α curves are nonlinear function of the parameters of the model. The intertwingled activity of excitatory-inhibitory populations gets self-consistently amplified by circulating the signal across a symmetric or asymmetric cyclic loop, a minimal computational unit which constitutes the fundamental building block of any large networks, notwith-

standing their diverse and variegated topology. In the following, we will continue elaborating along this line and show, from a thermodynamical perspective, that the reactivity promotes the out-of-equilibrium dynamics of the scrutinized system. As such, it holds promise to result in an additional ingredient to lay the foundation of stochastic thermodynamics from the micro to the macro realms.

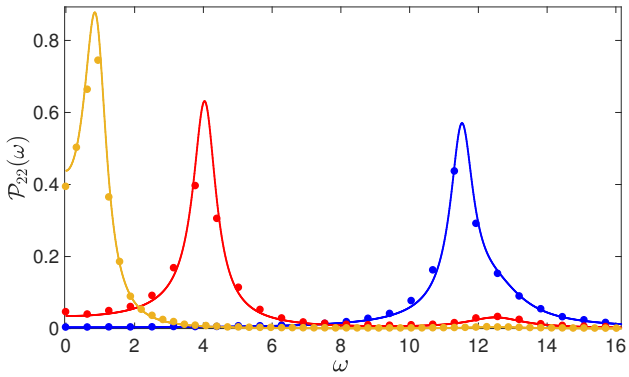

Figure 3.5: The theoretical power spectrum of the inhibitory species, $\mathcal{P}_{22}$, is plotted with a solid line against ω. Different curves refer to different choices of (D,ϵ) constrained to move across the iso-α line $\bar{\alpha} = -0.4$. The degree of reactivity, as quantified by the numerical abscissa $w(J)$, increases from right to left $(w(J) = 0.1, 4.6, 5.2)$: the peak of the power spectrum gains correspondingly in power. Symbols refer to direct numerical simulations, based on equations (3.15), averaging over $M = 200$ independent realizations. Here, $V_1 = V_2 = V_3 = 10^6$ and $r = 50$. Notice that $\mathcal{P}_{22} = \mathcal{P}_{44} = \mathcal{P}_{66}$, due to translational invariance across the loop.

3.2.4 Thermodynamics of a reactive loop

The goal of this section is to analyze the process of noise-driven amplification across the circular loop from a thermodynamic point of view. In doing so we shall provide a novel angle to contextualize the implications of reactive non-normality. To this end we recall that $\Pi(\boldsymbol{\zeta}, \tau)$, the distribution of fluctuations, obeys to the Fokker-Planck equation (3.52), in the linear noise approximation. Label with $F_i \equiv (\mathcal{J}\boldsymbol{\zeta})_i$ the nonlinear forces that define the

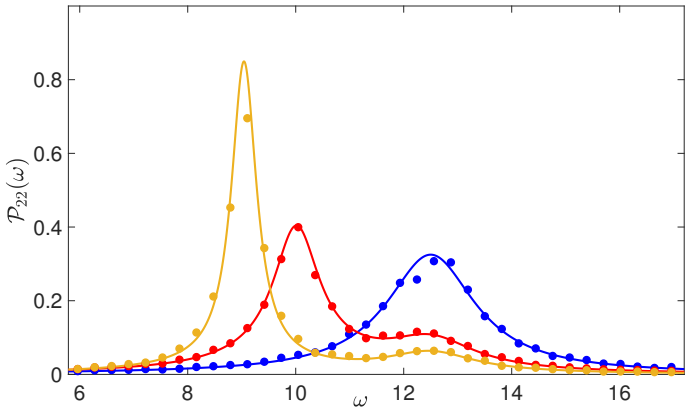

Figure 3.6: The theoretical power spectrum of the inhibitory species, $\mathcal{P}_{22}$, is plotted with a solid line against ω, for different choices of D. Symbols refer to direct numerical simulations, based on equations (3.15), averaging over $M = 200$ independent realizations. Here, $V_1 = V_2 = V_3 = 10^6$; $\mathcal{P}_{22} = \mathcal{P}_{44} = \mathcal{P}_{66}$, due to translational invariance across the loop and $r = 50$.

drift term in the aforementioned Fokker-Planck equation; $\mathcal{B}_i$ stands instead for the diffusive contribution.

The Fokker-Planck equation (3.52) can be written in the form of a continuity equation:

$$\frac{\partial \Pi}{\partial \tau} = -\boldsymbol{\nabla} \cdot \boldsymbol{\mathcal{I}} = -\sum_i \frac{\partial}{\partial z_i} \mathcal{I}_i \tag{3.61}$$

where we have defined the probability density current

$$\mathcal{I}_i = F_i \Pi - \frac{\mathcal{B}_i}{2} \frac{\partial}{\partial z_i} \Pi \tag{3.62}$$

In the limit $t \to \infty$, stationarity is achieved

$$\frac{\partial \Pi}{\partial \tau} = 0 \tag{3.63}$$

and the probability current is a solenoidal vector field

$$\boldsymbol{\nabla} \cdot \boldsymbol{\mathcal{I}} = 0 \tag{3.64}$$

Equilibrium represents a very specific stationary solution, attained by im-

posing a vanishing probability current, namely $\boldsymbol{\mathcal{I}} \equiv 0$. Hence,

$$F_i = \frac{\mathcal{B}_i}{2} \frac{\partial}{\partial z_i} \ln(\Pi). \tag{3.65}$$

If we suppose that the system is in contact with just one thermal bath, or restating the assumption in the context of interest, assuming that $\gamma_i = \gamma_1$ $\forall i$, the following consistency requirement should be matched:

$$\frac{\partial}{\partial z_j} F_i = \frac{\partial}{\partial z_i} F_j \tag{3.66}$$

The above expression implies that the forces must be conservative, i.e. they can be obtained by a generalized potential $\mathcal{U}$ satisfying

$$f_i = -\frac{\partial}{\partial z_i} \mathcal{U}. \tag{3.67}$$

The definition of the current becomes therefore

$$-\frac{\partial}{\partial z_i} \mathcal{U} = \frac{\mathcal{B}_i}{2} \frac{\partial}{\partial z_i} \ln(\Pi) \tag{3.68}$$

and the above expression can be readily integrated to return the usual Boltzmann-Gibbs distribution

$$\Pi(\mathbf{z}) = K \exp\left(-\frac{2}{\mathcal{B}_i} \mathcal{U}(\mathbf{z}) \right) \tag{3.69}$$

where K stands for a proper normalisation constant. More interesting is the setting where the forces are non conservatives and the system evolves towards a stationary state, different from the conventional equilibrium. To explore this possibility we set to introduce the entropy functional $\mathcal{S}(\tau)$ from the probability distribution $\Pi(\mathbf{z}, \tau)$ as [112, 114, 175]:

$$\mathcal{S}(\tau) = -\int_V d\mathbf{z} \Pi(\mathbf{z}, \tau) \ln\left(\Pi(\mathbf{z}, \tau) \right) \tag{3.70}$$

where V is the sample space of the dynamical variables. The Fokker-Planck equation sets the temporal evolution of the entropy. Taking the derivative of (3.70) with respect to time τ, and making use of the Fokker-Planck equation, one obtains [114, 175]:

$$\frac{d\mathcal{S}}{d\tau} = -\int_V \frac{\partial \Pi}{\partial \tau} (\ln \Pi + 1)\, d\mathbf{z} = \int_V \sum_i \frac{\partial \mathcal{I}_i}{\partial z_i} (\ln \Pi + 1)\, d\mathbf{z} \tag{3.71}$$

Assuming that the probability current vanishes at the boundary of the volume V, a simple integration by parts returns:

$$\frac{d\mathcal{S}}{d\tau} = -\sum_i \int_V \mathcal{I}_i \frac{\partial}{\partial z_i} \ln \Pi d\mathbf{z} \tag{3.72}$$

By recalling the definition of the probability current, one can write:

$$\frac{\partial}{\partial z_i} \ln \Pi = \frac{2}{\mathcal{B}_i} F_i - \frac{2}{\mathcal{B}_i} \frac{\mathcal{I}_i}{\Pi}. \tag{3.73}$$

Finally, by substituting the above expression in the formula for the temporal evolution of the entropy, one eventually gets [114, 175]:

$$\frac{d\mathcal{S}}{d\tau} = \mathit{\Pi}_S - \mathit{\Phi}_S \tag{3.74}$$

where

$$\mathit{\Pi}_S = \sum_i \frac{2}{\mathcal{B}_i} \int_V \frac{\mathcal{I}_i^2(\mathbf{z}, \tau)}{P(\mathbf{z}, \tau)} d\mathbf{z} \tag{3.75}$$

and

$$\mathit{\Phi}_S = \sum_i \frac{2}{\mathcal{B}_i} \int_V F_i(\mathbf{z}) \mathcal{I}_i(\mathbf{z}, \tau) d\mathbf{z}. \tag{3.76}$$

The quantity $\mathit{\Pi}_S$ is always positive and can be interpreted as the entropy production rate given by the non conservative forces f_i. On the other hand, $\mathit{\Phi}_S$ can be either positive or negative, and can be identified as the entropy flux rate. If $\mathit{\Phi}_S > 0$, the flux is from the system towards the environment, the opposite scenario corresponding to $\mathit{\Phi}_S < 0$. By invoking the definition of the current and performing a few integrations by parts, one derive a compact formula for the entropy flux rate:

$$\begin{aligned} \mathit{\Phi}_S &= \sum_i \frac{2}{\Gamma_i} \int_V F_i \mathcal{I}_i d\mathbf{z} = \sum_i \frac{2}{\Gamma_i} \int_V \left(f_i^2 P - \frac{\Gamma_i}{2} F_i \frac{\partial}{\partial z_i} P \right) d\mathbf{z} = \\ &= \sum_i \frac{2}{\Gamma_i} \int_V \left(F_i^2 P + \frac{\Gamma_i}{2} P \frac{\partial}{\partial z_i} F_i \right) d\mathbf{z} = \sum_i \left(\frac{2}{\Gamma_i} < F_i^2 > + < \frac{\partial}{\partial z_i} F_i > \right) \end{aligned} \tag{3.77}$$

which, by making explicit the forces F_i, yields:

$$\begin{aligned} \mathit{\Phi}_S &= \sum_{i,j,k} \frac{2}{\mathcal{B}_i} \mathcal{J}_{ij} \mathcal{J}_{ik} \mathcal{C}_{jk} + \sum_{i,j,k} \frac{2}{\mathcal{B}_i} \mathcal{J}_{ij} \mathcal{J}_{ik} < \zeta_j >< \zeta_k > + \sum_i \mathcal{J}_{ii} = \\ &= \sum_i \frac{2}{\mathcal{B}_i} \left(\mathcal{J} \mathcal{C} \mathcal{J}^t \right)_{ii} + \sum_i \frac{2}{\mathcal{B}_i} \left[\left(\mathcal{J} < \boldsymbol{\zeta} > \right)_i \right]^2 + Tr \mathcal{J}. \end{aligned} \tag{3.78}$$

In the stationary state:

$$(\Phi_S)_\infty = \sum_i \frac{2}{\mathcal{B}_i} \left(\mathcal{J}\mathcal{C}_s\mathcal{J}^t\right)_{ii} - 6 \tag{3.79}$$

where use has been made of the fact that the first moments of the distribution Π vanish in the stationary states and that $Tr\mathcal{J} = -2(1 + \frac{1}{\gamma_2} + \frac{1}{\gamma_3}) = -6$. Here, C_s stands for the stationary correlation matrix. Similarly, following an analogous pathway, one can prove that:

$$\begin{aligned} \mathit{\Pi}_S = &\sum_i \frac{2}{\mathcal{B}_i} \left(\mathcal{J}\mathcal{C}\mathcal{J}^t\right)_{ii} + 2Tr\mathcal{J} + \frac{1}{2}\sum_i \mathcal{B}_i\mathcal{C}_{ii}^{-1} + \\ &+ \sum_i \frac{2}{\mathcal{B}_i} \left[\left(\mathcal{J} < \boldsymbol{\zeta} >\right)_i\right]^2 + 4\left(\mathcal{J} < \boldsymbol{\zeta} >\right)_i \left(\mathcal{C}^{-1} < \boldsymbol{\zeta} >\right)_i + 2\mathcal{B}_i \left[\left(\mathcal{C}^{-1} < \boldsymbol{\zeta} >\right)_i\right]^2 \end{aligned} \tag{3.80}$$

In the stationary state, for the setting of interest where the nodes share the same volume ($\gamma_i = \gamma_1 \ \forall i$), the entropy production rate matches the expression:

$$(\mathit{\Pi}_S)_\infty = 2Tr\left(\mathcal{J}\mathcal{C}_s\mathcal{J}\right) + 2Tr\mathcal{J} + \frac{1}{2}Tr\mathcal{C}_s^{-1} \tag{3.81}$$

A straightforward, although lengthy calculation, confirms that $(\mathit{\Pi}_S)_\infty = (\Phi_S)_\infty$, i.e. the condition for stationarity should be obviouvsly met. The entropy can be calculated, at any time t, by inserting in the definition (3.70) the general solution of the Fokker-Planck equation (3.52). This is the multivariate Gaussian of equation (3.53). Carrying out the calculations return [115]:

$$\mathcal{S}(\tau) = \frac{1}{2}\int \Pi\left(\boldsymbol{\zeta}, \tau\right) \left[\left(\boldsymbol{\zeta} - < \boldsymbol{\zeta} >\right)^T \mathcal{C}^{-1} \left(\boldsymbol{\zeta} - < \boldsymbol{\zeta} >\right) + \ln\left(\left(2\pi\right)^n |\mathcal{C}|\right)\right] d\boldsymbol{\zeta} \tag{3.82}$$

The second term in the above integral gives simply $\ln\left(\left(2\pi\right)^n |\mathcal{C}|\right)$, because of the normalisation of the probability distribution The first term can be calculated as follows. Observe that $\mathcal{C}$ is a symmetric positive definite matrix and its elements are real. It is hence possible to construct its Cholesky decomposition $\mathcal{C} = EE^T$. Perform now the transformation $\boldsymbol{\zeta} = E\mathbf{s} + < \boldsymbol{\zeta} >$, which yields $\left(\boldsymbol{\zeta} - < \boldsymbol{\zeta} >\right)^T \mathcal{C}^{-1} \left(\boldsymbol{\zeta} - < \boldsymbol{\zeta} >\right) = \mathbf{s}^T\mathbf{s}$. The probability distribution expressed as a function of the variables $\mathbf{s}$ read

$$\mathit{\Pi}(\mathbf{s}) = \frac{1}{(2\pi)^n} \exp\left\{-\frac{1}{2}\mathbf{s}^T\mathbf{s}\right\} \tag{3.83}$$

and consequently the first integral in (3.82) gives

$$< \mathbf{s}^T \mathbf{s} >= n \tag{3.84}$$

In conclusion, $\mathcal{S}(\tau) = \frac{1}{2}\left[n + \ln\left((2\pi)^n |\mathcal{C}|\right)\right] = \frac{1}{2}\ln\left((2\pi e)^n |\mathcal{C}|\right)$ and $\mathcal{S}_\infty = \frac{1}{2}\ln\left((2\pi e)^n |\mathcal{C}_s|\right)$ with an obvious meaning of the involved symbols.

In Figure 3.7, the stationary entropy $\mathcal{S}_\infty$ is plotted against w moving on iso-α lines: the stationary entropy grows with reactivity of the system system. The reactivity, as stemming from non-normality, facilitates hence the exploration of the available phase space, pushing the system out of equilibrium. In the transient phase, $\Pi_S > \Phi_S$, as it can be appreciated in the main panel of Figure 3.8, where $\Pi_S - \Phi_S$ is represented against τ. The two curves refer to different pairs D, ϵ, chosen on the iso-α line $\bar{\alpha} = -0.6$. During the initial violent relaxation, the curves are almost indistinguishable, but then separate to proceed on distinct tracks. More importantly, the out-of-equilibrium regime seems to persist for longer times, when the value of w is made larger (solid vs. dashed lines). Indeed, the smaller w, the sooner the stationary condition $\Pi_S = \Phi_S$ is established, as illustrated in the inset of Figure 3.8. Here, the quantities Π_S and Φ_S are monitored as a function of time, in lin-log scale, for the same choice of parameters as in the main panel.

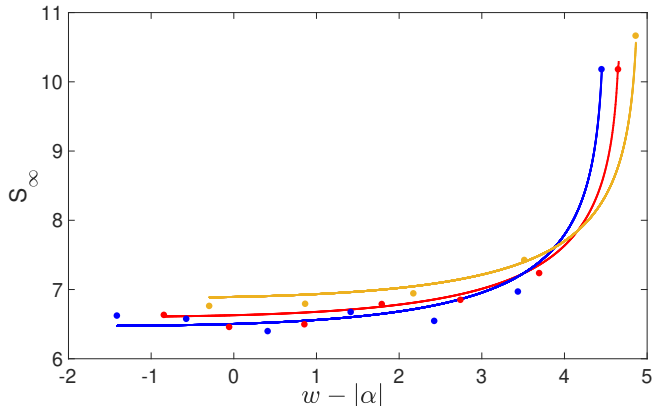

Figure 3.7: The stationary entropy $\mathcal{S}_\infty$ is plotted against w moving on iso-α lines. Here, $\bar{\alpha}$ $(= -0.8, -0.6, -0.4$, from bottom to top). Solid lines stands for the analytical solutions. Symbols follow from direct simulations of the Langevin equations (3.15), on averaging over $M = 300$ independent realizations. Here, $V_1 = V_2 = V_3 = 10^6$ and $r = 50$.

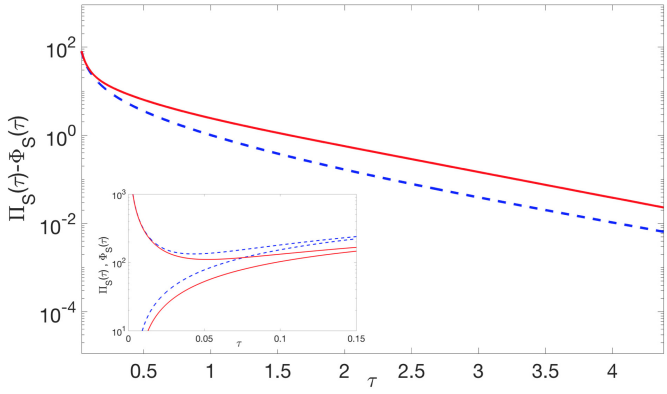

Figure 3.8: Main panel: $\Pi_S - \Phi_S$ is plotted in lin-log scale against τ, for two choices of the parameters D, ϵ constrained to return constant $\alpha = \bar{\alpha} = 0.6$. The solid (red) line refers to $w = 5.25$, while the dashed (blue) line stands for $w = -0.24$. In the inset Π_S and Φ_S are reported for the choices of parameters, as given in the main panel. Here, $r = 50$.

3.3 Conclusion

Finite size corrections represent an unavoidable source of endogenous disturbance, which can significantly impact the dynamics of the system under examination. Macroscopic order can materialize from the microscopic disorder, as stemming from the inherent demographic noise. Under specific operating conditions, quasi-cycles can develop via a resonant mechanism, triggered by the stochastic component of the dynamics. In general, quasi-cycles are modest in size and it is interesting to elaborate on the possible strategies, of either artificial or natural inspirations, that yield a coherent amplification of the stochastic signal. In a recent paper [70], it was shown that giant, noise assisted oscillations can develop when replicating a minimal model of excitatory and inhibitory units, on a large one dimensional lattice subject to unidirectional couplings. The parameters are assigned in such a way that the deterministic analogue of the scrutinized stochastic model displays a stable homogenous equilibrium. Fluctuations generated by the microscopic graininess, yield seemingly regular oscillations, with tunable frequency, which gain amplitude across the lattice. The rate of amplification is controlled by the

coupling constant, among adjacent patches. Motivated by this analysis, we have here considered a variant of the model discussed in [70] to shed light onto the fundamental ingredients which cooperate for the onset of the amplification. The species are assigned to populate a spatially extended loop made of three nodes. Triangular loops define the simplest non trivial closed path in large network complexes: for this reason, it is instructive to elaborate on their putative role in assisting the stochastic amplification of quasicycles. A sensible increase in the stochastic oscillations is indeed obtained when propagating the signal across the loop, while forcing the system in a region where the deterministic homogeneous fixed point proves stable. The larger the coupling constant the more pronounced the measured gain. When the coupling is made stronger, one approaches the boundary of stability for the underlying equilibrium: the damping of fluctuations is consequently reduced and this explains the increase of oscillations' amplitude against D. More interesting is the amplification detected when freezing the dispersion relation, i.e. setting to a constant the largest (negative real part of the) eigenvalue of the Jacobian. In this case, the degree of amplification is controlled by the reactivity index, a parameter that quantifies the short time growth of the norm of an imposed perturbation. The larger the reactivity of the non normal Jacobian matrix – associated to the spatially extended system – the more pronounced the stochastic driven oscillations. Nonconservative forces push the system out of equilibrium and the stationary value of the entropy is found to increase with the reactivity, here measured by the numerical abscissa. Based on these observations, we argue that non normality, and, more specifically, reactivity, should be thoroughly considered, when bridging stochastic dynamics and out-of-equilibrium thermodynamics. More than that, we want to remark that we are facing an important and unconventional thermodynamic scenario. In fact, in the presence of nonconservative forces the system converges asympotically to a genuine nonequilibrium steady state, after a transient during which the entropy production rate monotonically vanishes and the system reaches a maximum of the entropy. This shows that a variatonal principle based on entropy maximization is compatible with the presence of a nonzero (entropy) current. This is because in our model all nodes are subjected to the same effective temperature (i.e. $\gamma_i = \gamma_1 = 1 \forall i$). We conjecture that when assuming different values of the volumes of the nodes and of the corresponding temperatures, the system converges to the more standard scenario of another genuine nonequilibrium state, which is a consequence of the vari-

ational principle of minimization of the entropy production rate, constant at any node of the system. In conclusion, we have here shown that minimalistic loops of intertangled excitatory and inhibitory units might trigger a coherent amplification of the stochastic oscillations, as exhibited on each isolated patch. Moreover, deterministic non normality should be maximized for the stochastic system to grow giant coherent oscillations.

Chapter 4

Resilience for stochastic systems interacting via a quasi-degenerate network

The previous chapter highlights the consequences of nontrivial interplay between stochastic forcing and network arrangement for a model of reactive populations.

In this chapter, we show that a resonant amplification can be obtained when replicating a non-normal reactive scheme on the nodes of a directed and quasi-degenerate network, also for stable, hence resilient, systems. Non-normality and quasi-degenerate networks may, therefore, amplify the inherent stochasticity and so contribute to altering the perception of resilience, as quantified via conventional deterministic methods. Resilience represents the inherent ability of a given system to oppose external disturbances and eventually recover the unperturbed state. The concept of resilience is particularly relevant to ecology [87, 142]. Here, perturbations of sufficient magnitude may force the system beyond the stability threshold of a reference equilibrium. When the threshold is breached, recovery is not possible and the system under scrutiny steers towards an alternative attractor, distinct from the original one. The capacity of the system to withstand changes is however important in different fields ranging from climate change to material science, via information security and energy development [73].

To grasp the mathematical essence of the phenomenon, one can rely on a straightforward linear stability analysis of the governing dynamical,

supposedly deterministic, equations. If the largest real part of the Jacobian eigenvalues is negative, the examined system is deemed stable, against tiny disturbances [136, 170, 171]. However, a linearly stable equilibrium can be made unstable, through non-linearities, by a sufficiently large perturbation amount: this occurs for instance when the enforced disturbance takes the system outside the basin of attraction, i.e. the set of initial conditions leading to long-time behavior that approaches the attractor [130]. In the following, we shall focus on sufficiently small perturbations, so that the linear stability holds true. A transient growth can, however, take place, at short times, before the perturbation fades eventually away, as established by the spectrum of the Jacobian matrix. This short time amplification is instigated by the non-normal character of the interaction scheme and may trigger the system unstable, also when the eigenvalues of the Jacobian display a negative real part [176]. The elemental ability of a non-normal system to prompt an initial rise of the associated norm, can be made perpetual by an enduring stochastic drive [70,150], as described in Chapter 3. This evidence suggests that caution should be exercised when quantifying the resilience of systems driven by non-normal coupling and shaked by stochastic forcing. As a side remark, let us observe that non normal arrangement of coupled sensors could boost the performances of devices implementing the principle of stochastic resonance [28,78]. Suitable strategies of stochastic control could also be devised which exploit the ability of the system to trigger punctual amplification on key nodes of the collection [72].

We shall be, in particular, interested in interacting multi-species models, diffusively coupled via a networked arrangement [16, 19, 35, 41, 44, 61, 62, 93, 108, 138, 139, 153, 154]. The investigated systems are assumed to hold an homogeneous equilibrium. For a specific choice of the involved parameters, the homogeneous fixed point can turn unstable upon injection of a non homogeneous perturbation, which activates the diffusion component. The ensuing symmetry breaking instability, as signaled by the so called dispersion relation [159], constitutes the natural generalization of the celebrated Turing instability [178] to reaction-diffusion systems hosted on a complex network.

In [133], the authors showed that non-normal, hence asymmetric, networks may drive a deterministic system unstable, also if this latter is predicted stable under the linear stability analysis. As we shall here prove, the effect is definitely more remarkable when the non-normal system is made inherently stochastic [15, 22, 80, 182]. At variance with the analysis in [31],

it is the non-normality of the network to yield the self-consistent amplification of the noisy component, a resonant mechanism which prevents the resilient recovery. To elaborate along these lines, we will consider a generic reaction-diffusion model defined on a directed one-dimensional lattice, like that presented in Section 2.2. The degenerate spectrum of the Laplacian that governs the diffusive exchanges between adjacent nodes sits at the root of the generalized class of instability that we shall here address. Making the directed lattice longer, i.e. adding successive nodes to the one-dimensional chain, allows for the perturbation to grow in potency, and for the system to eventually cross the boundary of stability [188]. A similar scenario is met when the hosting network is assumed quasi-degenerate, meaning that the Laplacian eigenvalues are densely packed within a limited portion of the complex plane.

Many real networks have been reported to possess a pronounced degree of non-normality [17, 21]. In particular, it was shown that their adjacency matrix is almost triangular (when properly re-organizing the indexing of the nodes) which, in spectral terms, implies enhancing the probability of yielding a degenerate spectrum for the associated Laplacian matrix. Networks that display a triangular adjacency matrix are known as directed acyclic graphs (DAG).

The chapter is organized as follows. In Section 4.1, we shall introduce our reference setting, a reaction-diffusion system anchored on a directed one-dimensional lattice. In particular, we will show that a self-consistent amplification of the noisy component of the dynamics is produced, when successively incrementing the number of nodes that form the chain. Moving from this preliminary information, in Section 4.1 we will modify the lattice structure by accommodating for, uniform and random, return loops. This breaks the degeneracy that arises from the directed lattice topology. The coherent amplification of the stochastic drive is however persistent as long as the spectrum is close to degenerate. Random directed acyclic graphs with quasi-degenerate spectrum can also be created, so as to make reaction-diffusion systems equally prone to the stochastically driven instability. This topic will be discussed in Section 4.2.

4.1 Reaction-diffusion dynamics on a directed lattice

We begin by considering the coupled evolution of two species which are bound to diffuse on a (directed) network [1, 6, 33, 146]. Introduce the index $i = 1, ..., \Omega$ to identify the Ω nodes of the collection and denote by ϕ_i and ψ_i the concentration of the species on the i-th node. The local (on site) reactive dynamics is respectively governed by the non-linear functions $f(\phi_i, \psi_i)$ and $g(\phi_i, \psi_i)$. The structure of the underlying network is specified by the adjacency matrix $\mathbf{A}$: A_{ij} is different from zero if a weighted link exists which connects node j to node i. The species can relocate across the network traveling the available edges. With reference to species ϕ_i, the net flux at node i reads $D_\phi \sum_{j=1}^{\Omega} A_{ij}(\phi_j - \phi_i)$, where D_ϕ stands for the diffusion coefficient and the sum is restricted to the subset of nodes j for which $A_{ij} \neq 0$. Furthermore, we shall assume that the dynamics on each node gets perturbed by an additive noise component of amplitude σ_i. In formulae, the system under investigation can be cast as:

$$\frac{d}{dt}\phi_i = f(\phi_i, \psi_i) + D_\phi \sum_{j=1}^{\Omega} \Delta_{ij}\phi_j + \sigma_i(\mu_\phi)_i \tag{4.1a}$$

$$\frac{d}{dt}\psi_i = g(\phi_i, \psi_i) + D_\psi \sum_{j=1}^{\Omega} \Delta_{ij}\psi_j + \sigma_i(\mu_\psi)_i \tag{4.1b}$$

where $\Delta_{ij} = A_{ij} - k_i\delta_{ij}$ stands for the discrete Laplacian and $k_i = \sum_j A_{ij}$ is the incoming connectivity. Here, $(\mu_\phi)_i$ and $(\mu_\psi)_i$ are Gaussian random variables with zero mean and correlations $\langle(\mu_\phi)_i(t)(\mu_\phi)_j(t')\rangle = \langle(\mu_\psi)_i(t)(\mu_\psi)_j(t')\rangle = \delta_{ij}\delta(t-t')$ and $\langle(\mu_\phi)_i(t)(\mu_\psi)_j(t')\rangle = 0$. Here $\delta_{ij} = 1$ if and only if $i = j$ and $\delta_{ij} = 0$ otherwise, denotes the Kronecker delta. Conversely, $\delta(t - t") = 1$ if and only if $t = t'$ and $\delta(t - t') = 0$ otherwise, denotes the Dirac delta. In this section, we will assume a directed lattice as the underlying network. A schematic layout of the system is depicted in Fig. 4.1. The $\Omega \times \Omega$ Laplacian matrix associated to the directed lattice admits a degenerate spectrum, an observation that will become crucial for what follows. More precisely, the eigenvalues of the Laplacian operators are $\Lambda^{(1)} = 0$, with multiplicity 1, and $\Lambda^{(2)} = -1$, with multiplicity $\Omega - 1$. Notice that the eigenvalues are real, even though the Laplacian matrix is asymmetric.

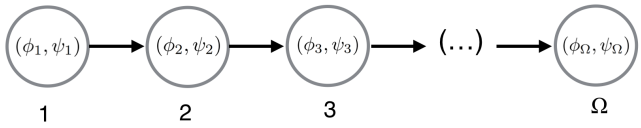

Figure 4.1: The scheme of the model is illustrated. Two populations, respectively denoted by ϕ and ψ, are distributed on a collection of Ω nodes. The nodes are arranged so as to form a one-dimensional lattice subject to unidirectional couplings, as outlined in the scheme. The weight of the link between adjacent nodes is set to one. The local, on site, interaction among species is ruled by generic nonlinear functions of the concentration amount.

4.1.1 The deterministic limit

To continue with the analysis, we will assume that the local reactive dynamics admits an equilibrium (ϕ^*, ψ^*), i.e. $f(\phi^*, \psi^*) = 0$ and $g(\phi^*, \psi^*) = 0$. In turn, this implies that the deterministic analogue of system (4.1a)-(4.1b) (obtained when setting $\sigma_i = 0$, $\forall i$) admits the homogeneous fixed point $\phi_i = \phi^*$ and $\psi_i = \psi^*$ for any i. Furthermore, we will assume that the aforementioned fixed point is stable against homogeneous perturbation, a working assumption which can be formally quantified by considering the associated Jacobian matrix:

$$\mathbf{J} = \begin{pmatrix} f_\phi & f_\psi \\ g_\phi & g_\psi \end{pmatrix} \tag{4.2}$$

where f_ϕ stands for the partial derivative of $f(\phi, \psi)$ with respect to ϕ, evaluated at the fixed point (ϕ^*, ψ^*). Similar definitions hold for f_ψ, g_ϕ and g_ψ. The homogeneous fixed point is stable provided that $tr(J) = f_\phi + g_\psi < 0$ and $det(J) = f_\phi g_\psi - f_\psi g_\phi > 0$. Here, $tr(...)$ and $det(...)$ denote, respectively, the trace and the determinant. When the above inequalities are met, the largest real part of the eigenvalues of the Jacobian matrix J is negative, pointing to asymptotic stability. Peculiar behaviors however arise when the spectrum of J is degenerate, namely when the eigenvalues come in identical pairs.

In this case, the solution to the linear problem ruled by matrix J contains a secular term, which, depending on the initial conditions, might yield a counterintuitive growth of the perturbation, at short time. For long enough time, the exponential damping takes it over and the system relaxes back to the stable equilibrium (or, equivalently, the imposed perturbation is damped

away). Short-time transients can also be found in stable linear systems, ruled by non-normal matrices. A matrix is said non-normal, if it does not commute with its adjoint [176] . For the case at hand, J is assumed to be real. Hence, taking the adjoint is identical to considering the transpose of the matrix. In formulae, J is non-normal, provided $[J, J^T] = JJ^T - J^T J \neq 0$, where the superscript T denotes the transpose operation. Assume that the non-normal matrix J is stable, hence its eigenvalues have negative real parts. Consider then the Hermitian part of J, a symmetric matrix defined as $H(J) = (J + J^T)/2$. If the largest eigenvalue of H is positive, then the linear system governed by J can display a short time growth, for a specific range of initial conditions. Systems characterized by stable Jacobian matrix, with an associated unstable Hermitian part, are termed reactive. In the following we shall consider a reactive two-component system, namely a two species model that possesses the elemental ability to grow the imposed perturbation at short times, also when deemed stable. This latter ability will be considerably augmented by replicating such fundamental unit on the directed chain, and so engendering a secular behavior which eventually stems from the degenerate structure of the associated Jacobian.

Heading in this direction we shall first make sure that the examined system is stable when formulated in its spatially extended variant, namely when the two species dynamical system is mirrored on a large set of nodes, coupled diffusively via unidirectional links. A non homogeneous perturbation can be in fact imposed, which activates the diffusion component and consequently turns, under specific conditions, the homogenous solution unstable. The subtle interplay between diffusion and reaction weakens therefore the resilience of the system, by opposing its ability to fight external disturbances and eventually regain the unperturbed (homogeneous) state. The conditions for the onset of the diffusion-driven instability are obtained via a linear stability analysis, that we shall hereafter revisit for the case at hand. The analysis yields a dispersion relation which bears information on the outbreak of the instability. This latter constitutes a straightforward generalization of the celebrated Turing mechanism [178] to the case of a discrete, possibly directed support [19].

To further elaborate along this axis, we focus on the deterministic version of system (4.1a)-(4.1b) and impose a, supposedly small, non homogeneous

perturbation of the homogenous equilibrium. In formulae, we set:

$$\begin{aligned} \phi_i &= \phi^* + \xi_i \\ \psi_i &= \psi^* + \eta_i \end{aligned} \tag{4.3}$$

where ξ_i and η_i stand for the imposed perturbation. In the following we will label $\boldsymbol{\zeta} = (\xi_1, \eta_1, ..., \xi_\Omega, \eta_\Omega)$ the vector which characterizes the fluctuations around the fixed point. Insert now the above condition in the governing equation and linearize around the fixed point, assuming the perturbation to be small. This readily yields a $2\Omega \times 2\Omega$ linear system in the variable $\boldsymbol{\zeta}$:

$$\frac{d}{dt}\boldsymbol{\zeta} = \mathcal{J}\boldsymbol{\zeta} \tag{4.4}$$

where

$$\mathcal{J} = \begin{pmatrix} \mathbf{J} & \mathbf{0} & \dots & \\ \mathbf{D} & \mathbf{J}-\mathbf{D} & \mathbf{0} & \dots \\ \mathbf{0} & \mathbf{D} & \mathbf{J}-\mathbf{D} & \\ \vdots & \ddots & \ddots & \ddots \end{pmatrix} \tag{4.5}$$

and $\mathbf{D} = \begin{pmatrix} D_\phi & 0 \\ 0 & D_\psi \end{pmatrix}$ is the diagonal diffusion matrix. The spectrum of the generalized Jacobian matrix $\mathcal{J}$ conveys information on the asymptotic fate of the imposed perturbation. If the eigenvalues display negative real parts, then the perturbation is bound to fade away, at sufficiently large times. The system hence recovers the unperturbed homogeneous configuration. Conversely, the perturbation grows when the eigenvalues possess a positive real part. A Turing-like instability sets in and the system evolves towards a different, non homogeneous, attractor.

To compute the eigenvalues λ of matrix $\mathcal{J}$, we label $\varepsilon_i = \mathbf{J} + \mathbf{D}\Delta_{ii}$ for $i = 1, \dots, \Omega$. Then, the characteristic polynomial of $\mathcal{J}$ reads:

$$0 = \det(\mathcal{J} - \lambda I) = \prod_{i=1}^{N} \det(\varepsilon_i - \lambda I) \tag{4.6}$$

$$= \det(\varepsilon_1 - \lambda I)\left[\det(\varepsilon_2 - \lambda I)\right]^{\Omega-1} \tag{4.7}$$

where I stands for the 2×2 identity matrix and

$$\det(\varepsilon_1 - \lambda I) = \lambda^2 - tr(\mathbf{J})\lambda + \det(\mathbf{J}) \tag{4.8}$$

$$\det(\varepsilon_2 - \lambda I) = \lambda^2 - tr(\mathbf{J}')\lambda + \det(\mathbf{J}')$$

where we have introduced the matrix $\mathbf{J}' = \mathbf{J} - \mathbf{D}$. The spectrum of the generalized Jacobian is hence degenerate if $\Omega > 2$ and the multiplicity of the degeneracy of the spectrum grows with Ω, the number of nodes that compose the lattice. In formulae:

$$\lambda_{1,2} = \frac{tr(\mathbf{J}) \pm \sqrt{tr^2(\mathbf{J}) - 4\det(\mathbf{J})}}{2} \tag{4.9}$$

and

$$\lambda_{3,4} = \frac{tr(\mathbf{J}') \pm \sqrt{tr^2(\mathbf{J}') - 4\det(\mathbf{J}')}}{2} \tag{4.10}$$

with degeneracy $\Omega - 1$. The stability of the fixed point (ϕ^*, ψ^*) to external non homogeneous perturbation is hence determined by $(\lambda_{re})_{max}$, the largest real part of the above eigenvalues.

For $\Omega > 2$, the solution of the linear system (4.4) can be cast in a closed analytical form, by invoking the concept of generalized eigenvectors. Denote with $\boldsymbol{v_0}$ and $\boldsymbol{w_0}$ the ordinary eigenvectors associated to the non degenerate eigenvalues λ_1 and λ_2. The ordinary eigenvectors $\boldsymbol{v_1}$ and $\boldsymbol{w_1}$, respectively associated to λ_3 and λ_4, are non degenerate (i.e. the geometric multiplicity is one). This can be proven for a generic dimension 2Ω of the matrix $\mathcal{J}$ due to the simple block structure of the matrix. We then introduce the generalized eigenvectors associated to λ_3, λ_4 as:

$$(\mathcal{J} - \lambda_3 I)^i \boldsymbol{v_{i+1}} = \boldsymbol{v_i}, \quad i = 1, \ldots, \Omega - 2 \tag{4.11}$$

$$(\mathcal{J} - \lambda_4 I)^i \boldsymbol{w_{i+1}} = \boldsymbol{w_i}, \quad i = 1, \ldots, \Omega - 2. \tag{4.12}$$

The solution of (4.4) reads therefore:

$$\begin{aligned}\boldsymbol{\zeta} = c_0 e^{\lambda_1 t}\boldsymbol{v_0} + d_0 e^{\lambda_2 t}\boldsymbol{w_0} \\ + [c_1\boldsymbol{v_1} + c_2(\boldsymbol{v_1}t + \boldsymbol{v_2}) + c_3(\boldsymbol{v_1}t^2 + \boldsymbol{v_2}t + \boldsymbol{v_3}) \\ + \cdots + c_{\Omega-1}(\boldsymbol{v_1}t^{\Omega-2} + \boldsymbol{v_2}t^{\Omega-3} + \cdots + \boldsymbol{v_{\Omega-1}})]e^{\lambda_3 t} \\ + [d_1\boldsymbol{w_1} + d_2(\boldsymbol{w_1}t + \boldsymbol{w_2}) + d_3(\boldsymbol{w_1}t^2 + \boldsymbol{w_2}t + \boldsymbol{w_3}) + \ldots \\ + d_{\Omega-1}(\boldsymbol{w_1}t^{\Omega-2} + \boldsymbol{w_2}t^{\Omega-3} + \cdots + \boldsymbol{w_{\Omega-1}})]e^{\lambda_4 t}.\end{aligned} \tag{4.13}$$

Secular terms, which bear the imprint of the spectrum degeneracy, may boost the short time amplification of the norm of the imposed perturbation. Remind that the transient growth occurs for $(\lambda_{re})_{max} < 0$, i.e. when the perturbation is bound to fade away asymptotically. Interestingly, the degree

of the polynomial increases with the lattice size. This implies, in turn, that the short time amplification of a stable system could progressively grow, as the number of lattice nodes gets increased.

Without loss of generality, and to test the implication of the above reasoning, we shall hereafter assume the Brusselator model, as a reference reaction scheme. The Brusselator is a paradigmatic testbed for nonlinear dynamics, and it is often invoked in the literature as a representative model of self-organisation, synchronisation and pattern formation [76]. Our choice amounts to setting

$$f(\phi_i, \psi_i) = 1 - (b+1)\phi_i + c\phi_i^2\psi_i \tag{4.14a}$$

$$g(\phi_i, \psi_i) = b\phi_i - c\phi_i^2\psi_i \tag{4.14b}$$

where b and c stand for positive parameters. The system admits a trivial homogeneous fixed point for $(\phi_i, \psi_i) = (1, b/c)$. This latter is stable to homogeneous perturbation provided that $c > b - 1$. We can then isolate, in the parameter plane (b, c), the domain where $(\lambda_{re})_{max} > 0$, or stated differently, the region that corresponds to a generalized Turing instability. The result of the analysis is displayed in Fig. 4.2, for a specific choice of the diffusion parameters, with $D_\phi > D_\psi$: the region of Turing instability falls inside the black solid lines (the red line follows the analysis of the stochastic analogue of the model, as we will explain in the following). The symbols identify two distinct operating points, positioned outside the region of deterministic instability. Working in this setting, after a short time transient, the perturbations get exponentially damped and the system relaxes back to its homogeneous equilibrium. The effect of the short time amplification should get more visible for increasing values of Ω, the lattice size, and the close the operating point is to the threshold of instability. This scenario is confirmed by inspection of Fig. 4.3, where the norm of the perturbation is plotted against time, for the chosen parameter values. To further elaborate on this observation, in Fig. 4.4 we display the density of species ϕ, on different nodes of the chain, versus time. Panel (a) refers to the choice of parameters that corresponds to the blue square in Fig. 4.2, while panel (b) follows for the parameters associated to the orange circle. By making the chain longer, one better appreciates the initial growth of the perturbation which materializes in transient patterns. For sufficiently long time, the patterns disappear and the system converges back to the unperturbed homogeneous fixed point. The time for equilibration grows with the size of the lattice, i.e. with the

number of nodes Ω. Transient patterns are more pronounced and persistent, the closer to the region of deterministic instability.

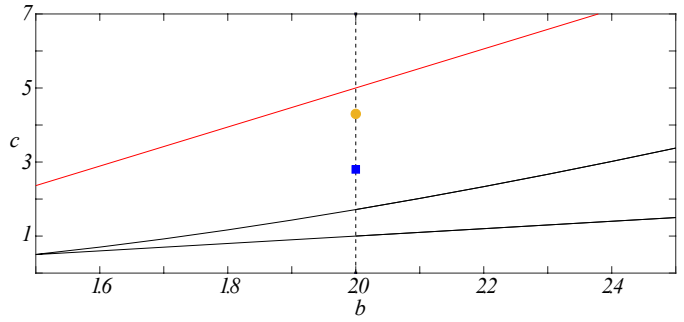

Figure 4.2: The region of instability is depicted in the parameter plane (b, c). This is the portion of the plane contained in between the two black solid lines. The symbols refer to two distinct operating points, positioned outside the domain of deterministic instability. The two points are located at $b = 2$, and have respectively $c = 2.8$ and $c = 4.3$. The red line delimits the upper boundary of the parameters region where the stochastic amplification can eventually take place, as discussed in the remaining part of the section. Here, $D_\phi = 1$ and $D_\psi = 10$.

4.1.2 The stochastic evolution

We shall here move on to consider the effect produced by a perpetual noise. This amounts to assuming $\sigma_i \neq 0$ in (4.1a)-(4.1b) [80]. For the sake of simplicity we will set in the following $\sigma_i = \sigma$. We anticipate however that our conclusions still hold when accounting for an arbitrary degree of heterogeneity in the strength of the noise. By linearizing the governing dynamical system around the fixed point yields a set of linear Langevin equations [30]:

$$\frac{d}{d\tau}\zeta_i = (\mathcal{J}\boldsymbol{\zeta})_i + \hat{\lambda}_i \tag{4.15}$$

where $\hat{\boldsymbol{\lambda}}$ is a 2Ω vector of random Gaussian entries with zero mean, $< \hat{\boldsymbol{\lambda}} >= 0$, and correlation given by $< \hat{\lambda}_i(\tau)\hat{\lambda}_j(\tau') >= \sigma^2\delta_{ij}\delta(\tau - \tau')$.

The linear Langevin equations (4.15) are equivalent to the following Fokker-Planck equation [89] for the distribution function Π of the fluctu-

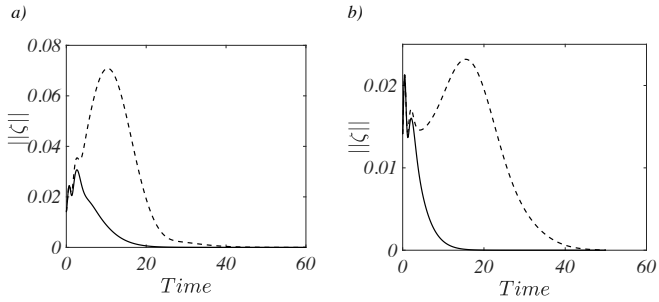

Figure 4.3: The evolution of the norm of the perturbation is displayed for different choices of the reaction parameter c, corresponding to the two points selected in Fig. 4.2 (at $b = 2$). (a) Here $c = 2.8$, the lower point (blue square) in Fig. 4.2. The solid line refers to $\Omega = 5$ while the dashed line is obtained for $\Omega = 10$. (b) Here $c = 4.3$, the upper point (orange circle) in Fig. 4.2. The solid line stands for $\Omega = 5$ while the dashed line refers to $\Omega = 25$. Notice that the amplification gets more pronounced the closer the working point is to the deterministic transition line. Also, the peak of the norm against time shifts towards the right as the power of the leading secular terms is increased. Here, $D_\phi = 1$ and $D_\psi = 10$.

ations

$$\frac{\partial}{\partial \tau}\Pi = -\sum_{i=1}^{2\Omega} \frac{\partial}{\partial \zeta_i}\left(\mathcal{J}\boldsymbol{\zeta}\right)_i \Pi + \frac{1}{2}\sigma^2 \frac{\partial^2}{\partial \zeta_i^2}\Pi \tag{4.16}$$

The solution of the Fokker-Planck equation is a multivariate Gaussian that we can univocally characterize in terms of the associated first and second moments. It is immediate to show that the first moment converges in time to zero. We focus instead on the $2\Omega \times 2\Omega$ family of second moments, defined as $\langle \zeta_l \zeta_m \rangle = \int \zeta_l \zeta_m \Pi d\boldsymbol{\zeta}$. A straightforward calculation returns [70]:

$$\frac{d}{d\tau} < \zeta_l^2 >= 2 < \left(\mathcal{J}\boldsymbol{\zeta}\right)_l \zeta_l > +\sigma^2 = 2\sum_{j=1}^{2\Omega} \mathcal{J}_{lj} < \zeta_l \zeta_j > +\sigma^2 \tag{4.17}$$

$$\frac{d}{d\tau} < \zeta_l \zeta_m >=< \left(\mathcal{J}\boldsymbol{\zeta}\right)_l \zeta_m > + < \left(\mathcal{J}\boldsymbol{\zeta}\right)_m \zeta_l >= \sum_{j=1}^{2\Omega} \mathcal{J}_{lj} < \zeta_m \zeta_j > +\mathcal{J}_{mj} < \zeta_l \zeta_j > \tag{4.18}$$

for respectively the diagonal and off-diagonal ($l \neq m$) moments. The stationary values of the moments can be analytically computed by setting to zero the time derivatives on the left hand side of equations (4.17)-(4.18) and solving the linear system that is consequently obtained. Particularly relevant for our purposes is the quantity $\delta_i = \langle \zeta_i^2 \rangle$, the variance of the displayed fluctuations, around the deterministic equilibrium, on node i. The value of δ_i, normalized to δ_1, is plotted in Fig. 4.5, for both species of the Brusselator model. The parameters correspond to the working point identified by the blue square in Fig. 4.2. The solid line stands for the, analytically determined, variance of the fluctuations predicted for species ϕ, while the dashed line refers to species ψ. The symbols are obtained after direct stochastic simulations of system (4.1a)-(4.1b), assuming the Brussellator as the reference reaction scheme. As it can be appreciated by visual inspection of Fig. 4.5, the fluctuations grow progressively node after node. The predicted variances nicely agree with the result of the simulations on the first nodes of the collection. For $\Omega > 15$, deviations are abruptly found and the linear noise approximation fails. Our interpretation goes as follows: the amplification mechanism is manifestly triggered by the imposed noise, which resonates with the peculiar topology of the embedding support. Due to this interplay, noise-seeded fluctuations grow across the chain and make it possible for the system to explore the phase space landscape, beyond the local basin of attraction to which it is deterministically bound.

From here on, it is no longer legitimate to simplify the dynamics of the system as if it was evolving in the vicinity of the homogeneous solution and the assumption that sits at the root of the linear noise estimate are consequently invalidated. The time evolution of species ϕ is plotted, with an appropriate color code, on different nodes of the chain and versus time in Fig. 4.6. Noise secures the stabilization of complex dynamical patterns, which are perpetually maintained in the stochastic version of the model, so breaking the spatial symmetry that characterizes the asymptotic deterministic solution. The amplification mechanism driven by the stochastic component can solely occur within a closed domain of the parameter space (b, c) adjacent to the region of deterministic instability. The domain of interest is delimited by the red solid line in Fig. 4.2: for the parameters that fall below the red line, the variance of the fluctuations is analytically predicted to increase along the chain. Even more importantly, the system may be frozen in the heterogenous state, when silencing the noise (so regaining the deterministic

limit) after a transient of the stochastic dynamics. This is clearly the case, provided that the deterministic dynamics possesses a stable non homogeneous attractor, for the chosen parameter set. In Fig. 4.7 (a) the pattern is stably displayed, only when the noise is active. When the stochastic forcing is turned off (at the time identified by the white dashed line), the system regains the homogenous equilibrium. A selection of individual trajectories, recorded on specific nodes of the chain, is plotted in Fig. 4.7 (b) and yields the same qualitative conclusion. A different scenario is instead met when operating with a slightly smaller value of the parameter c (still outside the region of deterministic Turing instability). When turning off the noise, the system spontaneously sediments in a Chimera like pattern, see Fig. 4.7 (c), a superposition of homogeneous (in the beginning of the chain) and heterogenous states (at the bottom of the chain) [2, 156, 168]. The same conclusion is reached upon inspection of Fig. 4.7 (d). Here, the deterministic attractor is represented with a collection of crosses. A straightforward calculation confirms that it is indeed one of the different non homogeneous and stable attractors displayed by the system in its deterministic version.

4.2 Quasi-degenerate directed lattice

This section is devoted to generalize the above analysis to the relevant setting where the degeneracy of the problem is removed by the insertion of return links, among adjacent nodes. More specifically we will assume that an edge with weight ϵ exists that goes from node i to nodes $i-1$, for all $i > 1$. At the same time the strength of the corresponding forward link is set to $1-\epsilon$, so as to preserve the nodes' strength (for $i > 1$), when modulating ϵ (see Fig. 4.8). In the following we will consider ϵ to be small. In particular, for $\epsilon \to 0$ one recovers the limiting case discussed in the previous section. On the other hand, the introduction of a tiny return probability suffices to break the degeneracy of the problem: the Ω eigenvalues become distinct and the eigenvectors of the Laplacian define a basis which can be used to solve the linear problem (4.4), which stems for the deterministic version of the inspected model [19, 139]. Denote by $\mathbf{v}^\alpha$ the eigenvector of $\mathbf{\Delta}$ relative to eigenvalue $\Lambda^{(\alpha)}$, with $\alpha = 1, .., \Omega$. In formulae, $\sum_{j=1}^{\Omega} \Delta_{ij} v_j^\alpha = \Lambda^\alpha v_i^\alpha$. The perturbation $\boldsymbol{\zeta}$ in equation (4.4) can be expanded as $\zeta_i = \sum_{\alpha=1}^{\Omega} c_\alpha e^{\lambda_\alpha t} v_i^\alpha$, where the constants c_α are determined by the initial condition. By inserting the aforementioned ansatz into the linear system (4.4) yields the self-consistent

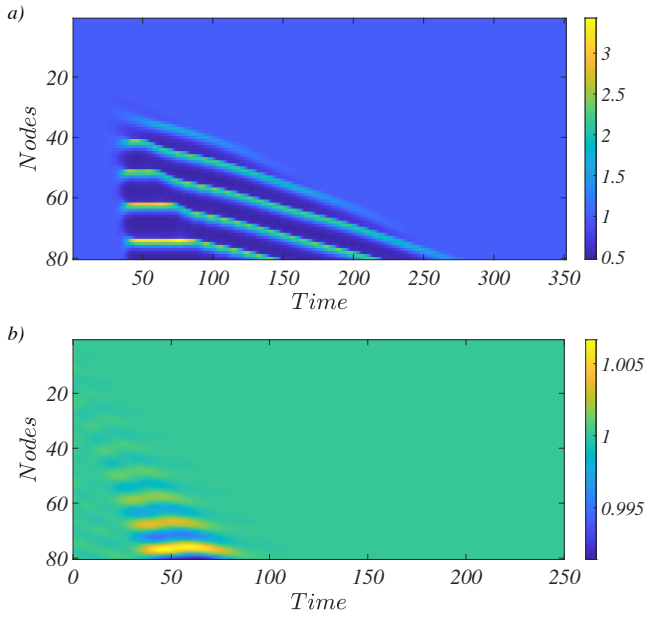

Figure 4.4: The time evolution of species ϕ is displayed with an appropriate color code, on different nodes of the chain and against time. The Brusselator reaction scheme is assumed. Diffusion constants are set to $D_\phi = 1$ and $D_\psi = 10$. Panel (a) refers to the values of b and c associated to the blue square in Fig. 4.2 (i.e. closer to the transition line), while panel (b) follows the parameters attributed by assuming the orange circle as the operating point (further away from the transition line).

condition

$$\det \begin{pmatrix} f_\phi + D_\phi \Lambda^\alpha - \lambda_\alpha & f_\psi \\ g_\phi & g_\psi + D_\psi \Lambda^\alpha - \lambda_\alpha \end{pmatrix} = 0. \tag{4.19}$$

The stability of the homogenous fixed point can therefore be determined from the above condition, by computing λ_α as a function of the Laplacian eigenvalues $\Lambda^{(\alpha)}$. This is the generalization of the so called dispersion relation to a setting where the spatial support is a network. In Fig. 4.9, we plot the dispersion relation for a chain made of $\Omega = 10$ nodes and for different values of ϵ, assuming the Brusselator model as the reference scheme. The reaction

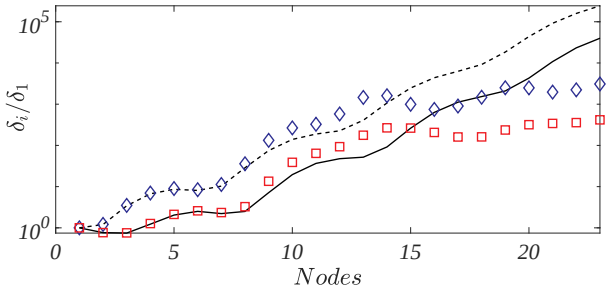

Figure 4.5: The phenomenon of noise driven amplification is illustrated: δ_i/δ_1 is plotted against the node's number along the chain. The solid (dashed) line refers to the variance of the fluctuations, as predicted for species ϕ (ψ). The symbols stand for the homologues quantities as computed via direct stochastic simulations. The Brussellator model is assumed as the reference reaction scheme and parameters refer to the blue square displayed in Fig. 4.2.

parameters are set so as to yield the square symbol in Fig.4.2. Remarkably, the spectrum of the Laplacian operator is real and the largest eigenvalue is $\Lambda^{(1)}$=0, as it readily follows by its definition. The remaining $\Omega-1$ eigenvalues are real and cluster in the vicinity of $\bar{\Lambda} = -1$, the smaller ϵ is, the closer they get to this value, as illustrated in Fig. 4.9. The case of a degenerate chain can be formally recovered by sending ϵ to zero, which in turn implies that the non trivial portion of the dispersion curve, as depicted in Fig. 4.9, collapses towards an asymptotic attractor located at $(\bar{\Lambda}, \lambda(\bar{\Lambda}))$. Building on this observation, it can be shown that the solution of the deterministic linear problem (4.4), for the system defined on a degenerate chain, can be obtained by performing the limit for $\epsilon \to 0$ of the non degenerate linear solution.

It is hence tempting to speculate that the stochastically driven instability, as outlined in the preceding section, can readily extend to a setting where the chain is non degenerate, provided that ϵ is sufficiently small. The remaining part of this section is entirely devoted to explore this interesting generalization.

Following the strategy discussed above, we can set to calculate the stationary values for the moments of the stochastic fluctuations. In Fig. 4.10, the stationary values of the moments $\delta_i = \langle \zeta_i^2 \rangle$ are normalized to δ_1 and

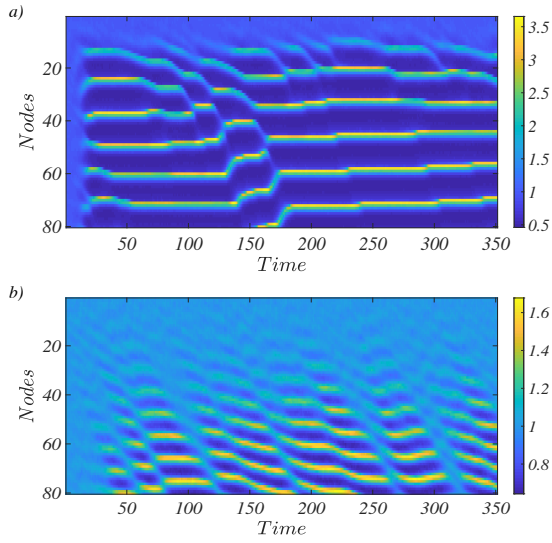

Figure 4.6: The time evolution of species ϕ is displayed with an appropriate color code, on different nodes of the chain and against time. The Brusselator reaction scheme is assumed and the choice of the parameters reflects that made in Fig. 4.4. The pattern displayed in panel a) is obtained for the parameters associated to the blue square in Fig. 4.2. Panel b) follows the position of the orange circle. By integrating the stochastic dynamics on a sufficiently long chain yields a robust pattern, which holds permanently, at variance with its deterministic analogue (see Fig. 4.4).

plotted against the node label across the chain. In analogy with the above, the solid line stands for the variance of the fluctuations associated to species ϕ, while the dashed line stands for species ψ. As expected, the fluctuations magnify along the chain, as it happens when the system is made to evolve with $\epsilon = 0$. The predicted variances agree with the results of the stochastic simulations, up to a critical length of the chain above which the system begins feeling the nonlinearities that will steer it towards a non homogeneous attractor. Noise stabilizes the heterogeneous patterns which become hence perpetual in the stochastic version of the model, as it can be appreciated by inspection of Fig. 4.11. As a further attempt to grasp the complexity of the phenomenon, we consider again a chain with return links, but assume the

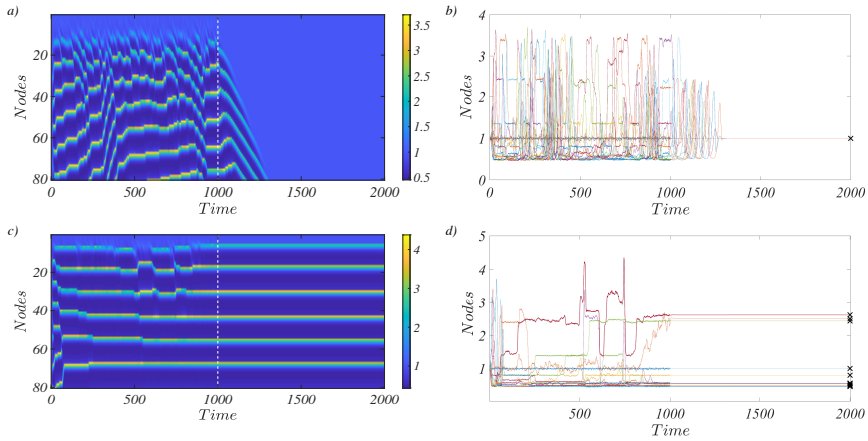

Figure 4.7: Panels (a) and (c). The time evolution of species ϕ is displayed with an appropriate color code, on different nodes of the chain and against time. The vertical dashed line identifies the instant in time when the external noise is turned off: from here on the system evolves according to a purely deterministic scheme. The Brusselator reaction scheme is assumed with the same parameters choice of Fig. 4.5, except for c. In (a), the pattern fades eventually away. Here $c = 2.8$, as in Fig. 4.5. In (c), the system sediments in a stationary pattern of the Chimera type. Here $c = 2.4$. In Figs. (b) and (d), the density of species ϕ is displayed on few nodes of the collection (one node each five, across the chain). In panel (b) (corresponding to pattern (a)), the system converges to the homogeneous fixed point (black cross). In panel (d) (corresponding to pattern (c)), the system reaches a stable heterogeneous attractor.

weights ϵ to be random entries drawn from a Gaussian distribution, centered in $\bar{\epsilon}$, with variance $\eta_{\bar{\epsilon}}$. The spectrum of the Laplacian operator is now complex (at variance with the case where the ϵ are all equal) and the discrete dispersion relation is no longer bound to the idealized continuum curve, see Fig. 4.12. For a sufficiently small $\bar{\epsilon}$, and modest scattering around the mean, the negative portion of the dispersion relation clusters in the vicinity of the point $(\bar{\Lambda}, \lambda(\bar{\Lambda}))$, which stems from the fully degenerate solution. Arguing as above, one can expect that noise and spatial coupling will cooperate also in this setting to yield robust stochastic patterns, in a region of the parameters

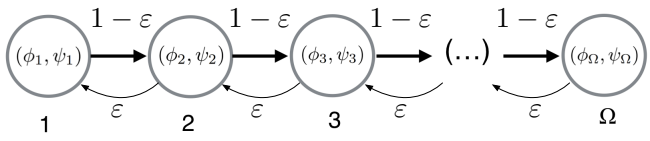

Figure 4.8: The scheme of the model is illustrated for the case where forward and backward links are present. The weights of the connections are modulated by the parameter ϵ.

for which deterministic stability is granted. In Fig. 4.13, we show that the signal amplification for the stochastic Brusselator model defined on a chain with random return weights, is on average identical to that observed when the ϵ are equal and set to the average value $\bar{\epsilon}$. The depicted points are computed after averaging over 100 realization of the random quasi-degenerate network and the error in the computed quantities is of the order of the symbols size. The ensuing stochastic pattern is reported in Fig. 4.14.

In conclusion, we have shown that a generic reaction model, which is stable when defined on a continuous or lattice-like support, can turn unstable due to the cooperative interplay of two effects, noise and the quasi-degenerate nature of the generalized Jacobian operator, as reflecting the specific spatial support here assumed. An increase in the node number yields a progressive amplification of the fluctuations on the rightmost end of the direct chain, a process which eventually drives the uniform attractor unstable. In the reciprocal space, one gains a complementary insight into the scrutinized phenomenon. Driving stochastically unstable a system, which is deemed stable under the deterministic angle, requires packing within a bound domain of the complex plane a large collection of Laplacian eigenvalues. The eigenmodes associated to the quasi-degenerate spectrum provide effective route to vehiculate the instability. One could therefore imagine to generate networks prone to the instability, by hierarchically assembling nodes in such a way that the associated Laplacian possesses a quasi-degenerate spectrum, according to the above interpretation. To challenge this view in the simplest scenario possible, we implemented a generative scheme which builds on the following steps. First we consider two nodes, linked via a direct edge that goes from the first to the second. The Laplacian associated to this pair displays two

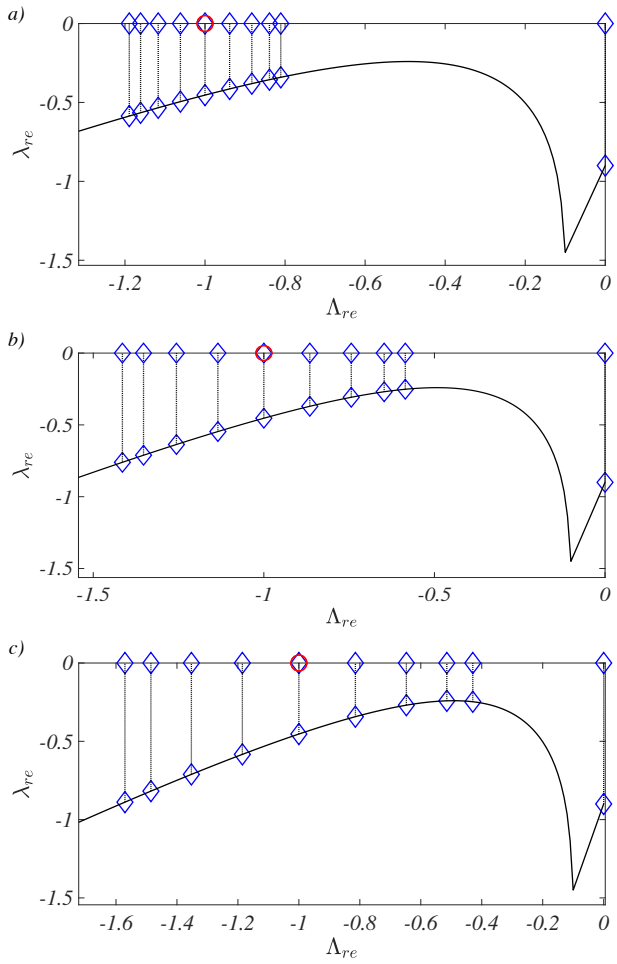

Figure 4.9: Laplacian eigenvalues on the real axis in correspondence with their respective points on the dispersion relation for different values of ϵ [(a) $\epsilon = 0.01$, (b) $\epsilon = 0.05$, (c) $\epsilon = 0.1$] and $\Omega = 10$. The solid lines stand for the dispersion curves obtained when placing the system on a continuous spatial support. Vertical dashed lines are a guide for the eye to project the discrete dispersion relation back to the real axis where the spectrum of the Laplacian falls. The red circle is positioned at -1, the value where the eigenvalues accumulates when sending $\epsilon \to 0$.

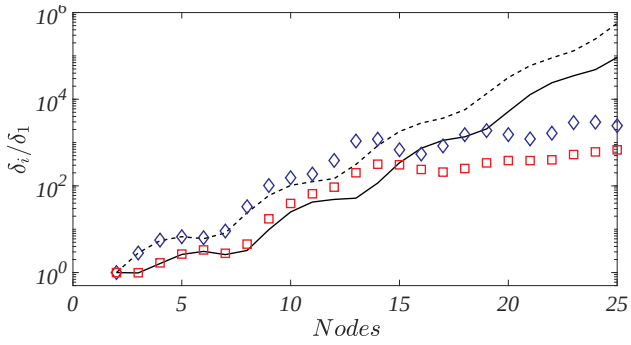

Figure 4.10: δ_i/δ_1 is plotted against the node's number along the chain. Here we set $\epsilon = 0.01$. The solid (dashed) line refers to the variance of the fluctuations as predicted for species ϕ (ψ). The symbols stand for the homologous quantities as computed via direct stochastic simulations. The parameters refer to the blue square displayed in Fig. 4.2.

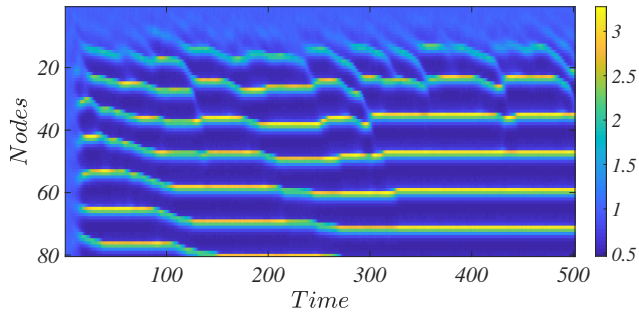

Figure 4.11: The time evolution of species ϕ is displayed with an appropriate color code, on different nodes of the chain and against time. Here $\epsilon = 0.01$ and the Brusselator reaction scheme is assumed with the same parameters choice of Fig. 4.10

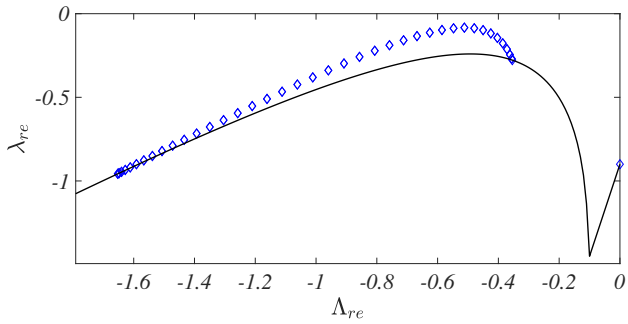

Figure 4.12: Dispersion relation for ϵ selected randomly, for each couple of nodes, from a Gaussian distribution with mean $\bar{\epsilon} = 0.01$ and variance $\eta_{\bar{\epsilon}} = 10^{-4}$. Here the chain is assumed to be $\Omega = 80$ node long.

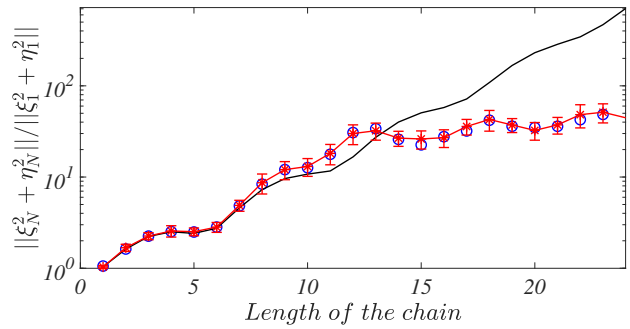

Figure 4.13: The ratio between the norm of the fluctuations on the last and first nodes of the chain is plotted against the length of the chain. The solid line refers to the norm as predicted. The symbols stand for the homologous quantities as computed via direct stochastic simulations. Blue diamonds refer to fixed weights $\epsilon = 0.01$, red squares to random weights (averaging over 25 realizations) chosen from a Gaussian distribution centered in $\bar{\epsilon} = 0.01$, with variance $\eta_{\bar{\epsilon}} = 10^{-4}$. The parameters are the same as those in Fig. 4.10.

eigenvalues, one in zero and the other localized in -1. We then add a third node to the collection. We select at random a node, from the pool of existing ones, and identify it as target of a link that originates from the newly added node. The strength of the link is chosen randomly from a Gaussian

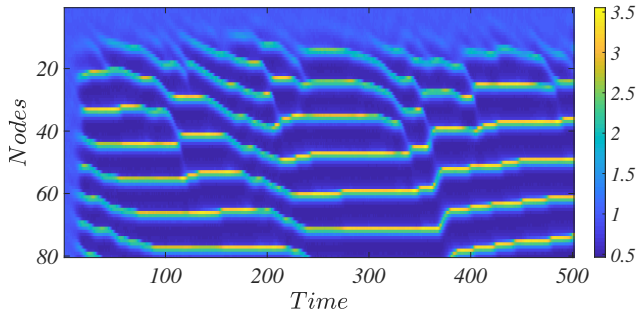

Figure 4.14: The time evolution of species ϕ is displayed with an appropriate color code, on different nodes of the chain and against time. Here we assume the weights ϵ to be random entries chosen from a Gaussian distribution centered in $\bar{\epsilon} = 0.01$ with variance $\eta_{\bar{\epsilon}} = 10^{-4}$. The parameters are the same as those in Fig. 4.10.

distribution with given mean and standard deviation. We then compute the spectrum of the obtained network and accept the move if the new eigenvalue falls sufficiently close to -1, or reject it otherwise. The procedure is iterated for a maximum number of times which scales extensively with the size of the network. Once the third node is aggregated to the initial pair, we move forward to adding the fourth node according to an identical strategy that we iterate forward. One exemplary of networks generated according to this procedure is displayed in Fig. 4.15. This is the skeleton of a distorted one-dimensional directed chain, short segments being added on the lateral sides, and fall in the class of the so called random directed acyclic graphs. The Brussellator model evolved on this network (see Fig. 4.16) returns noise triggered patterns which share similar features with those obtained earlier. In principle, one could devise more complicated networks, that would return a patchy distribution of eigenvalues, engineered to densely populate distinct regions of the complex plane. This extension is left for future work.

4.3 Conclusion

To investigate the stability of an equilibrium solution of a given dynamical system, it is customary to perform a linear stability analysis which aims

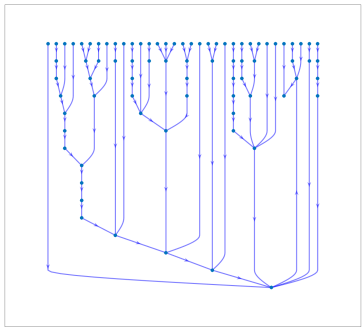

Figure 4.15: Example of network generated with the procedure described in the text made of $\Omega = 80$ nodes. The Brusselator reaction scheme is assumed with the parameter choice of blue square in Fig. 4.2.

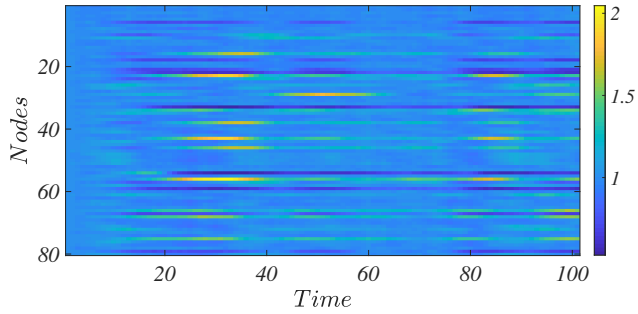

Figure 4.16: The time evolution of species ϕ is displayed with an appropriate color code, on different nodes of the network of Fig. 4.15 and against time.

at characterizing the asymptotic evolution of an imposed perturbation. In doing so, one obtains a Jacobian matrix, evaluated at the fixed point of interest, whose eigenvalues bear information on the stability of the system. If the eigenvalues of the Jacobian matrix display negative real parts, the system is resilient, meaning that it will eventually regain the equilibrium condition, by exponentially damping the initial perturbation. Non-normal reactive components may however yield a short time amplification of the disturbance, before the crossover to the exponential regime that drives the deterministic system back to its stable equilibrium. Particularly interesting is the interplay between noise, assumed as a stochastic perpetual forcing, and the inherent non-normality, as stemming from the existing interactions. Patterns have been for instance reported to occur for spatially extended stochastic models, with a pronounced degree of non-normal reactivity and outside the region of deterministic instability. Building on these premises, we have here taken one step forward towards the interesting setting where the degree of inherent non-normality is magnified by the embedding spatial support. Indeed, by replicating a two-species model on diffusively coupled patches of a directed lattice, we enhanced the ability of the system to grow perturbation at short time. This effect is the byproduct of the degeneracy in the spectrum of the Jacobian matrix associated to the examined system, and which ultimately reflects the architecture of couplings between adjacent units. A non trivial amplification of the noise across the lattice is observed and explained, which materializes in self-organized patterns, that are instead lacking in the deterministic analogue of the analyzed model. Our conclusions are then extended to a quasi-degenerate support: the ingredient that we have identified as crucial for the onset of the amplification is the presence of a compact region in the complex plane where the eigenvalues of the Laplacian operators accumulate. Beyond a critical size of the system, expressed in terms of number of nodes that define the support, the system may lose its deterministic resilience. In fact, it can eventually migrate towards another attractor that is stably maintained, also when the noise forcing is turned off. Taken all together, our investigations point out the importance of properly accounting for the unavoidable sources of stochasticity when gauging the resilience of a system: non normality and quasi-degenerate networks might alter dramatically the deterministic prediction turning unstable a system that would be presumed otherwise stable under a conventional deterministic perspective. Furthermore, our findings bear a remarkable similarity with the

phenomenon of convective instability, [59,103,117,118], a possible connection that we aim at investigating in a future contribution. In perspective, it would be also interesting to build an ideal bridge with the analysis reported in [65,166] where complex patterns of synchrony have been observed in feed-forward networks with degenerate architectures.

Chapter 5

Generating directed networks with prescribed Laplacian spectra

In Chapter 4 we introduced the concept of resilience, the ability of a given system to oppose to external perturbations. Moreover, we elaborated on the relation between resilience and stability for a class of networked systems.

As we have previously seen in Section 2.2, for reaction-diffusion systems defined on networks, the stability of the inspected equilibrium is ultimately dictated by the spectrum of the discrete Laplacian matrix [1, 146, 179]. The eigenvalues of the Laplacian define in fact the support of the dispersion relation, the curve that sets the rate for the exponential growth of the imposed perturbation. More specifically, external disturbances can, in general, be decomposed on the basis formed by the eigenvectors of the Laplacian operator. Each eigenvector defines an independent mode, which senses the web of intricate paths made accessible across the network: the perturbation can eventually develop, or, alternatively, fade away, along the selected direction, depending on the corresponding entry of the dispersion relation, as fixed by its associated eigenvalues.

Based on the above, it is hence essential to devise suitably tailored recipes for generating networks, which display a prescribed Laplacian spectrum, compatible with the stability constraint [41–43]. As a representative example, synchronization, a widespread phenomenon in distributed systems, can be enforced by properly adjusting the spectrum of the matrix which

encodes for intertwined pairings. Examples of control of Laplacian spectra are present in the literature. In [41], a method is presented to enforce stabilization for a spatially extended multispecies model, through the redefinition of the inter-node couplings. In [42], an ad hoc rewiring of the couplings is studied to stabilize an ecosystem, acting on the spectrum of the Jacobian matrix which governs the stability of the system. Our work represents a step forward in this direction.

The problem of recovering a network from a set of assigned eigenvalues has been tackled in the literature, both from an algorithmic [54,102,155] and formal [90, 128] standpoints. In [90], a procedure is discussed to generate an undirected and weighted graph from its spectrum. The result extends beyond the well-known theorem of Botti and Merris [37] which states that the reconstruction of non-weighted graphs is, in general, impossible since almost all (non-weighted) trees share their spectrum with another non-isomorphic tree. In [131], a method is proposed to obtain a, directed or undirected, graph whose eigenvalues are constrained to match specific bounds, which ultimately reflect the node degrees, as well as the associated weights. In [74], a mathematically rigorous strategy is instead developed to yield weighted graphs which *exactly* realize any desired spectrum. As discussed in [74], the method translates into an efficient approach to control the dynamics of various archetypal physical systems via suitably designed Laplacian spectra. The results are however limited to undirected Laplacians, characterized by a real spectrum.

The purpose of this chapter is to expand beyond these lines, by proposing and testing a procedure which enables one to recover a signed Laplacian operator which displays a prescribed complex spectrum. Signed Laplacians are often used in the literature for applications which relate to social contagion, cluster synchronization or repulsive-attractive interactions [7,39]. In engineering, they are often employed in modeling microgrid dynamics [45].

The chapter is organized as follows. Section 5.1 is devoted to illustrating the devised method, focusing on the mathematical aspects. We then turn to discussing the implementation of the scheme and elaborate on the sparsification algorithms that are run to cut unessential links. In Section 5.3.1, we elaborate on the conditions that are to be met to generate a positively weigthed network. This discussion is carried out with reference to a specific

setting. Then, we apply the newly introduced technique to the study of an ensemble made up of coupled Stuart-Landau oscillators [11, 79, 181] and to (a simplified version of) the Kuramoto model [110, 172].

5.1 A recipe to obtain a Laplacian with assigned complex eigenvalues

Consider a network consisting of Ω nodes and label with A the (weighted) adjacency matrix, were structural information is encoded. More precisely, the element A_{ij} is different from zero provided a directed link exists which goes from j to i. The entries of the matrix A are real numbers and their signs reflect the specificity of the interaction at play: negative signs stand for inhibitory (or antagonistic) couplings, while positive entries point to excitatory (or cooperative) interaction. From the adjacency matrix, one can define its associated Laplacian operator. This is the matrix L, whose elements read $L_{ij} = A_{ij} - k_i\delta_{ij}$, where $k_i = \sum_j A_{ij}$ represents the natural extension of the concept of (incoming) connectivity to the case of a weighted network.

We shall here discuss a procedure to generate a Laplacian matrix, which displays a prescribed set of eigenvalues. As anticipated above, we will focus in particular on directed Laplacians, which yield, in general, complex spectra. Concretely, we begin by introducing a collection of $\Omega = 2N + 1$ complex quantities defined as: [1]

$$\{\Lambda_i\} = \{\Lambda_1, \Lambda_2, \ldots, \Lambda_{2N}, \Lambda_{2N+1} = 0\} \tag{5.1}$$

The first $2N$ elements come in complex conjugate pairs and we set in particular $\Lambda_i = \Lambda^*_{i+N}$, $\forall\ i = 1, ..., N$, where $(\cdot)^*$ stands for the complex conjugate operation. The aim of this section is to develop a rigorous procedure to construct a directed (and weighted) graph G with $2N + 1$ vertices, whose associated Laplacian has $\{\Lambda_i\}$ for eigenvalues. Remark that $\{\Lambda_i\}$ contains the null element since this latter is, by definition, a Laplacian's eigenvalue.

The procedure that we are going to detail in what follows exploits the eigenvalue decomposition of the Laplacian matrix. To this end, we will seek

[1] We shall assume all the eigenvalues but 0 to be complex numbers. Let us remark that the method here developed straightforwardly generalizes to the case where also real eigenvalues are present. It is in fact sufficient to set to zero the imaginary components of a sub-portion of the selected eigenvalues.

to introduce a proper eigenvector basis such that

$$L = VDV^{-1} \tag{5.2}$$

is a Laplacian. In (5.2), D is a diagonal matrix where the sought Laplacian eigenvalues are stored. More specifically, $D_{ii} = \Lambda_{i-1}$ for $i = 2, .., 2N + 1$ and $D_{11} = \Lambda_{2N+1} = 0$. The problem is hence traced back to constructing V, whose columns are the right eigenvectors of L. We also recall that rows of the inverse matrix V^{-1} are the left eigenvectors of L. As outlined in [41], Laplacian (right and left) eigenvectors should satisfy a set of conditions. The columns of V which refer to complex conjugate eigenvalues, must be complex conjugate too. The same condition holds for the rows of V^{-1}. Moreover, the columns of V (resp. the rows of V^{-1}) corresponding to eigenvalues different from 0 should sum up to zero. Finally, the right eigenvector relative to the null eigenvalue ought to be uniform. In light of the above, we put forward for V the following structure:

$$V = \begin{pmatrix} c & v^T & v^{T*} \\ cu & iU & -iU \\ cu & U & U \end{pmatrix} \tag{5.3}$$

where c is an arbitrary constant, i stands for the imaginary unit, U is an $N \times N$ invertible matrix having real entries. Further, vector $u = (1 \dots 1)^T$ has dimension $N \times 1$ and vector v is defined as

$$v = -(1 + i)u^T U. \tag{5.4}$$

The first column of V is hence a uniform vector, candidate to be the eigenvector corresponding to the null eigenvalue. By construction, every other column sums up to zero, that is Eq. (5.4). In the following we will set $D_{jj} = \alpha_j + i\beta_j$, which in turn implies $D_{j+N,j+N} = \alpha_j - i\beta_j$, for $j = 2, \dots, N + 1$. Here, α_j and β_j are real quantities and respectively denote the real and imaginary parts of the j-th eigenvalue. To proceed further, one needs to determine the inverse of V.

To achieve this goal we begin by considering a generic matrix W, which satisfies the general constraints that are in place for V^{-1}. In formulae:

$$W = \begin{pmatrix} d & du^T & du^T \\ (1 - i)w & S & -iS^* \\ (1 + i)w^* & S^* & iS \end{pmatrix} \tag{5.5}$$

where

$$w = -\frac{1}{1-i}(Su - iS^*u) \tag{5.6}$$

Note that the jth and $(N+j)$th rows of W, for $j = 1, .., N+1$, are complex conjugated, as requested. Moreover, summing all the elements of each row (but the first) yields zero, a condition that the inverse of V should meet, as anticipated above. Building on these premises, we shall here determine the unknown S, w and d so as to match the identity $WV = I$, where I stands for the $(2N+1) \times (2N+1)$ identity matrix. This implies in turn that $W \equiv V^{-1}$ due to the uniqueness of the inverse matrix.

A straightforward manipulation yields the following conditions for respectively d and w

$$\begin{cases} d = \frac{1}{c(2N+1)} \\ wv^T = i(S - iS^*)EU \\ wv^{T^*} = (S - iS^*)EU \end{cases} \tag{5.7}$$

where use has been made of the identity $u^T u = N$ and where

$$E = uu^T = \begin{pmatrix} 1 & \dots & 1 \\ \vdots & \ddots & \vdots \\ 1 & \dots & 1 \end{pmatrix} \tag{5.8}$$

The quantity d is completely specified by the first of Eqs. (5.7) and solely depends on c and N, the size of the system. By making use of the identities (5.4) and (5.6), one can progress in the analysis of the second and third conditions (5.7) to eventually get:

$$SB + S^*A = I \tag{5.9}$$

$$SA - S^*B = 0 \tag{5.10}$$

where:

$$A = EU - iEU - iU \tag{5.11}$$

$$B = iEU + EU + iU \tag{5.12}$$

It is therefore immediate to conclude

$$S = (B + AB^{-1}A)^{-1} \tag{5.13}$$

$$S^* = (B + AB^{-1}A)^{-1}AB^{-1} \tag{5.14}$$

The analysis can be pushed further to eventually relate S to matrices U and E. The calculation, detailed in the annexed Appendix, yields

$$S = -\frac{i}{2}U^{-1}\left[I - \frac{1+i}{1+2N}E\right] \tag{5.15}$$

The expression for S^* can be immediately obtained by taking the complex conjugate of the above equation. In conclusion, the matrix W defined in (5.5) is the inverse matrix of V, provided d and S are respectively assigned as specified above.

Eventually, matrix L defined in (5.2) has the desired spectrum (5.1). We should however prove that L is a Laplacian. This amounts to show that L is a real matrix, whose columns sum up to zero. The proof is given in the following

Proposition: From (5.3) and (5.5), one can readily compute the elements of L via matrix products and taking advantage of the block structures of V and W, to prove that L is real. Notation-wise, $\mathrm{Re}(\cdot)$ is introduced to represent the real part of $(\cdot)$. The results of the calculation are reported below. The generic element L_{st} can be written as

$$L_{st} = (VDW)_{st} = \sum_{k=1}^{2N+1} V_{sk}(DW)_{kt} = \sum_{k=1}^{2N+1} V_{sk} \sum_{k'=1}^{2N+1} D_{kk'}W_{k't} \tag{5.16}$$

$$= \sum_{k=2}^{2N+1} V_{sk}D_{kk}W_{kt} \tag{5.17}$$

due to the diagonal structure of the matrix D, by recalling that $D_{11} = 0$. By making use of the specific form of V and W, one gets:

$$L_{st} = \sum_{k=2}^{N+1} V_{sk}D_{kk}W_{kt} + \sum_{k=N+2}^{2N+1} V_{sk}D_{kk}W_{kt} \tag{5.18}$$

$$= \sum_{k=2}^{N+1} V_{sk}D_{kk}W_{kt} + \sum_{k=2}^{N+1} (V_{sk}D_{kk}W_{kt})^* \tag{5.19}$$

$$= \sum_{k=2}^{N+1} 2\,\mathrm{Re}(V_{sk}D_{kk}W_{kt}) \tag{5.20}$$

since $\alpha\beta + \alpha^*\beta^* = 2\,\mathrm{Re}(\alpha\beta)$, for any complex numbers α and β. One can thus conclude that L, as generated by the above procedure, is real.

Proposition: Each column of L sums up to zero. Because of the diagonal structure of D:

$$\sum_i L_{ij} = \sum_{il} V_{il} D_{ll} V_{lj}^{-1} \tag{5.21}$$

Then:

$$\sum_i L_{ij} = \sum_l V_{lj}^{-1} D_{ll} \sum_i V_{il} = 0 \tag{5.22}$$

since (i) $D_{11} = 0$ and (ii) every eigenvector corresponding to eigenvalues different from 0, sums up to zero. Notice that this result can also be proven, by observing that the uniform vector $d\mathbf{1}$ is the left eigenvector corresponding to 0, that is

$$d\mathbf{1}L = 0 \tag{5.23}$$

From (5.23), it follows that $\sum_i L_{ij} = 0$, for every j.

Proposition: L is balanced. We can also show that $\sum_j L_{ij} = 0$ i.e. that the sum of all the elements of any given row i returns zero. According to (5.2), the first column of V is the right eigenvector corresponding to eigenvalue 0, namely

$$Lc\mathbf{1} = cL\mathbf{1} = 0 \tag{5.24}$$

This implies in turn $\sum_j L_{ij} = 0 \; \forall i$, which ends the proof. The Laplacian is hence balanced, as performing the sum on the rows and on the (corresponding) columns returns the same result.

From the generated Laplacian operator, one can readily calculate the adjacency matrix of the underlying network. In general, for any assigned spectrum, the recovered adjacency matrix is fully connected, meaning that links exist which connect every pair of nodes within the collection. Links are weighted and signed. The weights can be small or have a modest impact on the spectrum of the associated Laplacian. This motivates one to implementing a dedicated sparsification procedure, which seeks to remove unessential links, in terms of their reflection on the ensuing Laplacian spectrum. The next section is devoted to elaborating along these lines.

5.2 Results and discussion

5.2.1 Examples and sparsification

In this section we discuss a sparsification procedure, which aims at a posteriori simplifying the structure of the recovered network. To this end we begin by generating a network following the strategy outlined in the preceding section, and which yields an assigned spectrum for the associated Laplacian. The Laplacian spectrum that we seek to recover is made of $\Omega = 2N + 1$ complex entries, the eigenvalues, which we here confine in the left portion of the complex plane, by setting $\mathrm{Re}(\Lambda_j) = \alpha_j < 0$ for $j \geq 2$, see blue crosses in Fig. 5.1 (a). This choice is somehow arbitrary, and ultimately amounts to forcing stable a linear system of the type:

$$\frac{dx_i}{dt} = \sum_j L_{ij} x_j \tag{5.25}$$

where x_i is the i-th entry of the Ω-dimensional state vector x. In the final part of the paper we will turn to considering more complex scenarios where the stability of the examined dynamics is also influenced by local reaction terms being at play.

The network that we obtain, following the scheme outlined in the preceding Sections and which yields a Laplacian with the prescribed spectrum, is in general fully connected. In other words, a weighted link exists between each couple of nodes. The weights of the link can be in principle very small and, as such, bear a modest imprint on the ensuing Laplacian spectrum. Motivated by this observation, we perform an a posteriori sparsification of the obtained network: this is targeted to identifying and then removing, the finite subset of links that appear to have a modest impact on the eigenvalues of the associated Laplacian.

The first sparsification procedure that we have considered, aims at removing unessential links while confining the spectrum of the Laplacian operator within a bounded region of the complex plane. More precisely, we focus on the links which display a weight in the range (-σ, σ), where σ is a small, arbitrarily chosen, cut off. All links whose weight is smaller than σ in absolute value, are selected, in a random order. The selected link is removed and the modified Laplacian spectrum computed. Label $\tilde{\Lambda}_j$, for $j = 2, ..., 2N + 1$, the Laplacian eigenvalues obtained upon removal of the link. The change to the network arrangement becomes per-

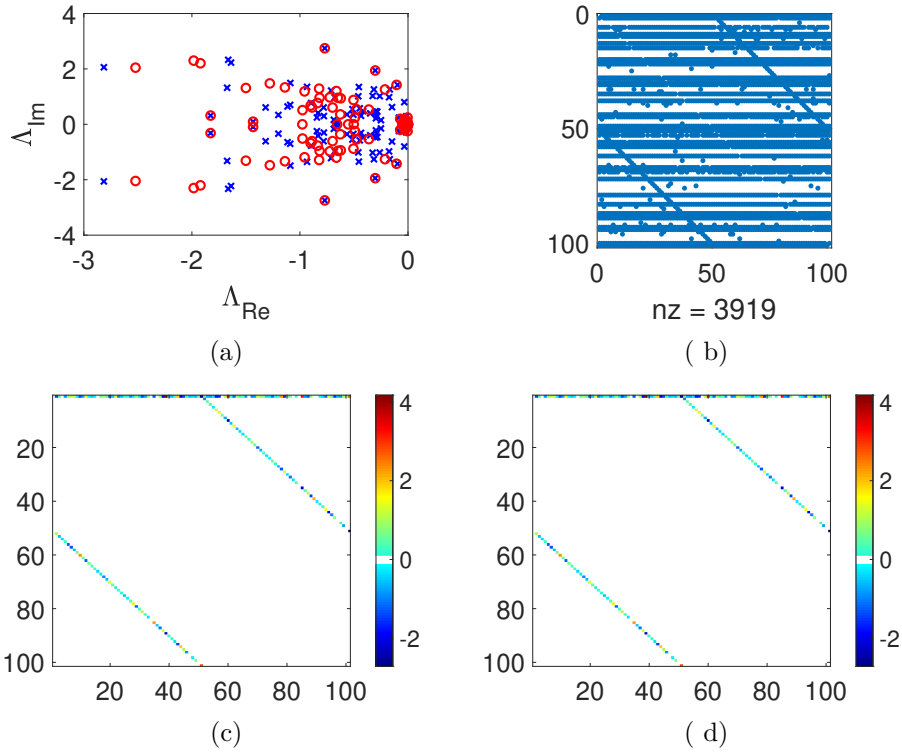

Figure 5.1: *The recipe discussed in the main text is applied to generate a network of* $\Omega = 2N + 1 = 101$ *nodes, whose associated Laplacian displays the spectrum depicted (blue stars) in panel (a). The spectrum of the Laplacian obtained from the sparsified network is shown with red circles. We here follow the first sparsification recipe as illustrated in the main body of the paper. More specifically, we trim unessential links, chosen among those that bear very modest weights, while confining the Laplacian spectrum in a bounded domain, located in the negative portion of the complex plane. Here,* σ *is* 0.01 *and* $\delta = 0.5$*. In panel (b), the sparsity pattern of the adjacency matrix obtained upon application of the sparsification algorithm is shown. The entries of the adjacency matrices, before and after the sparsification are respectively plotted, with an apt color-code, in panels (c) and (d). The main structure of the network is preserved upon application of the devised sparsification protocol.*

manent, if $|min_j \left[\mathrm{Re}(\tilde{\Lambda}_j)\right] - min_j \left[\mathrm{Re}(\Lambda_j)\right]| < \delta$ and $|max_j \left[\mathrm{Im}(\tilde{\Lambda}_j)\right] - max_j \left[\mathrm{Im}(\Lambda_j)\right]| < \delta$, for $j = 2, ..., N$. Here $\mathrm{Im}(\cdot)$ stands for the imaginary part of $(\cdot)$ and δ is an arbitrary threshold which quantifies the amount of perturbation that is deemed acceptable for the problem at hand. As a further condition, we check that $\mathrm{Re}(\tilde{\Lambda}_j) < 0$ for $j = 2, ..., 2N+1$, which in turn corresponds to preserving the stability of the linear system (5.25). Clearly, the order of extraction of the links which are candidate to be trimmed matters. Different realizations of the procedure of progressive sparsification illustrated above might hence result in distinct final outcomes. In Fig. 5.1(a), the eigenvalues obtained after the sparsification algorithm are plotted (red circles) for two choices of the cutoff δ. The sparsity pattern of the adjacency matrix obtained at the end of the above procedure is displayed in panel (b) of Fig. 5.1. In panels (c) and (d) of Fig. 5.1 we plot, with an appropriate color code, the entries of the adjacency matrices, before and after the sparsification. Only weights which are significantly different from zero (see annexed colorbars) are displayed. As appreciated by visual inspection, the skeleton of the network is not altered by the applied sparsification. To monitor how the eigenvalues get redistributed within the bounded domain to which they belong, we introduce the following indicators:

$$I_x = \sum_{i=2}^{2N+1} (\beta_i)^2 \tag{5.26}$$

$$I_y = \sum_{i=2}^{2N+1} \left(\alpha_i - \frac{1}{2N+1} \sum_{j}^{2N+1} \alpha_j \right)^2 \tag{5.27}$$

The quantity I_x measures the dispersion along the imaginary axis, by weighting the squared distance of each eigenvalue from the horizontal axis. Conversely, I_y reflects the scattering of the eigenvalues about their mean, in the direction of the real axis. In Fig. 5.2, I_x and I_y, normalized to their respective values obtained before application of the sparsification algorithm, are shown against N, an indicator of the size of the generated networks. The sparsification procedure shrinks the eigenvalues in the x-direction, while the opposite tendency is observed for the distribution along the y-direction.

The second sparsification method implements a more stringent constraint. Just like before, we select the links with weights in the range (-σ, σ), where σ acts as a small threshold amount. At variance with the former case, we now eliminate the selected link only if the change produced on the norm of

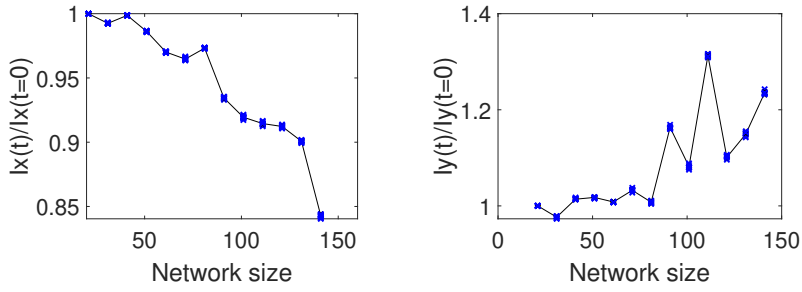

(a) (b)

Figure 5.2: *Panel (a): I_x as measured at the end of the sparsification and normalized to the corresponding value, before the sparsification is plotted against N, the size of the explored network. Panel (b): I_y, calculated after the sparsification and normalized to the corresponding value, before the sparsification is depicted versus N. In both cases, blue symbols are computed, as the average over* 15 *different realizations of the generated network (with the same given spectrum). For each value of N, the real and imaginary components of the eigenvalues are random number, drawn from a normal distribution. The solid line is a guide for the eye. Here, $\delta = 0.5$ and $\sigma = 0.01$.*

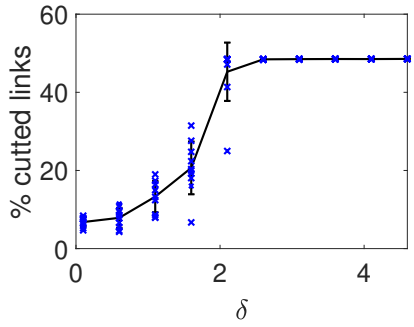

Figure 5.3: *The percentage of links that are cut against the imposed perturbation δ. Blue symbols refer to* 10 *indendent realizations, for each value of δ. The black line goes through the average values, computed from the collection of independent runs, at fixed δ. Here, $N = 50$ ($\Omega = 2N + 1 = 101$) and $\sigma = 0.01$.*

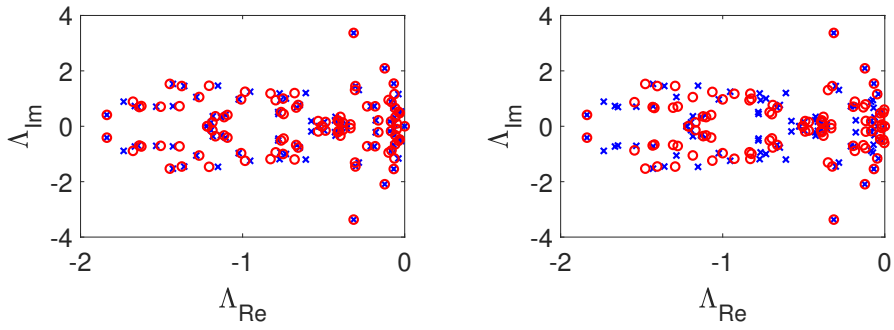

(a) (b)

Figure 5.4: *Effect of the second method of sparsification on a network made of* $\Omega = 2N + 1 = 101$ *nodes. The original spectrum is plotted with (blue) stars. The modified one with (red) circles. Panel (a) refers to* $\delta = 0.5$ *while panel (b) to* $\delta = 1$*. Here,* $\sigma = 0.01$*.*

each of the N eigenvalues is smaller than δ, namely if $|\Lambda_j - \tilde{\Lambda}_j| < \delta$, for $j = 2, ..., 2N + 1$. In Fig. 5.4, the eigenvalues obtained after the sparsification algorithm are plotted (red circles) for two choices of the cutoff δ. The number of links that can be effectively removed grows with δ, the size of the allowed perturbation, as clearly demonstrated in Fig. 5.3.

As mentioned above, this latter method implements a local, hence stringent, constraint. By allowing modest re-arrangements of individual eigenvalues yields a spectral distribution in the complex plane which is by construction close to the original one. This method is better suited when the room for maneuver is limited, due to the specific constraint that the reactive model implements. On the other hand, the number of pruned links can be scanty, when small local perturbations are solely allowed for. A global re-organization of the operator's spectrum, which entails a significant reduction in the associated number of active links, might be instead accomplished when the eigenvalues are constrained to fall within a compact domain in the complex plane, as follows the former sparsification procedure.

Summing up, we have developed and tested a procedure to generate a network which returns an associated Laplacian matrix with a prescribed complex spectrum. The weighted network obtained following the above pro-

cedure is in general fully connected. Dedicated sparsification strategies can be applied to remove the links which carry a small weight, and bear a modest imprint in the ensuing Laplacian spectrum. In the following, we will consider a specific setting of the aforementioned generation scheme, which makes it possible for the Laplacian elements to be accessed analytically.

5.3 Focusing on the special case $U = qI$

In the previous sections, we described a general method to generate a Laplacian matrix which displays a designated spectrum. The method assumes a generic matrix U, which can be randomly assigned. In the following, we will focus on the specific case where U is proportional to the identity matrix and progress with the analytic characterization of the obtained Laplacian. As we shall argue in the following, working in this framework allows us to derive a set of closed conditions for constraining the weights of the underlying network to strictly positive values. To proceed in this direction we set:

$$U = qI \tag{5.28}$$

where I stands for the identity matrix and q is a scalar quantity.

A straightforward calculation returns the following expression for matrix S:

$$S = \begin{pmatrix} a+ib & a-ia & \dots & a-ia \\ a-ia & a+ib & \ddots & a-ia \\ \dots & \ddots & \ddots & \vdots \\ a-ia & \ddots & \ddots & a+ib \end{pmatrix} \tag{5.29}$$

while w is a uniform vector with identical entries equal to $Na+((N-1)a-b)i$ and the quantities d, a, b are specified by

$$d = \frac{1}{(2N+1)c} \tag{5.30}$$

$$a = \frac{-1}{2(2N+1)q} \tag{5.31}$$

$$b = 2Na \tag{5.32}$$

The equations (5.16), (5.18) open up the possibility to obtain a closed expression for each element of the Laplacian matrix, as function of the eigenvalues entries. The interested reader can find the detailed computations in

Appendix A.2; we thus limit ourselves to hereby report the final formulas. The diagonal elements satisfy:

$$L_{11} = \frac{2}{2N+1}\sum_{k=2}^{N+1}\alpha_k \tag{5.33}$$

$$L_{ss} = \frac{2N\alpha_s+\beta_s}{2N+1} \quad s=2,\dots,N+1 \tag{5.34}$$

$$L_{ss} = \frac{2N\alpha_s-\beta_s}{2N+1} \quad s=N+2,\dots,2N+1\,, \tag{5.35}$$

where use has been made of the identity $\mathrm{Re}(D_{kk})=\alpha_k$. The first row and column are given by:

$$L_{t1} = \frac{-\alpha_t+\beta_t}{2N+1} \quad t=2,\dots,N+1 \tag{5.36}$$

$$L_{t1} = \frac{-\alpha_t-\beta_t}{2N+1} \quad t=N+2,\dots,2N+1 \tag{5.37}$$

$$L_{1t} = \frac{1-2N}{1+2N}\alpha_t-\beta_t+\frac{2}{2N+1}\sum_{k=2,k\neq t}^{N+1}\alpha_k \quad t=2,\dots,N+1 \tag{5.38}$$

$$L_{1t} = \frac{1-2N}{1+2N}\alpha_t+\beta_t+\frac{2}{2N+1}\sum_{k=2,k\neq t-N}^{N+1}\alpha_k \quad t=N+2,\dots,2N+1 \tag{5.39}$$

while the remaining elements are obtained as:

$$L_{st} = \frac{-\alpha_s+\beta_s}{2N+1} \quad s=2,\dots,N+1 \text{ and } t=N+2,\dots,2N+1 \text{ with } t\neq s-N \tag{5.40}$$

$$L_{st} = \frac{-\alpha_s-\beta_s}{2N+1} \quad s=N+2,\dots,2N+1 \text{ and } t=2,\dots,N+2 \text{ with } t\neq s-N \tag{5.41}$$

$$L_{s,s+N} = \frac{-\alpha_s - 2N\beta_s}{2N+1} \quad s = 2, \ldots, N+1 \tag{5.42}$$

$$L_{s,s-N} = \frac{-\alpha_s + 2N\beta_s}{2N+1} \quad s = N+2, \ldots, 2N+1 \tag{5.43}$$

$$L_{st} = \frac{-\alpha_s + \beta_s}{2N+1} t, s = 2, \ldots, N+1 \text{ and } s \neq t \tag{5.44}$$

$$L_{st} = \frac{-\alpha_s - \beta_s}{2N+1} s, t = N+2, \ldots, 2N+1 \text{ and } s \neq t. \tag{5.45}$$

5.3.1 Controlling the sign of non-diagonal Laplacian entries

The Laplacian matrix that one obtains with the procedure illustrated above has both positive and negative entries. Signed Laplacian are often used in consensus problems, where negative weights model antagonistic interactions. In other contexts, when e.g. the Laplacian are stemming from diffusive interactions, non diagonal entries are constrained to positive values. In the following, we will provide a set of necessary conditions for the assigned spectrum to eventually yield a Laplacian with positive extra diagonal elements, $L_{ij} > 0$ for $i \neq j$. Clearly, $L_{ii} < 0$, as summing on the rows should return zero. The underlying network displays hence positive weights, as its adjacency matrix is basically found from the Laplacian matrix by replacing the diagonal elements with zeros.

Further, we will set $\mathrm{Re}(\Lambda_j) = \alpha_j < 0$ for $j \geq 2$, an assumption which, we recall, corresponds to dealing with a stable linear system of the type given in ((5.25)). This request immediately yields $L_{11} < 0$, as it follows from relation (A.9). We will also operate in the setting analyzed above, i.e. assuming $U = I$. The obtained expressions for the Laplacian elements allow to recast the sought conditions on their signs as:

$$\begin{cases} 2N\alpha_t < \beta_t < -2N\alpha_t \\ \beta_t > -\frac{1-2N}{2N+1}\alpha_t - \frac{2}{2N+1}\sum_{k=2,k\neq t}^{N+1}\alpha_k \\ \beta_t < \frac{1-2N}{2N+1}\alpha_t + \frac{2}{2N+1}\sum_{k=2,k\neq t}^{N+1}\alpha_k \\ \alpha_t < \beta_t < -\alpha_t \\ \frac{\alpha_t}{2N} < \beta_t < -\frac{\alpha_t}{2N} \end{cases} \tag{5.46}$$

where the inequalities hold for $t = 2, \ldots, N+1$.

The above conditions can be simplified using some algebraic manipula-

tions to return

$$\frac{4N}{4N^2-1}\sum_k \alpha_k < \alpha_t < \frac{2}{2N+1}\sum_k \alpha_k \tag{5.47}$$

and

$$\alpha_t - \frac{2}{2N+1}\sum_k \alpha_k < \beta_t < -\alpha_t + \frac{2}{2N+1}\sum_k \alpha_k\,. \tag{5.48}$$

The interested reader can access the detailed steps in Appendix A.3.

Assume that the assigned Laplacian spectrum matches the above conditions, while having $\alpha_k < 0$ for $k > 2$. Then the Laplacian matrix that we obtain following the procedure outlined above, with $U = I$, displays positive non diagonal entries.

Let us explore the consequences of conditions (A.75) and (A.76). To this end, introduce $\bar{\alpha}$, the average of the non-negative real parts of the Laplacian eigenvalues. In formulae, $\bar{\alpha} = (\sum_k \alpha_k)/(2N)$. A straightforward analysis allows us to conclude that the generated Laplacian returns positive non-diagonal elements, if the assigned non trivial eigenvalues (i.e. Λ_k, with $k > 1$) fall in a bounded rectangular domain of the complex plane. More specifically, the rectangular region is symmetric, with respect to the horizontal (real) axis, and extends along the vertical direction (imaginary axis) of $\pm 2N\bar{\alpha}/(4N^2-1)$. The rectangle is completed by two vertical sides, positioned at $\frac{4N^2}{4N^2-1}\bar{\alpha}$ and $\frac{2N}{2N+1}\bar{\alpha}$. Working at fixed N, the larger $|\bar{\alpha}|$ the more extended the rectangle along the vertical direction. Conversely, when making N larger, the rectangle shrinks in the horizontal direction and becomes eventually degenerate for $N \to \infty$. In other words, for large values of N, eigenvalues should align on a vertical segment positioned at $\bar{\alpha}$, and whose extension increases linearly with $|\bar{\alpha}|$ (while decreasing with N). This is shown in Fig. 5.5, where three different spectra are depicted (for different choices of $\bar{\alpha}$) which yield a Laplacian with positive off diagonal elements.

In the following section we will apply the method of Laplacian generation here discussed to the study of two prototypical examples of dynamical systems on networks.

5.4 Selected applications

In this section we consider two different models of interacting oscillators, defined on a network. In both cases, the coupling between individual oscillators

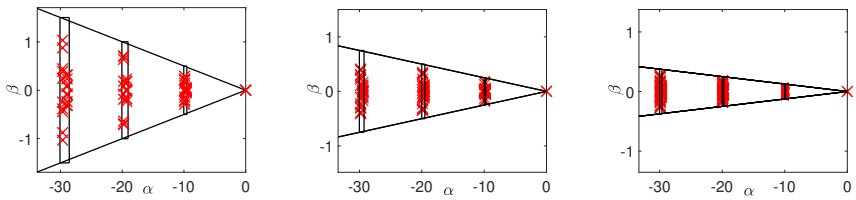

(a) (b) (c)

Figure 5.5: *Examples of discrete spectra (red symbols) which yield a Laplacian with positive non diagonal entries. The rectangular boxes identify the region where eigenvalue should fall for the ensuing network to display positive weights and are traced according to the conditions derived in the main body of the paper. Here,* $\Omega = 2N + 1 = 21$ *(a),* $\Omega = 2N + 1 = 41$ *(b) and* $\Omega = 2N + 1 = 81$ *(c).*

is implemented via a discrete Laplacian operator, which reflects the specific network arrangement. We will show that a suitable network arrangement can be a priori established, building on the procedure illustrated above, so as to make the inspected systems stable against external perturbations.

5.4.1 Coupled Stuart-Landau oscillators

Consider an ensemble made of $2N + 1$ nonlinear oscillators and label with W_i their associated complex amplitude. We assume the oscillators to be mutually coupled via a diffusive-like interaction which is mathematically exemplified via a discrete Laplacian operator. Each oscillator obeys a complex Ginzburg-Landau equation. The dynamics of the system can be cast in the form:

$$\frac{d}{dt}W_j = W_j - (1 + ic_2)|W_j|^2 W_j + (1 + ic_1)K \sum_k L_{jk} W_k \tag{5.49}$$

where c_1 and c_2 are real parameters. The index j runs from 1 to $2N + 1$, the total number of oscillators. Here, K is a suitable parameter setting the coupling strength. Without loss of generality, in what follows we suppose $K = 1$; $L_{ij} = A_{ij} - k_i\delta_{ij}$ is the Laplacian, A_{ij} a directed and weighted adjacency matrix and $k_i = \sum_j A_{ij}$.

The system admits a homogeneous limit cycle solution in the form $W_{LC}(t) = e^{-ic_2 t}$. To characterize the stability of the cycle, one can introduce a non

homogeneous perturbation in polar coordinates as:

$$W_i(t) = W_{LC}[1 + \rho_i(t)]e^{i\theta_i(t)} \tag{5.50}$$

By linearizing around the limit cycle solution ($\rho_i(t) = 0$, $\theta_i(t) = 0$), one gets:

$$\frac{d}{dt}\begin{pmatrix}\rho_j \\ \theta_j\end{pmatrix} = \begin{pmatrix}-2 & 0 \\ -2c_2 & 0\end{pmatrix}\begin{pmatrix}\rho_j \\ \theta_j\end{pmatrix} + \begin{pmatrix}1 & -c_1 \\ c_1 & 1\end{pmatrix}\sum_k \Delta_{jk}\begin{pmatrix}\rho_k \\ \theta_k\end{pmatrix} \tag{5.51}$$

To proceed further one expands the perturbations ρ_j and θ_j on the Laplacian eigenvectors basis, that is

$$\begin{pmatrix}\rho_j \\ \theta_j\end{pmatrix} = \sum_{\alpha=1}^{2N+1}\begin{pmatrix}\rho^{(\alpha)} \\ \theta^{(\alpha)}\end{pmatrix} e^{\alpha t}(v_{(\alpha)})_i \tag{5.52}$$

By inserting this expansion in (5.51) and using the relation

$$\sum_j L_{ij}(v_{(\alpha)})_j = \Lambda^{(\alpha)}(v_{(\alpha)})_i \tag{5.53}$$

for $\alpha = 1, \ldots, 2N + 1$, we obtain a condition formally equivalent to the expression of the continuous dispersion relation

$$\lambda_{max}(\Lambda^{(\alpha)}) = -\Lambda^{(\alpha)} - 1 + \sqrt{-c_1^2\left(\Lambda^{(\alpha)}\right)^2 - 2c_1c_2\Lambda^{(\alpha)} + 1} \tag{5.54}$$

If $\lambda_{Re} = \mathrm{Re}(\lambda_{max})$ is positive for some $\Lambda^{(\alpha)}$, the perturbation grows exponentially in time, and the initial homogeneous state proves unstable. Conversely, if $\lambda_{Re} = \mathrm{Re}(\lambda_{max}) \leq 0$, for every $\Lambda^{(\alpha)}$, the perturbation gets re-absorbed and the system converges back to the fully synchronized state. The condition $\lambda_{Re} < 0$ can be further processed analytically, as discussed in [41]. In particular, one can show that the latter condition is fulfilled, if the Laplacian eigenvalues fall in a specific portion of the parameter plane, which reflects the choice made for the reaction parameters c_1, c_2 and K. The region of interest is the one enclosed between the two solid lines, displayed in Fig. 5.6(a) for the specific selection of the parameters operated. The blue symbols depicted in Fig. 5.6(a) are randomly generated so as to fall in the region of the complex plane where stability holds. They represent the spectrum of the Laplacian that we seek to recover following the method illustrated above. In Fig. 5.6(b), λ_{Re} is plotted against $-\Lambda_{Re} = -\mathrm{Re}(\Lambda)$, confirming the stability of the homogeneous solution.

We now proceed by generating a Laplacian matrix, which is constructed so as to yield the spectrum depicted in Fig. 5.6(a), see crosses (in blue). Circles (in red) refer to the spectrum obtained after the sparsification. In this case we operated with the more sparsification protocol, the second of those introduced above. This latter appears more suited to the case at hand because of the shape of the domain where the eigenvalues should eventually fall to enforce stability. As an additional condition to the algorithm, we accepted only the sparsification moves which prevent the eigenvalues to invade the region of the complex plane associated to instability.
The sparsified adjacency matrix A defines the network of interactions between coupled oscillators, as follows (5.49). We hence integrate numerically the governing equations, assuming the initial state to be a perturbation of the homogenous synchronized equilibrium. As expected, the perturbation fades away and the system regains its unperturbed, fully synchronized, equilibrium.

5.4.2 Coupled Kuramoto oscillators

As a second example we set to study a Kuramoto model. Consider a system made up of $2N+1$ oscillators, label θ_i the phase of the i-th oscillator, and ω_i its natural frequency. The oscillators evolve as dictated by the following system of $2N+1$ coupled differential equations:

$$\dot{\theta}_i = \omega_i + \sum_{j=1}^{2N+1} A_{ij} \sin(\theta_j - \theta_i) \qquad i = 1, .., 2N+1 \tag{5.55}$$

Here, A_{ij} stands for the entries of the adjacency matrix A which sets the interactions between pairs of oscillators. The matrix is, in principle, weighted, and may display positive and negative entries as reflecting the specific interaction (excitatory or inhibitory) being at play.

As an additional assumption, we will here focus on the simplified setting where $\omega_i = \omega \ \forall i$. We can then introduce the new variable $\psi_i = \theta_i - \omega t$, and write the governing equations in the equivalent form:

$$\dot{\psi}_i = \sum_{j=1}^{2N+1} A_{ij} \sin(\psi_j - \psi_i) \qquad i = 1, .., 2N+1 \tag{5.56}$$

A homogeneous solution always exists with $\Psi = \psi_i \ \forall i$, and for any constant $\Psi \in [0, 2\pi)$, as it can be immediately checked by substitution. To assess

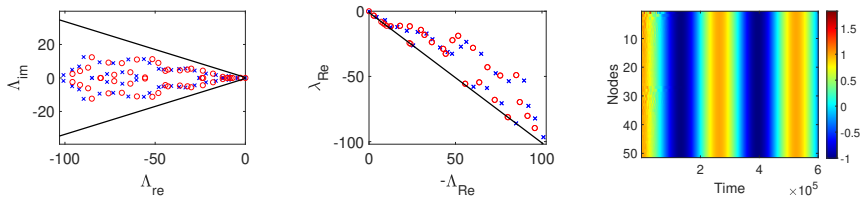

(a) (b) (c)

Figure 5.6: *Panel (a): the system of coupled Landau-Stuart oscillators is stable if the eigenvalues of the Laplacian operator fall in the portion of the complex plan comprised in between the two solid lines. Crosses (in blue) represent the (randomly assigned) eigenvalues of the Laplacian that we aim at recovering following the procedure introduced in the early part of this paper. Circles (in red) refer to the spectrum obtained as follows the sparsification (see main body of the paper). In the sparsification procedure we assumed* $\sigma = 0.01$ *and* $\delta = 5$. *The percentage of the pruned links is around* 35% *of the total. Panel (b):* λ_{Re} *is plotted against* $-\Lambda_{Re} = -\mathrm{Re}(\Lambda)$. *This is an alternative way to show that the system is stable with the prescribed Laplacian spectrum. The solid line stands for dispersion relation obtained in the continuum limit, when the discrete Laplacian is replaced by a standard differential operator. Panel (c): the time evolution of the real components* $\mathrm{Re}(W_j)$ *is shown, with an appropriate color code. Here, the weighted network which specifies the coupling between the nodes is obtained from the sparsified Laplacian. Here,* $c_1 = 3$, $c_2 = 2.4224$ *and* $K = 1$.

the stability of the solution one sets $\psi_i = \Psi + \delta_i$, and expands (5.56) at the leading order in the δ_i. In doing so, one gets:

$$\dot{\delta_i} = \sum_{j=1}^{2N+1} A_{ij}(\delta_j - \delta_i) = \sum_{j=1}^{2N+1} L_{ij}\delta_j \tag{5.57}$$

where $L_{ij} = A_{ij} - k_i\delta_{ij}$ is the Laplacian operator which stems from A_{ij}. The stability of the simplified Kuramoto model here considered is eventually controlled by a linear system of the type introduced in (5.25), with the obvious replacement of x_i with δ_i. The system proves hence stable if the (non trivial) eigenvalues of the Laplacian operator display negative real parts. Our aim is here to generate a Laplacian (and therefore a matrix of binary weighted connections among oscillators) which warrants the stability of the system. To this end, we assign the eigenvalues (which appear in conjugate pairs) to belong to the negative portion of the complex plane, see Fig. 5.7(a). The null eigenvalue is clearly included into the pool. Running the procedure discussed in the first part of the paper, we obtain the corresponding Laplacian and compute the associated adjacency matrix. The first of the two sparsification procedures is then applied to remove unessential links, yielding the spectrum of the associated Laplacian depicted with (red) circles in Fig 5.7(a). The Kuramoto model (5.56) is then integrated numerically by assuming the recovered expression for A. As predicted, the system is stable to external perturbations as one can clearly appreciate by inspection of Fig. 5.7(b).

5.5 Conclusion

Studying the dynamics of an ensemble made of interacting units on a network is central for a large plethora of applications. In many cases of interests, individual units evolve under the influence of homologous constituents, the interaction being in general mediated by binary exchanges. Distinct fundamental units are assigned to different nodes of the collection, paired via physical or virtual links. For a relevant subclass of problems, the stability of the ensuing equilibrium can be traced back to the spectrum of the Laplacian operator, computed from the adjacency matrix which defines the network arrangement. Symmetric networks yields Laplacian operators with real spectrum, while directionality in the couplings reflects in an imaginary spectrum. Methods exist which allow one to generate symmetric network, hence Laplacian, with a prescribed real spectrum. Starting from these premises,

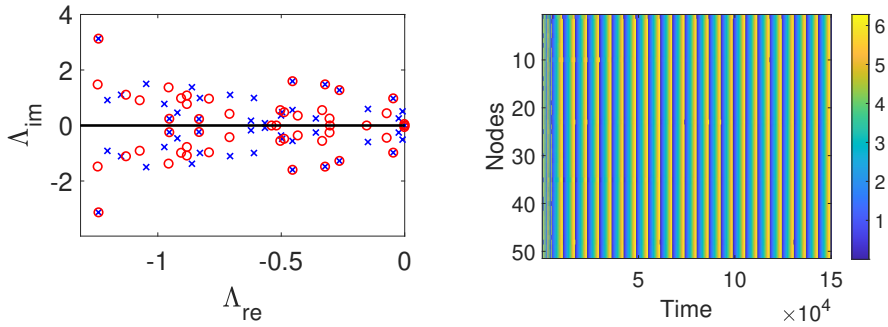

Figure 5.7: *Panel (a): crosses (in blue) represent the spectrum of the Laplacian operator that we seek to recover. The eigenvalues are distributed in the left portion of the complex plane to assure stability of the inspected Kuramoto model. Circles (in red) stand for the spectrum of the Laplacian after the sparsification procedure. We here apply the first sparsification algorithm as discussed in the main body of the paper. More specifically, unessential links with modest weights are removed, while confining the Laplacian spectrum in a bounded domain, locate in the negative portion of the complex plane. Here,* $\sigma = 0.01$ *and* $\delta = 0.2$*. The percentage of trimmed links is around* 9% *of the total. Panel (b):* θ_i *vs. time. Here, the adjacency matrix employed in the numerical integration follows from the sparsified. As an initial condition, we perturb the homogenous solution (assumed* $\Psi = 0$*) by a random heterogeneous amount. After a transient, the perturbation gets absorbed and the oscillators evolve in unison. Here* $\Omega = 2N + 1 = 51$*.*

we have here proposed and tested a novel procedure to generate a (signed and directed) Laplacian which returns an a priori assigned (complex) spectrum. A special case has also been considered, which enables one to recover closed analytical expressions for the entries of the sought Laplacian matrix. Working in this setting, we can elaborate on the conditions that are to be matched for the ensuing Laplacian to solely display positive non diagonal elements. Dedicated sparsification procedures are also discussed to help removing unessential links in terms of their impact on the associated spectrum. The algorithm for Laplacian generation has been successfully tested with reference to two prototypical examples of coupled oscillators. Taken together, our work explores possible strategies for network generation with the emphasis placed on dynamical, rather than structural, features. The dynamics is indirectly modulated by the spectrum of the Laplacian operator, which is here constraining the generative algorithm.

Chapter 6

Many body interactions systems

So far we considered systems defined on networks. As known, networks encode for binary relationships among units. This descriptive framework is sufficiently accurate in many cases of interest, although several examples exist of systems for which it holds true just as a first order approximation [27, 113]. The relevance of high-order structures has been indeed emphasised in the context of functional brain networks [120,162], in applications to protein interaction networks [68], to the study of ecological communities [85] and co-authorship networks [40,158].

Starting from this observation, higher-order models have been developed so as to capture the many body interactions among interacting units whose most notable examples are simplicial complexes [51, 60, 161] and hypergraphs [29, 67, 81], non trivial mathematical generalisations of ordinary networks that are currently attracting a lot of interest. The concept of simplicial complexes has been for instance invoked to address problems in epidemic spreading [36, 101] or synchronisation phenomena [77, 122].

Our work is positioned in the framework of hypergraphs, a domain of investigation which is still in its infancy. In this respect, we mention applications to social contagion models [57], to the modeling of random walks [40] and to the study of synchronisation [109,132] and diffusion [71]. Hypergraphs constitute indeed a very flexible paradigm: an arbitrary number of agents are allowed to interact, thus extending beyond the limit of binary interactions of conventional network models. On the other hand, hypergraphs define a leap forward as compared to simplicial complexes. In this latter case, in fact, if (say) 3 agents form a 2-simplex, also all binary interactions are accounted

for. On the other hand, agents interacting via a hypergraph do form a hyperedge, a unifying frame which encompasses the many body interactions as a whole. Imagine that a subgroup of agents organized in the hyperedge, also interact with each other, via a distinct channel. This yields a new hyperedge, included in the former. A hypergraph can reproduce, in a proper limit, a simplicial complex and, in this respect, provides a more general tool for addressing many body simultaneous interactions. Furthermore, the analysis of the models in the framework of hypergraphs turns out to be simpler as compared to their simplicial complexes homologues. In these latter settings, the involved formulas get rapidly cumbersome and, for this reason, applications are limited to low dimensional simplexes, i.e. 2 or 3-simplex. At variance, one can efficiently handle very large hyperedges and, even more importantly, heterogenous distribution of hyperedges' sizes, because all the information on the high-order structure of the embedding support are stored in a matrix whose dimension depends only on the number of nodes.

Starting on these premises, it is clear that many body interactions constitute a relevant and transversal research field that is still in its embryonic stage, in particular as concerns studies that relate to hypergraphs. Indeed, novel light could be shed on a large plethora of systems, usually defined on standard networks, by accounting for generalized hypergraph architectures. This chapter aims at taking one first step in this direction, by expanding along different axis. We will begin by adapting to the hypergraph setting the Master Stability Function [159] formalism. We will then consider the condition for the emergence of Turing patterns [178] for reaction-diffusion systems on hypergraphs, the synchronisation of nonlinear oscillators [12] and of chaotic orbits. It is here anticipated that for theoretical progress to be made one needs to characterize the spectral properties of a properly defined operator, which implements diffusion on hypergraphs.

The Master Stability Function (MSF), is a powerful technique developed in [159] to analyse synchronisation and it basically amounts to performing a linear stability analysis around a given equilibrium, for a system of coupled interacting units. A straightforward application of linear stability analysis is for instance found in the context of the celebrated Turing instability, once the reference orbit is indeed a homogeneous fixed point. In his seminal paper [178], Alan Turing set the mathematical basis of pattern formation. Initially proposed to explain the richness and diversity of forms displayed in Nature, it is nowadays an universally accepted paradigm of self-

organisation [23, 135, 151]. The onset of patterns originates from the loss of stability of an homogeneous equilibrium, as triggered by diffusion. Turing instabilities have been initially studied for systems defined on continuous spatial domains and regular lattices [152]. More recently, the realm of application of Turing ideas has been extended to account for reaction-diffusion dynamics hosted on a complex network [140] and other related structures, such as multilayer network [13, 107] or multigraph [14] just to mention a few. It is hence a natural question to generalise these studies to the broad framework of hypergraphs.

Turing patterns emerge from the destabilisation of a homogeneous equilibrium, that is a stationary solution of the examined model. In many real cases, however the system is not bound to evolve close to a stationary solution, but instead displays periodic oscillations. Examples ranges from biology to ecology, passing through physics [12, 163]: individual nonlinear oscillators can synchronise and thus exhibit a coherent collective behaviour. Synchronization, the spontaneous ability of coupled oscillators to operate in unison, has been studied for systems interacting via a complex and heterogeneous network of interlaced connections. To the best of our knowledge, however, this analysis has never been attempted for systems defined on hypergraphs of the type here considered. Let us observe that, although similar in their conception, the works [32, 169] deal with hypernetworks, namely a network where several different links can connect two nodes, also called multigraph in the literature. The interactions are hence pairwise.

The formalism of the MSF can be also applied to chaotic oscillators. The synchronisation of chaotic systems defined on hypergraphs has been studied in [109] using the formalism of the MSF under two main assumptions: (i) the work has been limited to p-hypergraphs, namely assuming all the hyperedges have the same size; (ii) the coupling function was assumed to be invariant with respect to permutations of the nodes, within each hyperedge. In this paper, we will relax both assumptions to deal with general hypergraphs with heterogenous hyperedge size distribution and without putting forward any hypothesis on the form of the coupling function.

In a recent work [132], the synchronisation phenomenon has been studied again by means of the MSF, by using however a Laplace operator [104] which cannot fully account for the high interaction at play. The employed operator is defined from the hyper-adjacency matrix, which is solely capable to encode for the number of incident hyperedges withouth gauging their

sizes. Moreover authors assumed the coupling function to depend on the average (arithmetic or geometric) value of the involved variables. Again, both assumptions are relaxed in the present work, because our Laplace operator takes into account both the number of incident hyperedges but also their size. We will moreover make use of a generic coupling function.

We already introduced the formalism of hypergraphs in Section 2.5 and, among other relevant quantities to be used in the subsequent analysis, a new Laplace matrix for hypergraphs; hence, the chapter is organised as follows. We discuss on the spectrum of the newly introduced Laplacian by emphasising its localisation properties. We perform also a numerical analysis using the perturbation theory to predict these eigenvector properties. We present the analytical derivation and we present the results about the eigenvalues approximation. Then, we present three applications, following the logic path outlined above, and elaborate on the impact of the high-order structures.

6.1 Localisation of eigenvectors

One can prove [40] that the Laplace matrix $\mathbf{L}^H$ (2.25) defined in Chapter 2, is symmetric, non-negatively defined and the smallest eigenvalue equals 0. Moreover let $(\Lambda_H^\alpha)_{1\leq\alpha\leq n}$ be the set of its eigenvalues, then $\Lambda_H^n \geq \dots \Lambda_H^2 > \Lambda_H^1 = 0$, and its eigenvectors, $\left(\vec{\phi}^\alpha\right)_{1\leq\alpha\leq n}$ form an orthonormal basis, $\vec{\phi}^\alpha \cdot \vec{\phi}^\beta = \delta_{\alpha\,\beta}$. As already observed $\vec{\phi}^1 \propto (1,\dots,1)$. Finally $\mathbf{L}^H$ reduces to the Laplace matrix defined on networks once all the hyperedges have size 2. In the following we will denote by $(\Lambda^\alpha)_{1\leq\alpha\leq n}$ the eigenvalues of the Laplace operator of the projected network, L and $\left(\vec{\psi}^\alpha\right)_{1\leq\alpha\leq n}$ the associated eigenvectors. Based on the well known properties of L and assuming the network to be connected, we have $\Lambda^n \geq \dots \Lambda^2 > \Lambda^1 = 0$ and the eigenvectors do form an orthonormal basis.

Localisation of eigenmodes is a phenomenon relevant to many fields of science, e.g. the Anderson localisation in disordered systems [8, 84], with a particular relevance to the dynamics. For this reason we decided to start our analysis by studying the localisation properties of the Laplacian eigenvectors for the hypergraph (2.25) and compare them with the corresponding quantities obtained for the projected network. Results reported in Fig. 6.1 show that the localisation is more evident for a hypergraph, than for the

associated projected network. In the left panel of Fig. 6.1, we present the eigenvectors for the Laplace matrix stemming from the hypergraph (ordered for increasing eigenvalue Λ_H^α) as a function of the nodes indexes (ordered for increasing k_i^H). In the right panel, the same quantity is displayed for the Laplace matrix computed from the projected network. By visual inspection (entries larger than 0.015 are coloured in black while the remaining ones are drawn in white), one can clearly appreciate the dark squarish zones, associated to small or medium rank eigenvectors, which appear in the left panel of Fig. 6.1: eigenvectors are found with relatively large entries, i.e. a strong localisation, on a subset of nodes. On the right panel, similar structures are present but much weaker. A substantially analogous behaviour is observed for high ranked eigenvectors, e.g. $\alpha \gtrsim 400$ in the left panel and $\alpha \sim 500$ in the right one, for which only few entries display very large values, pointing hence to an even stronger localisation (see the thin dark "line" in the top right corners in both panels).

To illustrate our results, we employed as projected network a Scale Free network made by $n = 500$ nodes, built using the configuration model with $\gamma = -2$ and $k_{min} = 2$ [116]. The associated hypergraph is obtained by transforming all the maximal m-cliques into hyperedges of size m. The distribution of hyperedges sizes is reported in Fig. 6.2.

A more quantitative measure of the localisation can be obtained using the *Inverse Participation Ratio* (IPR) [126], that for a n-dimensional vector, $\mathbf{v}$, it is defined by

$$P(\mathbf{v}) = \frac{\sum_i v_i^4}{\left(\sum_i v_i^2\right)^2} \,. \tag{6.1}$$

The above quantity ranges in $[1/n, 1]$, where the lower bound is attained for a vector with uniform entries. The upper limit is hit when all the entries are 0 but one which equals 1. In Fig. 6.3 we report the IPR computed for the eigenvectors of the hypergraph (blue dots) and the projected network (black dots) used in Fig. 6.1. We can observe that in the case of the hypergraph, the IPR is always larger than the same quantity computed for the projected network, except for very high ranked eigenvectors (say the last 5 ones).

In the next sections, we will show that the localisation which manifests on hypergraphs, leaves macroscopic imprints on the dynamics of systems subject to many-body, higher-order interactions.

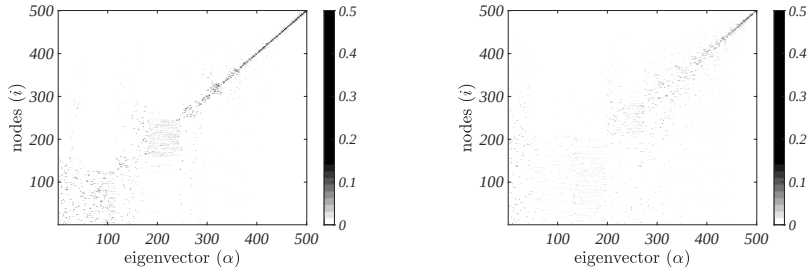

Figure 6.1: **Laplacian eigenvectors**. We report the absolute values of the components of the eigenvectors, $\vec{\phi}^{\alpha}$, ordered for increasing eigenvalues and nodes degree (right panel) and nodes hyper degree (left panel). Entries larger than 0.015 are pictured in black, while the remaining ones in white. The projected network is a scale free network made of 500 nodes and generated by using the configuration method with $\gamma = -2$ and $k_{min} = 2$. The corresponding hypergraph is obtained from the latter by transforming all the m-cliques into a hyperedge of size m.

6.1.1 Perturbation analysis of the Laplacian matrix

It is known [92] that localization properties of random networks can be predicted by using the perturbation theory. This approach is indeed used in [92] to analyze eigenvalues and eigenvectors for scale-free networks generated by the Barabási-Albert preferential attachment algorithm, classical Erdös-Rényi random network and real neural network of *C. elegans*. A similar method was used by Kim and Motter to analyze the Laplacian eigenvalues of scale-free networks [106].

Does this theory also work for hypergaphs? In this section, we try to answer to this question. For this reason, we apply the perturbation theory [95, 167] to the Laplacian matrix (2.25). The diagonal elements of matrix (2.25) are of the order $\mathcal{O}(< k^H >)$, while non-diagonal elements are $\mathcal{O}(K^H_{ij})$. We introduce an expansion parameter $\epsilon =< K^H > / < k^H >$ and we rewrite the Laplacian matrix as

$$\mathbf{L}^H = \mathbf{L}_0 + \epsilon \mathbf{L}_1 \tag{6.2}$$

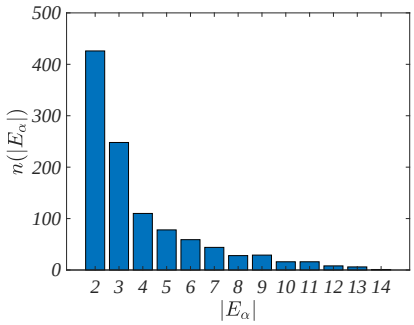

Figure 6.2: **Distribution hyperedges sizes**. We report the distribution of hyperedges sizes for a hypergraph whose Scale Free projected network is made by 500 nodes and built using the configuration method with $\gamma = -2$ and $k_{min} = 2$. One can observe the presence of relatively large hyperedges responsible for the high-order interactions.

whose elements

$$L_{0,ij} = -k_i^H \delta_{ij} \tag{6.3}$$

$$L_{1,ij} = \frac{< k^H >}{< K^H >} \mathbf{K}_{ij}^H \tag{6.4}$$

are of the same order $\mathcal{O}(< k^H >)$. With the same arguments discussed in [92], we observe that, if the hypergraph is sufficiently dense, the inequality $< k^H > \gg K_{ij}^H$ holds generally and it is expected that the perturbation theory yields accurate approximation results.

First of all, note that L_0 is not a Laplacian matrix because its rows do not sum up to zero. Also, the zeroth-order eigenvalue Λ_0^N is not zero as usual, but equal to the smallest hyper degree $-k_N$. It is convenient to employ the bra-ket notation to denote the Laplacian eigenvector, i.e. $\vec{\phi}^{(\alpha)} = |\alpha\rangle$, and drop the summation symbol as $\sum_{j=1}^N L_{ij}\phi_j^{(\alpha)} = L\,|\alpha\rangle$. We expand the

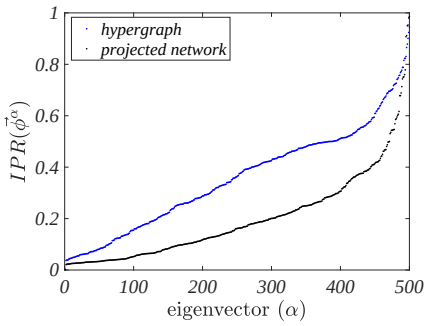

Figure 6.3: **Inverse Participation Ratio**. We report the IPR of the eigenvectors of the hypergraph (blue dots) and of the associated projected network (black dots) used in Fig. 6.1. We can observe that in the case of the hypergraph the IPR is always larger than that obtained for the corresponding projected network, while the eigenvectors associated to the largest eigenvalues are more localised for the case of the network.

Laplacian eigenvectors $|\alpha\rangle$ and eigenvalues $\Lambda^{(\alpha)}$ in series of ϵ as

$$|\alpha\rangle = |\alpha\rangle_0 + \epsilon\,|\alpha\rangle_1 + \epsilon^2\,|\alpha\rangle_2 + \dots \tag{6.5}$$

and

$$\Lambda^{(\alpha)} = \Lambda_0^{(\alpha)} + \epsilon\Lambda_1^{(\alpha)} + \epsilon^2\Lambda_2^{(\alpha)} + \dots \tag{6.6}$$

and we substitute these expressions into the eigenvalue equation

$$L^H\,|\alpha\rangle = \Lambda^{(\alpha)}\,|\alpha\rangle \tag{6.7}$$

where $\alpha = 1, 2, \dots, N$ is the index of the α-th eigenvector. The resulting equations up to the second order are:

$$(L_0 - \Lambda_0^{(\alpha)})\,|\alpha\rangle_0 = 0 \tag{6.8}$$

$$(L_0 - \Lambda_0^{(\alpha)})\,|\alpha\rangle_1 = -(L_1 - \Lambda_1^{(\alpha)})\,|\alpha\rangle_0 \tag{6.9}$$

$$(L_0 - \Lambda_0^{(\alpha)})\,|\alpha\rangle_2 = -(L_1 - \Lambda_1^{(\alpha)})\,|\alpha\rangle_1 + \Lambda_2^{(\alpha)}\,|\alpha\rangle_0\,. \tag{6.10}$$

These three equations allow to derive the zeroth- ($|\alpha\rangle_0$) and first-order ($|\alpha\rangle_1$) perturbations for the eigenvectors, and the zeroth- ($\Lambda_0^{(\alpha)}$), first- ($\Lambda_1^{(\alpha)}$) and second- ($\Lambda_2^{(\alpha)}$) order perturbations for the eigenvalues.

Consider at first the unperturbed system (6.8); the eigenvectors $|\alpha >_0$ and eigenvalues $\Lambda_0^{(\alpha)}$ are given exactly as

$$|\alpha\rangle_0\,(i) = 0 \quad \text{for} \quad i \neq \alpha \tag{6.11}$$

$$|\alpha\rangle_0\,(i) = 1 \quad \text{for} \quad i = \alpha \tag{6.12}$$

and

$$\Lambda_0^{(\alpha)} = -k_{(\alpha)} \tag{6.13}$$

for $\alpha = 1, \ldots, N$. Each eigenvector is characterized by a single non-zero element at the hypergraph node $i = \alpha$, and the corresponding eigenvalue $\Lambda_0^{(\alpha)}$ is equal to the negative of the characteristic node hyper degree k_α. The hypergraph generally possesses multiple nodes with same degrees and, from the zeroth-order solution (6.8), it is evident that such nodes have corresponding degenerate eigenvectors. For this reason, we should consider the higher-order perturbation terms and employ the degenerate perturbation theory [95,167]. From (6.8)-(6.10) we compute the approximated eigenvectors and eigenvalues up to the second order. The complete derivation of the perturbation corrections for a general class of degenerate system has been reported, for example, in [95].

6.1.2 Degenerate perturbation theory

This section is inspired by the work of Hata and Nakao [92] and represents a generalization of this study to the emerging field of hypergraphs. The applications could be several, being the localization an aspect that influence the dynamics of systems defined on top of networks and high-order structures, as we will show in the following.

The derivation is analogous to the one reported in [92]. We differentiate the eigenvectors into three classes, depending on their degeneracy: non-degenerate vectors, vectors whose degeneracy is solved at the first order and vectors who are still degenerate at the first order. For the sake of completeness, we remind the expressions of each term of the expansion. We consider

perturbation terms up to the second-order for eigenvalues, and terms up to the first-order for the eigenvectors.

For non-degenerate eigenvalues the first-order correction term read as

$$|\alpha\rangle_1 = \sum_{\beta\neq\alpha} \frac{{}_0\langle\beta|\mathbf{L}_1|\alpha\rangle_0}{\Lambda_0^{(\alpha)} - \Lambda_0^{(\beta)}} |\beta\rangle_0 \,, \tag{6.14}$$

while, the first order correction to the eigenvalue is zero

$$\Lambda_1^{(\alpha)} = {}_0\langle\alpha|\mathbf{L}_1|\alpha\rangle_0 \,, \tag{6.15}$$

because of the diagonal elements of $\mathbf{L}_1$ are zero. The second-order correction term to the eigenvalue is given by

$$\Lambda_2^{(\alpha)} = {}_0\langle\alpha|\mathbf{L}_1|\alpha\rangle_1 \,. \tag{6.16}$$

For eigenvalues whose degeneration is solved at the first order, we denote the degenerate eigenvectors corresponding to the same eigenvalue $\Lambda_0^{\alpha)}$ as $\alpha_1, \ldots, \alpha_m$. We introduce new zeroth-order eigenvectors so that the degeneration is solved at the first-order perturbation; they are defined as

$$|\tilde{\alpha}_i\rangle_0 = \sum_{j=1}^{m} b_{i,j} |\alpha_j\rangle_0 \,, \tag{6.17}$$

where the mixing coefficients b_{ij} are the eigenvectors of the matrix $\mathbf{V}$ defined by $V_{ij} = {}_0\langle\alpha_i|\mathbf{L}_1|\alpha_j\rangle_0 \, (i,j = 1,\ldots,m)$; in other words, they satisfy the eigenvalue equation $\sum_{j=1}^{m} V_{kj} b_{ij} = \Lambda_1^{(\alpha_i)} b_{ik}$, where $\Lambda_1^{(\alpha_i)}$ gives the first-order perturbation to the Laplacian eigenvalues.

The first-order correction term for eigenvectors is given by

$$|\tilde{\alpha}_i\rangle_1 = \sum_{\beta\neq\alpha} \frac{{}_0\langle\beta|\mathbf{L}_1|\tilde{\alpha}_i\rangle_0}{\Lambda_0^{(\alpha)} - \Lambda_0^{(\beta)}} \left[\sum_{j=1}^{m} \frac{{}_0\langle\tilde{\alpha}_j|\mathbf{L}_1|\beta\rangle_0}{\Lambda_1^{(\alpha_i)} - \Lambda_1^{(\alpha_j)}} |\tilde{\alpha}_j\rangle_0 + |\beta\rangle_0 \right] \tag{6.18}$$

where the summation symbol with $\beta \neq \alpha$ indicates that the index β runs over all eigenvectors except for the degenerate ones, i.e. $\alpha_1, \ldots, \alpha_m$.

The second order correction to the eigenvalue is given by

$$\Lambda_2^{(\alpha_i)} = {}_0\langle\tilde{\alpha}_i|\mathbf{L}_1|\tilde{\alpha}_i\rangle_1 \,. \tag{6.19}$$

Let us consider now the eigenvalues whose degeneration is not eliminated at the first order. Suppose that a subset of eigenvalues $\tilde{\alpha}_1, \ldots, \tilde{\alpha}_m$ $(n \leq m)$

are still degenerate at the first order perturbation. In this case, the zeroth-order eigenvectors are redefined as

$$\left|\tilde{\tilde{\alpha}}_i\right\rangle_0 = \sum_{j=1}^{n} c_{ij} \left|\tilde{\alpha}_j\right\rangle_0 , \tag{6.20}$$

where c_{ij} are the eigenvectors of the matrix

$$W_{kj} = \sum_{\beta \neq \alpha} (\ {}_0\langle \tilde{\alpha}_k | \mathbf{L}_1 | \beta \rangle_0 \ \ {}_0\langle \beta | \mathbf{L}_1 | \tilde{\alpha}_j \rangle_0) / (\Lambda_0^{(\alpha)} - \Lambda_0^{(\beta)}). \tag{6.21}$$

The first-order correction to the eigenvectors is in this last case given by

$$\left|\tilde{\tilde{\alpha}}_i\right\rangle_1 = \sum_{\beta \neq \alpha} \frac{{}_0\left\langle \beta \middle| \mathbf{L}_1 \middle| \tilde{\tilde{\alpha}}_i \right\rangle_0}{\Lambda_0^{(\alpha)} - \Lambda_0^{(\beta)}} \left[\sum_{k=n+1}^{m} \frac{{}_0\langle \tilde{\alpha}_k | \mathbf{L}_1 | \beta \rangle_0}{\Lambda_1^{(\alpha_i)} - \Lambda_1^{(\alpha_k)}} \left|\tilde{\alpha}_k\right\rangle_0 + \left|\beta\right\rangle_0 \right]. \tag{6.22}$$

and the first-order perturbation term $\Lambda_1^{(\alpha_i)}$ for the eigenvalues is defined as in the previous case.

In conclusion, the second-order correction $\Lambda_2^{(\alpha_i)}$ is determined from the equation

$$\sum_{j=1}^{m} W_{kj} c_{ij} = \Lambda_2^{(\alpha_i)} c_{ik}. \tag{6.23}$$

If some eigenvectors are still degenerate even at the second-order perturbation, one can introduce new zeroth-order eigenvectors so that the degeneracy is solved at the third-order perturbation. In principle, one can proceed iterating this method until the degeneration is resolved.

We applied the introduced theory to hypergraphs. We show here the preliminary results about the eigenvalues approximation.
As in the previous sections, we start considering a scale free network made of 500 nodes, generated by using the configuration method with $\gamma = -2$ and $k_{min} = 2$. The corresponding hypergraph is obtained from this network by transforming all the m-cliques into a hyperedge of size m. Via a numerical implementation of the formulae presented above, we calculate an approximation for Laplacian eigenvalues at zeroth- and second-order, corresponding respectively to Eq. (6.13) and Eq. (6.15)-(6.16). The comparison between approximated and true eigenvalues calculated by direct numerical analysis is illustrated in Figure 6.4. As one can clearly appreciate, the original quantities are well reproduced, and the zeroth-order perturbation provide an already qualitatively good estimate of eigenvalues.

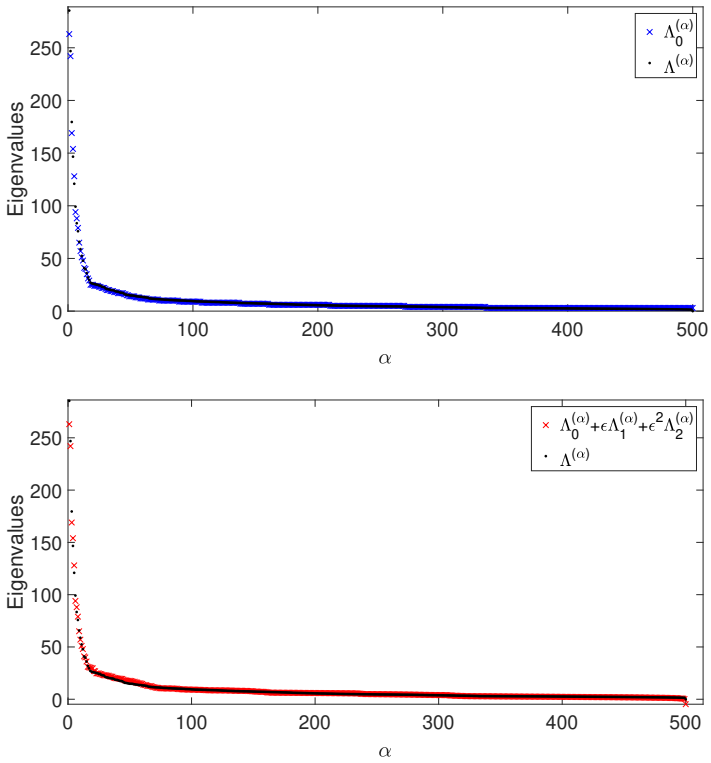

Figure 6.4: Approximation of the Laplacian eigenvalues using the perturbation theory. The hypergraph is obtained transforming all the m-cliques of a scale-free network made of 500 nodes into a hyperedge of size m. The network is constructed using the configuration method with parameters $\gamma = -2$ and $k_{min} = 2$. The comparison between the true and the zeroth-order (upper panel) and second-order (bottom panel) approximated eigenvalues is shown. We point out the plateaux at the zeroth-order approximation displayed in the upper panel; these correspond to degenerate eigenvectors relative to eigenvalues who share the same hyperdegrees, according to (6.13). The second-order perturbation terms smooth the curve, as one can appreciate from the bottom panel. The recovered quantities are, in both cases, in good agreement with the original ones.

Using the same approach, an approximation of the Laplacian eigenvectors can be obtained. In this case, depending on the degeneracy of each node, we should consider the correction terms written above, for all the zeroth-, first and second-order of approximation.

Predict the localization properties of Laplacian eigenvectors for hypergraphs will be the subject of our future research. In principle, a random generated hypergraph does not possess a set of strongly localized eigenvectors. In this respect, it could be interesting to devise a method to design hypergraphs with desired properties. A solution could be given by a variant of the procedure presented in Chapter 5, where we recover a network starting from a set of assigned Laplacian eigenvalues. More specifically, once we fixed a properly basis of Laplacian eigenvectors, with an analogous procedure based on the eigenvalue decomposition, we are able to construct a hypergraph with specific properties. At variance with Chapter 5, in this case the eigenvalues are located in a (a priori) unknown region of the complex plane.

6.2 Dynamical systems on hypergraphs

In this section we will consider the behaviour of dynamical systems defined on hypergraphs. In particular, we will analyse the consequences of dealing with higher-order couplings, exploiting to this end the spectral characteristics highlighted above. More specifically, assume n copies of the same low dimensional dynamical system to be hosted on each node of a given collection. This defines the local dynamics of the inspected system. Units belonging to different nodes are assumed to interact through higher-order structures identified as hyperedges. Many body interactions promote a preferential interaction among nodes belonging to the same large hyperedge. The nodes can be imagined to identify different spatial locations. For this reason, we will denote by aspatial the system composed by one isolated dynamical unit, and use spatial to refer to its multi-dimensional version made of mutually entangled components.

As already mentioned, the newly introduced (combinatorial) Laplace matrix (2.25) admits a homogeneous eigenvector associated to the zero eigenvalue. This will allow us to probe (in)stability of interconnected systems evolving close to reference orbits. For the sake of completeness, we will consider three applications that cover several relevant research domains. We

will begin by imposing a generalised diffusive coupling among nodes as exemplified by the aforementioned Laplace matrix (2.25). Working in this framework, we will study the emergence of Turing patterns, that is the existence of a stable heterogeneous solution. We will then turn to considering the synchronisation between nonlinear oscillators, diffusively coupled via higher-order combinatorial Laplacians. Finally, we will analyse the synchronisation of chaotic oscillators, in the setting of interest where higher-order interactions are at play. The formalism of the Master Stability Function will be used to tackle the problem analytically. Projected networks will be employed as reference benchmarks to bring into evidence the role of hypergraphs and related higher order interactions.

Consider a d-dimensional system described by local, i.e. aspatial, equations:

$$\frac{d\mathbf{x}}{dt} = \mathbf{F}(\mathbf{x}) \quad \mathbf{x} \in \mathbb{R}^d \,, \tag{6.24}$$

and fix a reference orbit, $\mathbf{s}(t)$. Let us observe that the latter can also be a fixed point. Assume further n identical copies of the above system coupled through a hypergraph, namely each copy is represented by a node of a hypergraph. Moreover, each system belongs to one (or more) hyperedge. Units sharing the same hyperedge are tightly coupled, due to existing many body interactions. In formulas:

$$\frac{d\mathbf{x}_i}{dt} = \mathbf{F}(\mathbf{x}_i) - \varepsilon \sum_{\alpha: i \in E_\alpha} \sum_{j \in E_\alpha, j \neq i} (C_{\alpha\,\alpha} - 1) \left(\mathbf{G}(\mathbf{x}_i) - \mathbf{G}(\mathbf{x}_j)\right) \,,$$

where $\mathbf{x}_i$ denotes the state of the i-th system, i.e. sitting on the i-th node, ε the strength of the coupling and $\mathbf{G}$ a generic nonlinear coupling function. The elements $C_{\alpha\alpha}$ of matrix $\mathbf{C}$ denote the size of the hyperedge E_α. The factor -1 accounts for the fact that j should be different from i. Recalling the definition of $e_{i\alpha}$ one can rewrite the previous formula as

$$\begin{aligned}
\frac{d\mathbf{x}_i}{dt} &= \mathbf{F}(\mathbf{x}_i) - \varepsilon \sum_{\alpha,j} e_{i\alpha} e_{j\alpha} (C_{\alpha\,\alpha} - 1) \left(\mathbf{G}(\mathbf{x}_i) - \mathbf{G}(\mathbf{x}_j)\right) \\
&= \mathbf{F}(\mathbf{x}_i) - \varepsilon \sum_j k_{ij}^H \left(\mathbf{G}(\mathbf{x}_i) - \mathbf{G}(\mathbf{x}_j)\right) = \mathbf{F}(\mathbf{x}_i) - \varepsilon \sum_j \left(\delta_{ij} k_i^H - k_{ij}^H\right) \mathbf{G}(\mathbf{x}_j) \\
&= \mathbf{F}(\mathbf{x}_i) - \varepsilon \sum_j L_{ij}^H \mathbf{G}(\mathbf{x}_j) \,,
\end{aligned} \tag{6.25}$$

where we have used the definition of $k_i^H = \sum_j k_{ij}^H$ and L_{ij}^H given by (2.25). Let us stress once again that all the high-order structure is encoded in a

$n \times n$ matrix and there is no need for tensors as in the case of simplicial complexes: this simplifies the resulting analysis.

By exploiting the fact that $\sum_j L^H_{ij} = 0$ for all $i = 1, \dots, n$, it is immediate to conclude that the aspatial reference solution $\mathbf{s}(t)$ is also a solution of (6.25). A natural question that arises is hence to study the stability of the homogeneous solution for the system in its coupled variant.

To answer to this question one introduces the deviations from the reference orbit, i.e. $\delta\mathbf{x}_i = \mathbf{x}_i - \mathbf{s}$. Assuming this deviation to be small, one can derive a self-consistent set of linear equations for tracking the evolution of the perturbation in time. To this end, we make use of the above expression in (6.25) and perform a Taylor expansion by neglecting terms of order larger than two, to eventually get:

$$\frac{d\delta\mathbf{x}_i}{dt} = D\mathbf{F}(\mathbf{s}(t))\delta\mathbf{x}_i - \varepsilon \sum_j L^H_{ij} D\mathbf{G}(\mathbf{s}(t))\delta\mathbf{x}_j \,, \tag{6.26}$$

where $D\mathbf{F}(\mathbf{s}(t))$ (resp. $D\mathbf{G}(\mathbf{s}(t))$) denotes the Jacobian matrix of the function $\mathbf{F}$ (resp. $\mathbf{G}$) evaluated on the trajectory $\mathbf{s}(t)$.

Remember that $\mathbf{L}^H$ is symmetric. Hence, there exists a basis formed by orthonormal eigenvectors, $\vec{\phi}^\alpha$, associated to eigenvalues Λ^α_H (see Section 6.1). We can then project $\delta\mathbf{x}_i$ on this basis and obtains for all α:

$$\frac{d\delta\mathbf{y}_\alpha}{dt} = \left[D\mathbf{F}(\mathbf{s}(t)) - \varepsilon\Lambda_\alpha D\mathbf{G}(\mathbf{s}(t))\right]\delta\mathbf{y}_\alpha \,, \tag{6.27}$$

where $\delta\mathbf{y}_\alpha$ is the projection of $\delta\mathbf{x}_i$ on the α-th eigendirection.

Let us finally conclude this section by observing that from Eq. (6.27) one can derive the Master Stability Function, i.e. the most general framework to address questions that pertain to the stability of the reference orbit. Despite its generality, the latter can only be handled numerically, except very few exceptions. In the following, we begin by studying the setting where $\mathbf{s}(t)$ is a constant solution. In this case, the previous equation simplifies because the right hand side is no longer time dependent and the problem translates into the onset of (generalised) Turing instability. Indeed, the rightmost term in (6.25) can be seen as a sort of generalised Fick's diffusion (see Section 6.2.1). If the reference orbit is instead periodic in time, one can investigate the conditions which drive the synchronisation of regular oscillators. In this case, the Master Stability Function can be analysed by resorting to the Floquet machinery. In the following, we have however chosen to study the synchronisation of Stuart-Landau oscillators via higher-order couplings

(see Section 6.2.2). Working in this setting, the Master Stability Function becomes again time independent and the analysis closely resembles the one carried out for addressing the onset of Turing instabilities. As a final step, we will turn to studying the case where $\mathbf{s}(t)$ is a chaotic trajectory (see Section 6.2.3).

6.2.1 Turing patterns on hypergraphs

The Turing instability takes place for spatially extended systems: a stable homogeneous equilibrium becomes unstable upon injections of a heterogeneous, i.e. spatially dependent, perturbation once diffusion and reaction terms are simultaneously at play. Let us first consider two generic nonlinear functions $f(u, v)$ and $g(u, v)$ describing the local dynamics

$$\begin{cases} \dot{u} &= f(u, v) \\ \dot{v} &= g(u, v) \end{cases} . \tag{6.28}$$

Then assume to replicate such system on all the nodes of a given hypergraphs, and label u_i and v_i the corresponding concentrations. Here, the index i refers to the specific node to which the dynamical variables are bound. Finally, assume that two nodes, i and j, communicate if they belong to the same hyperedge and moreover the strength of the interaction (which results into an effective transport across the involved nodes) is mediated by both the number of shared hyperedges and their sizes. Indeed, nodes belonging to the same hyperedge exhibit a higher-order interaction and we consequently assume that spreading among them is more probable than with nodes associated with other hyperedges or smaller ones. From a microscopic point of view, imagine to deal with a walker belonging to a given node. The walker assigns to all its neighbours a weight that gauges the size of the hyperedges and the number of incident hyperedges, and then performs a jump with a probability proportional to this weight. This represents a higher-order extension of Ficks' law: the rate of change of u_i is proportional to

$$\dot{u}_i \sim \sum_{\alpha : i \in E_\alpha} \sum_{j \in E_\alpha, j \neq i} (C_{\alpha\,\alpha} - 1)(u_i - u_j) \,, \tag{6.29}$$

where use has been made of matrix $\mathbf{C}$, as introduced above. Recalling the definition of $e_{i\alpha}$, one can rewrite the previous formula as

$$\begin{aligned}\dot{u}_i &\sim \sum_{\alpha,j} e_{i\alpha}e_{j\alpha}(C_{\alpha\,\alpha}-1)(u_i-u_j)\\ &= \sum_j k_{ij}^H(u_i-u_j) = \sum_j \left(\delta_{ij}k_i^H - k_{ij}^H\right)u_j = \sum_j L_{ij}^H u_j\,, \end{aligned} \quad (6.30)$$

where we have used the definition of $k_i^H = \sum_j k_{ij}^H$ and L_{ij}^H.

Hence, in conclusion a reaction-diffusion process on hypergraphs, where the diffusion takes into account the higher-order interactions among nodes in the same hyperedge, can be described by the following system

$$\begin{cases} \dot{u}_i &= f(u_i,v_i) + D_u \sum_j L_{ij}^H u_j \\ \dot{v}_i &= g(u_i,v_i) + D_v \sum_j L_{ij}^H v_j \end{cases}, \quad (6.31)$$

where D_u and D_v are the diffusion coefficients of species u and v. At first sight, the above model seems to solely account for binary interactions. However, higher-order interactions are also present, as encoded in the matrix $\mathbf{L}^H$. This is thus a compact formalism allowing to overcome the computational issues intrinsic to simplicial complexes. Finally, let us observe that if the hypergraph is a network, i.e. the hyperedges have size 2, $|E_\alpha| = 2 \quad \forall\alpha$, then $\mathbf{L}^H$ reduces to the standard Laplace matrix. Thus (6.31) converges to the standard reaction-diffusion system defined on a network.

The condition for the emergence of a Turing instability can be detected by performing a linear stability analysis about the homogeneous equilibrium. More precisely, the latter is assumed to be stable with respect to homogeneous perturbations, while it loses its stability for heterogeneous perturbations once diffusion is at play, i. e. $D_u > 0$ and $D_v > 0$. The linear stability analysis can be performed by following the standard procedure: (i) by linearising the model (6.31) around the equilibrium, $(u_i, v_i) = (\bar{u}, \bar{v})$ for all i; (ii) by expanding the perturbations on the eigenbasis of $\mathbf{L}^H$, and (iii) by calculating the dispersion relation, i.e. the linear growth rate $\lambda_\alpha = \lambda(\Lambda_H^\alpha)$ of the eigenmode α as a function of the Laplacian eigenvalue Λ_H^α. The linear growth rate is the real part of the largest root of the second order equation

$$\lambda_\alpha^2 - \lambda_\alpha\left[tr\mathbf{J}_0 + \Lambda_H^\alpha(D_u+D_v)\right] + \det\mathbf{J}_0 + \Lambda_H^\alpha(D_u\partial_v g + D_v\partial_u f) + D_uD_v(\Lambda_H^\alpha)^2 = 0\,, \quad (6.32)$$

where $\mathbf{J}_0 = \begin{pmatrix} \partial_u f & \partial_v f \\ \partial_u g & \partial_v g \end{pmatrix}$ is the Jacobian matrix of the reaction part evaluated at the equilibrium $(u_i, v_i) = (\bar{u}, \bar{v})$, tr (resp. det) is its trace (resp. determinant). The concept of dispersion relation is close to that of Lyapunov exponent: the existence of eigenvalues Λ_H^α for which the dispersion relation takes positive values, implies that the system goes unstable via a typical path first identified by Alan Turing in his seminal work. At variance, if the dispersion relation is negative, the system cannot undergo a Turing instability: any tiny perturbation fades away and the system settles back to the homogeneous equilibrium.

To provide a concrete example, we assume the reaction kinetic to be modelled by the Brusselator scheme [151, 164]. This is a nonlinear model defined by $f(u, v) = 1 - (b + 1)u + cu^2v$ and $g(u, v) = bu - cu^2v$, where b and c act as tunable parameters. We first show an example of Turing pattern emerging in both the hypergraph and projected network (the same used in the previous section). In the main panels of Fig. 6.5 the dispersion relations are reported: a subset of eigenvalues exist which is associated to positive values of the relation dispersion, for both the hypergraph -(panel (a))- and the projected network -(panel (b)). In the insets of Fig. 6.5 we display the ensuing patterns. Nodes are ordered for increasing hyper degree (resp. degree) for the hypergraph (resp. the projected network). One can clearly observe that, in the case of the hypergraph, patterns are strongly localised in nodes associated to larger hyper degree.

From Fig. 6.5 one can also observe that the domain of the eigenvalues for the hypergraph covers a much wider range, as compared to that associated projected network. This observation can open the way to settings where patterns emerge only for systems defined on top of hypergraphs and not on the corrsponding projected networks. In this case, patterns are the result of the higher-order interaction among nodes. To challenge this scenario, let us thus consider a small network built using the Barabási-Albert algorithm [5] with 20 nodes. For each iteration of the generative algorithm, 3 new nodes are attached to the already existing ones, according to a preferential attachment scheme; because of the small size of the network, our goal here is not to resolve the scale free nature of the network but to obtain a hierarchical structure where 3-cliques, and larger ones, are mutually connected. We identify the complete cliques and build the associated hypergraph by assuming each m-clique to form a hyperedge of size m. We then turn to consider the resulting hypergraph and the associated projected network as the underlying

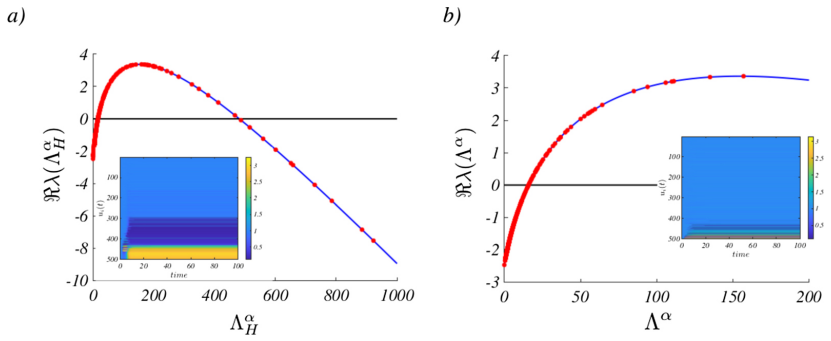

Figure 6.5: **Turing patterns on hypergraphs**. Main panels: The **Dispersion relation** for the Brusselator model defined on the hypergraph (panel (a)) and the projected network (panel (b)). One can observe that in both cases there are eigenvalues for which the dispersion relation is positive (red dots); the blue line represent the dispersion relation for the Brusselator model defined on a continuous regular support. Being both Laplace matrices symmetric, the dispersion relation computed for the discrete spectra lies on top pf the one for the continuous support. Insets: The **Turing Patterns** on the hypergraph (panel (a)) and the projected network (panel (b)). We report the time evolution of the concentration of the species $u_i(t)$ in each node as a function of time, by using an appropriate colour code (yellow associated to large values, blue to small ones). In the former case nodes are ordered for increasing hyper degree while in the second panel for increasing degree. One can hence conclude that nodes associated to large hyper degrees display a large concentration amount for species u_i. This yields a very localised pattern. The hypergraph and the projected network are the same used in Fig. 6.1.

support for the dynamics (6.31). The dispersion relations can be computed (see main panels of Fig. 6.6): observe that the homogenous equilibrium is stable even in presence of diffusion on the network while it looses its stability in the case of the hypergraph. In this latter setting, the Turing patterns are hence expected to develop. This can be checked by computing the time evolution of the species density $u_i(t)$ both on the hypergraph and the projected network. By inspection of Fig. 6.6, one can appreciate that heterogenous patterns develop in the former case (see inset in the panel (a) of Fig. 6.6). Patterns are instead lacking in the latter scenario, i.e. when the Brusselator

model hosted on the projected network (see inset in the panel (b) of Fig. 6.6).

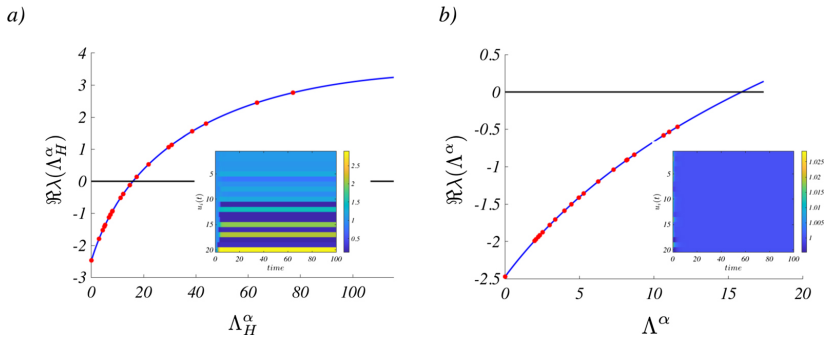

Figure 6.6: **Many body induced Turing patterns**. Main panels: The **Relation dispersion** for the Brusselator model defined on the hypergraph (panel (a)) and the projected network (panel (b)). In the former case eigenvalues are found for which the dispersion relation is positive (red dots) while for the system defined on the projected network this conclusion does not hold. The blue line represents again the dispersion relation for the Brusselator model on a continuous support. Insets: because the condition for Turing instability is satisfied for the hypergraph Laplace matrix, **Turing Patterns** emerge on the hypergraph (panel (a)). At variance, patterns do not manifest on the projected network (panel (b)). We report the time evolution of the concentration of species $u_i(t)$, on each node, as a function of time by using a proper colour code (yellow associated to large values, blue to small ones). In the former case nodes are ordered for increasing hyper degree while in the latter for increasing degree. The hypergraph and the projected network are obtained by means of the Barabási-Albert algorithm [5] with 20 nodes. Every iteration, 3 newly nodes are attached to the existing ones.

6.2.2 Synchronisation of Stuart-Landau oscillators on hypergraphs

In the previous section we studied the emergence of Turing patterns for reaction-diffusion systems defined on a hypergraph so as to account for many body interactions. These patterns originate from a symmetry breaking instability induced by an externally imposed perturbation acting on systems initially close to a stationary homogeneous equilibrium. In many relevant

problems, systems display periodic solutions. It is therefore important to investigate the stability of isolated periodic orbits and, even more essential, to study the dynamics of extended systems which combine several replicas of the same nonlinear oscillators. Imagine that individual oscillators are evolving in phase and introduce a non homogeneous perturbation. If the system is globally stable, the perturbation gets eventually re-absorbed and the oscillators display a synchronous dynamics [12]. Otherwise, the perturbation develops in time and the system evolves towards a distinct, heterogeneous, attractor.

To study the synchronisation via a hypergraph, we consider individual units obeying to a Stuart-Landau (SL) equation [111,174]. This is a paradigmatic model of nonlinear oscillators, often invoked for modelling a wide range of phenomena, from nonlinear waves to second-order phase transitions, from superconductivity and superfluidity to Bose-Einstein condensation [10]. Besides, the SL equation can be considered as a normal form for systems close to a supercritical Hopf-bifurcation. In this respect, the results here presented are more general than the specific setting explored.

Consider an ensemble made of n nonlinear oscillators and label with W_i their associated complex amplitude. Each oscillator obeys a complex Stuart-Landau equation

$$\frac{d}{dt}W_j = W_j - (1 + ic_2)|W_j|^2 W_j \,,$$

where c_2 is a real parameter and $i = \sqrt{-1}$. Let us observe that the former admits the limit cycle solution $W_{LC}(t) = e^{-ic_2 t}$.

We then assume the oscillators to be coupled via a many body diffusive-like interaction which can be described by the discrete Laplacian matrix (2.25), returning thus the system

$$\frac{d}{dt}W_j = W_j - (1 + ic_2)|W_j|^2 W_j - (1 + ic_1)K \sum_k L^H_{jk} W_k \,, \tag{6.33}$$

where c_1 is a second real parameters and K is a suitable parameter setting the coupling strength. Based on the properties of the Laplace matrix, one can prove that the limit cycle solution, $W_{LC}(t)$, is also a solution of (6.33). To characterise the stability of the latter to heterogeneous perturbation, we rewrite W_j using polar coordinates as:

$$W_j(t) = W_{LC}[1 + \rho_j(t)]e^{i\theta_j(t)} \,. \tag{6.34}$$

Assuming $|\rho_i(t)|$ and $|\theta_i(t)|$ to be small, one can insert (6.34) into (6.33) and then linearise the resulting equation, to get:

$$\frac{d}{dt}\begin{pmatrix}\rho_j\\ \theta_j\end{pmatrix} = \begin{pmatrix}-2 & 0\\ -2c_2 & 0\end{pmatrix}\begin{pmatrix}\rho_j\\ \theta_j\end{pmatrix} - K\begin{pmatrix}1 & -c_1\\ c_1 & 1\end{pmatrix}\sum_k L^H_{jk}\begin{pmatrix}\rho_k\\ \theta_k\end{pmatrix}. \qquad (6.35)$$

Remark that, even if we are perturbing around a limit cycle, namely a time dependent solution, the coefficients of the linearised equations do not depend on time, owing to the specific structure of the GL equation. This observation will simplify the successive analysis, which will follow closely that discussed in the preceding section for the case of a Turing instability. In the next section we will instead deal with a problem for which the linearised dynamics yields a time dependent Jacobian.

To proceed further we expand the perturbations ρ_j and θ_j on the Laplacian eigenvectors basis

$$\begin{pmatrix}\rho_j\\ \theta_j\end{pmatrix} = \sum_{\alpha=1}^{n}\begin{pmatrix}\rho_\alpha\\ \theta_\alpha\end{pmatrix}\phi_j^\alpha\,, \qquad (6.36)$$

and inserting the latter into (6.35), and by using the orthonormality of the eigenvectors, we obtain:

$$\frac{d}{dt}\begin{pmatrix}\rho_\alpha\\ \theta_\alpha\end{pmatrix} = \begin{pmatrix}-2 & 0\\ -2c_2 & 0\end{pmatrix}\begin{pmatrix}\rho_\alpha\\ \theta_\alpha\end{pmatrix} - K\Lambda^H_\alpha\begin{pmatrix}1 & -c_1\\ c_1 & 1\end{pmatrix}\begin{pmatrix}\rho_\alpha\\ \theta_\alpha\end{pmatrix}. \qquad (6.37)$$

We put forward the ansatz of exponential growth for each mode, that is $\rho_\alpha \sim e^{\lambda_\alpha t}$ and $\theta_\alpha \sim e^{\lambda_\alpha t}$ and we eventually obtain a condition formally equivalent to the dispersion relation

$$\lambda(\Lambda^\alpha) = -(1+K\Lambda^\alpha) + \sqrt{(1+K\Lambda^\alpha)^2 - K\Lambda^\alpha\left[2(c_1c_2+1)+(1+c_1^2)K\Lambda^\alpha\right]}\,. \qquad (6.38)$$

Let us observe that $\lambda(\Lambda^1)=0$, signifying that the reference orbit is a limit cycle and thus neutrally stable. On the other hand if $\mathrm{Re}\,\lambda(\Lambda^\alpha)$ is positive for some $\alpha > 1$, the perturbation grows exponentially in time, and the initial homogeneous state proves unstable. Conversely, if $\mathrm{Re}\,\lambda(\Lambda^\alpha) < 0$, for every α, the perturbation fades away and the system converges back to the fully synchronised state. Expanding (6.38) for small $K\Lambda^\alpha$ we get

$$\lambda(\Lambda^\alpha) \sim -K\Lambda^\alpha(1+c_1c_2) + \dots\,,$$

By recalling that $\lambda(0)=0$, $K>0$ and $\Lambda^\alpha > 0$ for $\alpha > 1$, one can conclude [41] that $\lambda(\Lambda^\alpha) > 0$ for some α if and only if $1 + c_1c_2 < 0$, that

is a necessary and sufficient condition for the loss of stability of the fully synchronised solution.

The numerical results reported in Fig. 6.7 complement the previous analytical theory. In panel (a) of Fig. 6.7 we present the dispersion relation and the heterogeneous patterns emerging for both the hypergraph and the associated projected network, for $K = 1$, $c_1 = 0.5$ and $c_2 = -10$. The dispersion relation is positive over a finite domain and the patterns (represented by $\mathrm{Re}\, W_j(t)$) that develop as follow the instability are pretty localised. In panel (b) of Fig. 6.7, the parameters are set to the values $K = 1$, $c_1 = 1$ and $c_2 = -0.9$. The dispersion relation is non positive and the system displays synchronised oscillations: the imposed perturbation dies out and the oscillators evolve at unison.

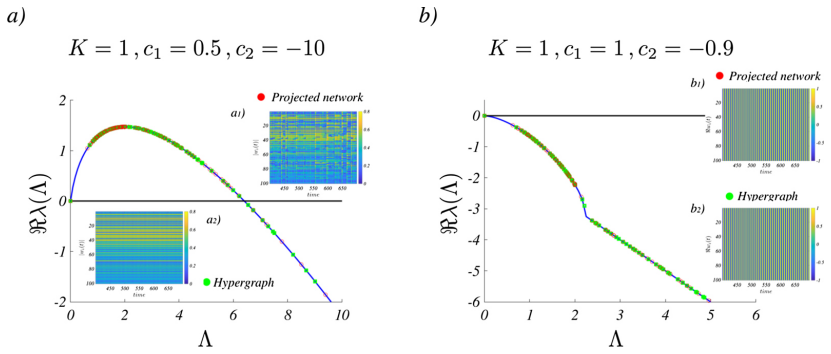

Figure 6.7: **Synchronisation for Stuart-Landau system**. Main panels: The **Relation dispersion** for the Stuart-Landau system defined on the hypergraph and the projected network is shown for two sets of parameters. In panel (a) ($K = 1$, $c_1 = 0.5$ and $c_2 = 10$) this choice yields to a loss of synchronisation. Indeed there are eigenvalues associated to positive values of the dispersion relation and the resulting patterns are heterogeneous (see insets (a_1) for the projected network and (a_2) for the hypergraph). In both insets nodes are ordered for increasing hyper degree, resp. degree, for hypergraph, resp. projected network. The localisation is stronger when the dynamics is hosted on the ypergraph. In panel (b) the chosen parameters ($K = 1$, $c_1 = 1$ and $c_2 = -0.9$) result in the emergence of a globally synchronised state, the dispersion relation being always negative. This can be appreciated by looking at the insets ((b_1) for the projected network and (b_2) for the hypergraph) where we report $\mathrm{Re}\, W_j$ as function of time.

6.2.3 Master Stability Function on hypergraphs

In the previous section we have analysed the synchronisation of an ensemble of Stuart-Landau (SL) oscillators defined on a hypergraphs. To this end we employed a straightforward generalisation of the techniques presented in the section 6.2.1, when investigating the emergence of Turing patterns. The use of the dispersion relation has been made possible because, for coupled SL equations, the variational problem yields a time independent Jacobian, once evaluated on the periodic homogeneous solution (6.35). This is not true for generic nonlinear oscillators. To overcome this problem one can however resort to the formalism of the Master Stability Function (MSF) [159], as introduced above. The aim of this section is thus to study the MSF in its fully generality for systems defined on hypergraph. In particular, we will set to analyse the to the hypergraph and thus to study the synchronisation of nonlinear chaotic oscillators coupled through a hypergraph and compare the outcome of the analysis to that obtained when operating the system on the corresponding projected network.

Let us consider again (6.27) ans replace now in the latter equation $\varepsilon\Lambda_\alpha$ by a generic parameter $\kappa > 0$ and thus also the projection $\delta\mathbf{y}_\alpha$ by a generic "perturbation" vector $\delta\mathbf{y}$

$$\frac{d\delta\mathbf{y}}{dt} = [D\mathbf{F}(\mathbf{s}) - \kappa D\mathbf{G}(\mathbf{s})]\,\delta\mathbf{y}\,. \tag{6.39}$$

The largest Lyapunov exponent of Eq. (6.39) is called the Master Stability Function [159]. Let us denote it by $\lambda(\kappa)$ to emphasise its dependence on the parameter $\kappa > 0$. If for all κ, $\lambda(\kappa) < 0$, then $\delta\mathbf{y}$ decays to 0. At variance, if there exists $\kappa > 0$ such that $\lambda(\kappa) > 0$, then $\delta\mathbf{y}$ will grow. Back to Eq. (6.27) one can conclude that if for a given ε there exists α such that $\lambda(\varepsilon\Lambda_\alpha) > 0$, then the associated $\delta\mathbf{y}_\alpha$ grows in time. Thus individual units deviate from the reference solution $\mathbf{s}(t)$. On the other hand if for all α one has $\lambda(\varepsilon\Lambda_\alpha) < 0$ then the system reaches a globally synchronised state: all units will follow at the unison the same chaotic orbit. Let us observe that $\lambda(0) > 0$ being the reference orbit, $\mathbf{s}(t)$, a chaotic one.

To procees in the analysis we assume linear coupling functions [98]: in this way the MSF simplifies, since $D\mathbf{G}$ is a constant matrix. Moreover, we will assume the matrix $D\mathbf{G}$ to have only one non zero element, say DG_{ba}, denoting a coupling between the a–th and the b-th component of $\mathbf{x}$.

Let us observe that the variational equation still contain explicitly the time variable through the Jacobian of the reaction part, $D\mathbf{F}(\mathbf{s}(t))$, which

is indeed evaluated on the chaotic orbit. Hence to compute the MSF we have to solve a non autonomous system of ODEs, to study the evolution of the norm of $\delta\mathbf{y}(t)$ and then use the definition of the maximum Lyapunov exponent $\lambda(\kappa) = \lim_{t\to\infty} \frac{\log ||\delta\mathbf{y}(t)||}{t}$. This can result in a tricky exercise. Indeed if $\lambda(\kappa) > 0$ then the norm can quickly increase to produce an overflow. On the other hand if $\lambda(\kappa) < 0$, then $||\delta\mathbf{y}(t)||$ shrinks below round-off error. For this reason we employed in our analysis the *Mean Exponential Growth of Nearby Orbits*, (MEGNO) [47, 48]. This is an improved chaos indicator that allows to rapidly discriminate between chaotic and regular orbits. The method allows for the Lyapunov exponent to be consequently recovered. For these reasons, MEGNO has been largely used in the framework of planetary systems [83, 119], satellites and spatial debris [50, 99, 180] and also generic nonlinear dynamical systems [47]. The method overcomes the above mentioned issues being based on a sort of time average of the norm of the deviation vector (see Appendix B.1).

Without loss of generality we will use the Lorenz model [121] for a demonstrative application:

$$\begin{cases} \dot{x} &= \sigma(y - x) \\ \dot{y} &= x(\rho - z) - y \\ \dot{z} &= xy - \beta z\,. \end{cases} \tag{6.40}$$

In the following we will fix the model parameters to the "standard values", $\beta = 2$, $\sigma = 10$ and $\rho = 28$. Once we couple the above ODE using high-order interactions, i.e. the hypergraph, we get

$$\frac{d}{dt}\begin{pmatrix} x_i \\ y_i \\ z_i \end{pmatrix} = \begin{pmatrix} \sigma(y_i - x_i) \\ x_i(\rho - z_i) - y_i \\ x_i y_i - \beta z_i \end{pmatrix} - \sigma \sum_j L^H_{ij} \mathbf{E} \begin{pmatrix} x_j \\ y_j \\ z_j \end{pmatrix}, \tag{6.41}$$

where the constant 3×3 matrix $\mathbf{E}$ encodes the coupling among the three variables and its entries take values 0 has only a non zero en or 1try by hypothesis. For instance if $E_{21} = 1$, (noted for short $1 \to 2$) then the growth rate of the second variable, y, depends of the first one, x, that is $\dot{y}_i \sim -\varepsilon \sum_j L^H_{ij} x_j$ (discarding the reaction part).

We are now in a position to adapt the above described theory, i.e. linearise about the reference orbit and project the perturbation on the eigenbase of the Laplace matrix, to rewrite (6.27) for the Lorenz system and eventually compute the MSF to check the stability property of the chaotic Lorenz oscillator. In the main panel of Figs. 6.8 we report the MSF for the coupling scheme, $1 \to 1$, that in the classification proposed in [98] corresponds to the

class Γ_1, namely the MSF is monotone decreasing and it has a single root, for two values of the coupling strength $\varepsilon = 3$ (panel (a)) and $\varepsilon = 10$ (panel (b)). For (sufficiently) small coupling strength (panel (a)), the MSF evaluated on the discrete spectrum of the Laplace matrix for the hypergraph (green dots) is always negative and thus the system synchronises to the chaotic reference orbit as shown in the inset (a_2). On the other hand the MSF for the projected network (red dots) takes positive values: the chaotic oscillators cannot synchronise, as we can appreciate in the inset (a_1). For large enough coupling strength (panel (b)) both spectra yield a negative MSF (green and red dots in panel (b)) and hence, in both cases, the systems do synchronise (see insets (b_1) and (b_2)).

From these results one can draw a first conclusion. Once we fix the coupling strength ε, the sign of the MSF depends on the spectrum of the Laplace matrix for the hypergraph, $\mathbf{L}^H$. Similarly for the projected network. However, as we observed in Section 6.1 the eigenvalues of the hypergraph Laplacian extend over a large portion of the real axis, as compared to what it happens when considering the projected network. Hence the coupling scheme $1 \to 1$ favours the synchronisation on the hypergraph, provided the coupling strength is sufficiently small. Said figuratively, one can act on the "knob" ε and have the spectra to slide on the MSF: by prograssively reducing the value of ε one can force the spectrum of the projected network to enter the zone where the MSF is positive, whereas for the same value of ε the spectrum of the hypergraph is still associated to a negative MSF.

In Fig. 6.9 we report a similar analysis for the coupling schemes $1 \to 2$ (panel (a)) and $3 \to 3$ (panel (b)). In the classification proposed in [98] the former corresponds the class Γ_2, two zeros, while the latter to Γ_3, three zeros. From the results shown in the Figure, one can conclude that the system behaves similarly for couplings $3 \to 3$ and $1 \to 1$: if the coupling is sufficiently large (here $\varepsilon = 20$) synchronisation is found on the hypergraph but not on the corresponding projected network. This generalises our previous observation to all couplings belonging to an odd class Γ_{2m+1}.

The reported behaviour is reversed once we consider coupling that belong to an even class. As we can appreciate in Fig. 6.9 panel (a)) one can chose a sufficiently small coupling to have the MSF negative on the projected network (red dots), while it takes also positive values, when the problem formulated on the hypergraph (green dots).

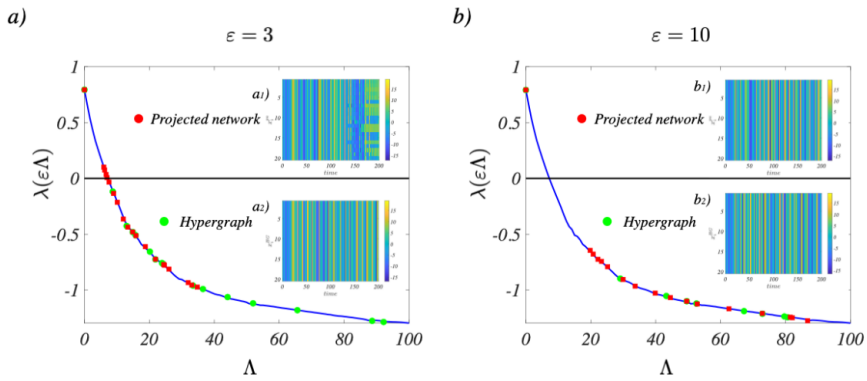

Figure 6.8: **Master Stability Function and synchronisation for the Lorenz system I**. We report the MSF for the Lorenz model for linear couplings, $1 \to 1$ (main panels) and two choices of the coupling strengths $\varepsilon = 3$ ((a) panel) and $\varepsilon = 10$ (panel (b)). For a small coupling strength (panel (a)), the MSF is negative in correspondence of the eigenvalues of the Laplace matrix defined on the hypergraph (green dots), while the MSF can assume positive values once evaluated on the spectrum of the Laplace matrix for the projected network (red dots). In the former case, the system synchronises (see inset (a_2)) while in the latter it does not (see inset (a_1)). For larger coupling strengths (panel (b)) the MSF is negative for both the hypergraph and the projected network and thus, in both cases, the systems do synchronise (see insets (b_1) and (b_2)).

6.3 Conclusion

In this work we took a step forward in modelling dynamical systems processes on networks. The aim of the work is to account for high-order interactions among coupled units. In particular we focused on the hypergraphs, a very versatile setting where to model systems endowed with many-body interactions. Indeed one can easily represent such high-order interactions via the hyperedge, so as to overcome the limitations intrinsic to dealing with binary exchanges. Starting from a microscopic process which takes place on the hypergraph, i.e. a random walk biases toward the size and the number of hyperedges a node belongs to, we defined a new combinatorial Laplace operator which generalises the concept of diffusive interaction to a multi-

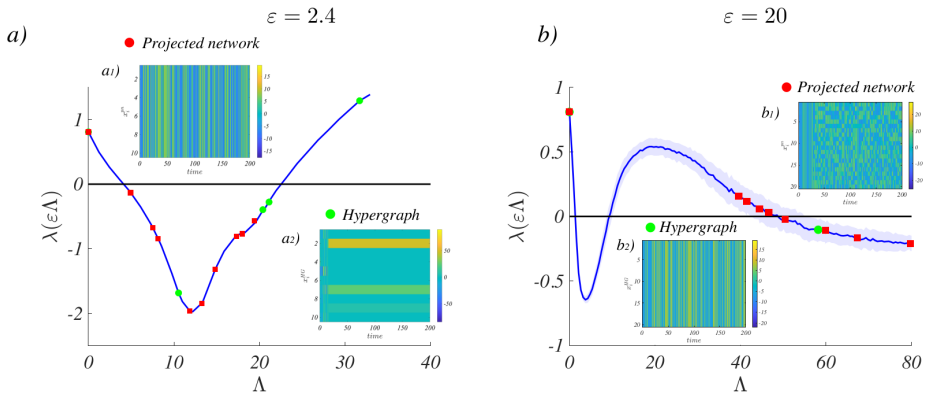

Figure 6.9: **Master Stability Function and patterns for the Lorenz system II**. We report the MSF for the Lorenz model using the linear couplings, $1 \to 2$ (panel (a)) and $3 \to 3$ (panel (b)). In the former case we can observe that, for the chosen value of the coupling strength, $\varepsilon = 2.4$, the projected network yields a negative MSF (red dots) and thus the system synchronises (inset (a_1)). Conversely, the hypergraph possesses unstable eigenmodes (green dots) and the systems goes consequently unstable (inset (a_2)). The opposite behaviour is displayed in the case of the $3 \to 3$ coupling for $\varepsilon = 20$ (panel (b)): here the projected network exhibits unstable eigenmodes (red dots) while the hypergraph shows a negative MSF (green dots). The inset (b_1) testifies on the absence of synchronisation for the projected network, while in the inset (b_2) synchronisation is shown to occur on the hypergraph. Due to the coupling, the MSF is less regular in the case shown in the panel (b), we thus reported the average of the MSF (blue curve) computed over 200 independent simulations and the associated standard deviation (light blue area).

dimensional setting. This operator reduces to the standard combinatorial Laplacian once the hypergraph converges back to an ordinary network. In this respect, the newly introduced Laplacian can be rationalised as a natural extension of the usual operator. In this framework we considered dynamical systems defined on top of hypergraphs and analysed the stability of the associated homogeneous equilibria. In particular we extended the Master Stability Function to this formalism and investigated the specificity of

Turing patterns for the generalised proxy of reaction-diffusion systems on hypergraphs. We also analysed the synchronisation of periodic and chaotic orbits, shedding light on the role exerted by high-order couplings. In all the analysed cases, the spectral property of the novel Laplace operator are central in shaping the ensuing patters, which appear remarkably localised, as illustrated with reference to the Turing setting. Further, hypergraphs can enhance or impede the synchronisation, as compared to what it happens on the corresponding projected network, depending on the specificity of the imposed couplings.

Chapter 7

Conclusion

Many real-world phenomena, from physics to biology, passing through social science, can be qualitatively described via dynamical models hosted on networks. In this respect, network science is a powerful tool to investigate the behavior arising from such systems, whenever networks constitute the underlying support of the dynamics. Stochastic contributions must be considered when formulating realistic models of complex systems: macroscopic order can emerge from the microscopic disorder and noise can completely change the behavior predicted following a deterministic approach.

In this thesis we examined various reaction-diffusion models with a special consideration for the role of the noise, which can be either external to the system or intrinsically related to it. Finite size corrections represent a source of endogeneous noise which can significantly affect the dynamics of the investigated systems. This topic represent the main part of Chapter 3, where a simplified version of the celebrated Wilson-Cowan model hosted on a triangular loop made of three nodes is presented. The stochastic component, due to demographic noise, boosts the emergence of quasicycles whose amplitude increases with the reactivity index, a parameter that quantifies the short-time growth of the norm of an imposed perturbation. Quasicycles are often characterized by small amplitude oscillations and broad signal in the power spectrum; our work overcome these gaps, resulting in a possible strategy to amplify noise-assisted oscillations.

Non-normality and reactivity proved to be essential to enhance stochastic oscillations. This observation was also confirmed in Chapter 4 where we

considered a two-species models arranged on the diffusively coupled nodes of a directed lattice. Carrying on the above premises, we studied the interplay between the degree of non-normality and the degeneracy in the spectrum of the Jacobian matrix, which reflects the structure of the couplings between adjacent nodes. Self-organized patterns are observed as consequence of the strong amplification process of the noise along the lattice, due to the organization of the Laplacian eigenvalues that overlap on the same point. This allowed us to generalize the result to a quasi-degenerate lattice, in the sense that the eigenvalues accumulates in a compact region (a point, potentially) of the complex plane. The eigenmodes associated to a quasi-degenerate spectrum represent thus a route to drive instability. Our first algorithm of network generation arose starting from this observation: the idea is to generate networks assembling nodes in such a way that the associated Laplacian possesses a quasi-degenerate spectrum. The networks obtained with this procedure are distorted one-dimensional directed chains and belong to the class of the so called random directed acyclic graphs (DAG).

Network generation is an interesting challenge in research community. The stability of many dynamical systems is related to the spectrum of the Laplacian matrices associated to the underlying networks. Designing network with desired Laplacian spectrum is the subject of Chapter 5 where we provide a recipe to construct a graph with any desired set of Laplacian eigenvalues. Our result represents the generalization of an existing method to generate undirected network with, by construction, real Laplacian spectrum. The networks obtained are directed and fully connected; since complete graphs can be difficult to realize physically, we presented two sparsification methods to remove unessential links from the original networks, without altering the structure of the underlying adjacency matrices. The effects of these procedures are investigated simulating two models of oscillators hosted on top of the sparsified networks. In a particular case of working setting, we were able to compute analytical expressions of the recovered Laplacians and derivate conditions to guarantee positive entries for that matrices.

The aim of Chapter 6 was to expand our research to high-order structures, in particular to hypergraphs. We started defining a new combinatorial Laplace operator which generalises the concept of diffusive interaction to this multidimensional setting. In this framework we considered dynamical systems defined on top of hypergraphs and, to analyze the stability of the associated homogeneous equilibria, we employed the Master Stability Func-

tion. Further, we analysed the synchronisation of periodic and chaotic orbits. The spectral properties of the Laplacian proved fundamental in studying the evolution of such dynamical models. For this reason, we were interested in predicting localization properties of the eigenmodes via the perturbation theory. We showed the comparison between the true Laplacian eigenvalues computed by direct numerical analysis and the approximated quantities, up to the zeroth- and the second-order, obtained applying the perturbation theory to the Laplacian matrix. The results were in good agremeent with the original eigenvalues, and the theory provided an accurate estimate already at the zeroth-order. In future we want to extend this analysis to Laplacian eigenvectors, in order to to predict their localization property, developing a novel research field with several possible applications.

Appendix A

Generating directed networks: supplementary materials

A.1 On the explicit expression of S

Given two arbitrary constants α and β the following identity holds

$$(I + \alpha E)(I + \beta E) = I + (\alpha + \beta)E + \alpha\beta E^2 \tag{A.1}$$

for every matrix E. If E is the matrix defined in (5.8) one gets:

$$E^2 = NE \tag{A.2}$$

and then

$$(I + \alpha E)(I + \beta E) = I + (\alpha + \beta + \alpha\beta N)E \tag{A.3}$$

If $\beta = -\frac{\alpha}{1+\alpha N}$, from (A.3) we get

$$(I + \alpha E)^{-1} = (I + \beta E) \tag{A.4}$$

The above result can be used to derive the structure of matrix S, as reported in the main body of the paper. To do this end we begin by rewriting the matrices A and B as

$$A = [(1 - i)E - iI]U = -i[I + (i + 1)E]U \tag{A.5}$$

$$B = [(i + 1)E + iI]U = i[I + (1 - i)E]U \tag{A.6}$$

From (A.4) we obtain

$$B^{-1} = -iU^{-1}[I + (i+1)E]^{-1} = -iU^{-1}\left[I + \frac{i-1}{1+(1-i)N}E\right] \tag{A.7}$$

and then, after some calculations, we get

$$\begin{aligned} B + AB^{-1}A &= i\left[I + (1-i)E + I + \frac{3i + 2iN + 1}{1+(1-i)N}E\right]U \\ &= 2i\left[I + \frac{1+i}{1+(1-i)N}E\right]U \end{aligned}$$

In conclusion

$$\begin{gathered} S = (B + AB^{-1}A)^{-1} = \\ -\frac{i}{2}U^{-1}\left[I - \frac{1+i}{1+2N}E\right] \end{gathered}$$

because of

$$\left[I + \frac{1+i}{1+(1-i)N}E\right]^{-1} = \left[I - \frac{1+i}{1+2N}E\right] \tag{A.8}$$

which proves the results.

A.2 About the computation of L_{ij}

The aim of this section is to detail the computations needed to obtain explicitly the entries of the Laplace matrix L under the assumption $U = qI$ starting thus from Eqs. (5.16) and (5.18).

Let us begin by computing the diagonal elements of L , namely L_{ii} for $i = 1, .., N,$. For $i = 1$, one gets:

$$L_{11} = \sum_{k=2}^{N+1} V_{1k} D_{kk} W_{k1} \tag{A.9}$$

From (5.4) and (5.6) we obtain for $k = 2, \ldots, N+1$:

$$V_{1k} = -1 - i \tag{A.10}$$

$$W_{k1} = \frac{-1+i}{2(2N+1)} \tag{A.11}$$

Then

$$L_{11} = 2\sum_{k=2}^{N+1} Re\left[(-1-i)D_{kk}\frac{-1+i}{2(2N+1)}\right] \quad (A.12)$$

$$= 2\sum_{k=2}^{N+1} Re\left[D_{kk}(-1-i)\frac{-1+i}{2(2N+1)}\right] \quad (A.13)$$

$$= \frac{2}{2N+1}\sum_{k=2}^{N+1}\alpha_k \quad (A.14)$$

where use has been made of the identity $Re(D_{kk}) = \alpha_k$.

We can proceed in analogy for the others diagonal elements of the Laplacian matrix. In particular, for $s = 2, \ldots, N+1$, we have that

$$W_{ss} = S_{ss} = \frac{-2Ni-1}{2(2N+1)}, \quad (A.15)$$

and then

$$L_{ss} = 2\sum_{k=2}^{N+1} Re[D_{kk}V_{sk}W_{ks}] \quad (A.16)$$

$$= 2Re(D_{ss}V_{ss}W_{ss}) \quad (A.17)$$

$$= 2Re\left[(\alpha_s + i\beta_s)i\frac{-2Ni-1}{2(2N+1)}\right] \quad (A.18)$$

$$= \frac{2N\alpha_s + \beta_s}{2N+1} \quad (A.19)$$

Instead, for $s = N+2, \ldots, 2N+1$, we have

$$W_{ss} = iS_{ss} = i\frac{-2Ni-1}{2(2N+1)}, \quad (A.20)$$

and consequently:

$$L_{ss} = 2Re\left[(\alpha_s - i\beta_s)i\frac{-2Ni-1}{2(2N+1)}\right] \quad (A.21)$$

$$= \frac{2N\alpha_s - \beta_s}{2N+1} \quad (A.22)$$

Let us proceed now with the other elements of the first row of L. For

$t = 2, \ldots, N+1$ we can write

$$\begin{aligned}
L_{1t} &= 2\sum_{k=2}^{N+1} Re(V_{1k}D_{kk}W_{kt}) && \text{(A.23)}\\
&= 2\Big[Re(V_{1t}D_{tt}W_{tt}) + \sum_{k=2,k\neq t}^{N+1} Re(V_{1k}D_{kk}W_{kt})\Big] && \text{(A.24)}\\
&= 2\Big\{Re\Big[(-1-i)(\alpha_t+i\beta_t)\frac{-2Ni-1}{2(2N+1)}\Big] + && \text{(A.25)}\\
&\quad \sum_{k=2,k\neq t}^{N+1} Re\Big[(-1-i)(\alpha_k+i\beta_k)\frac{i-1}{2(2N+1)}\Big]\Big\} && \text{(A.26)}\\
&= \frac{1-2N}{1+2N}\alpha_t - \beta_t + \frac{2}{2N+1}\sum_{k=2,k\neq t}^{N+1}\alpha_k && \text{(A.27)}
\end{aligned}$$

and for $t = N+2, \ldots, 2N+1$ we get

$$\begin{aligned}
L_{1t} &= 2\Big\{Re\Big[(-1+i)(\alpha_t-i\beta_t)i\frac{-2Ni-1}{2(2N+1)}\Big] + && \text{(A.28)}\\
&\quad \sum_{k=N+2,k\neq t}^{2N+1} Re\Big[(-1+i)(\alpha_k-i\beta_k)i\frac{i-1}{2(2N+1)}\Big]\Big\} && \text{(A.29)}\\
&= \frac{1-2N}{1+2N}\alpha_t + \beta_t + \frac{2}{2N+1}\sum_{k=N+2,k\neq t}^{2N+1}\alpha_k && \text{(A.30)}\\
&= \frac{1-2N}{1+2N}\alpha_t + \beta_t + \frac{2}{2N+1}\sum_{k=2,k\neq t-N}^{N+1}\alpha_k && \text{(A.31)}
\end{aligned}$$

For $s = 2, \ldots, N+1$ and $t = N+2, \ldots, 2N+1$ with $t \neq s-N$, we get:

$$\begin{aligned}
L_{st} &= \sum_{k=2}^{2N+1} V_{sk}D_{kk}W_{kt} && \text{(A.32)}\\
&= V_{ss}D_{ss}W_{st} + V_{s,s+N}D_{s+N,s+N}W_{s+N,t} && \text{(A.33)}\\
&= i(\alpha_s+i\beta_s)(-i)\frac{-i-1}{2(2N+1)} + && \text{(A.34)}\\
&\quad (-i)(\alpha_s-i\beta_s)i\frac{i-1}{2(2N+1)} && \text{(A.35)}\\
&= \frac{-\alpha_s+\beta_s}{2N+1} && \text{(A.36)}
\end{aligned}$$

while, for $s = N+2, \ldots, 2N+1$ and $t = 2, \ldots, N+2$ with $t \neq s-N$, the following expression holds:

$$\begin{aligned} L_{st} &= V_{ss} D_{ss} W_{st} + V_{s,s-N} D_{s-N,s-N} W_{s-N,t} && \text{(A.37)} \\ &= (\alpha_s - i\beta_s)\frac{-i-1}{2(2N+1)} + (\alpha_s + i\beta_s)\frac{i-1}{2(2N+1)} && \text{(A.38)} \\ &= \frac{-\alpha_s - \beta_s}{2N+1} && \text{(A.39)} \end{aligned}$$

For $s = 2, \ldots, N+1$

$$\begin{aligned} L_{s,s+N} &= && \text{(A.40)} \\ & V_{ss} D_{ss} W_{s,s+N} + V_{s,s+N} D_{s+N,s+N} W_{s+N,s+N} && \text{(A.41)} \\ &= i(\alpha_s + i\beta_s)(-i)\frac{2Ni-1}{2(2N+1)} + && \text{(A.42)} \\ & (-i)(\alpha_s - i\beta_s) i \frac{-2Ni-1}{2(2N+1)} = && \text{(A.43)} \\ & \frac{-\alpha_s - 2N\beta_s}{2N+1} && \text{(A.44)} \end{aligned}$$

instead, for $s = N+2, \ldots, 2N+1$, we obtain:

$$\begin{aligned} L_{s,s-N} &= && \text{(A.45)} \\ & V_{ss} D_{ss} W_{s,s+N} + V_{s,s-N} D_{s-N,s-N} W_{s-N,s-N} && \text{(A.46)} \\ &= (\alpha_s - i\beta_s)\frac{2Ni-1}{2(2N+1)} + (\alpha_s + i\beta_s) i \frac{-2Ni-1}{2(2N+1)} = && \text{(A.47)} \\ & \frac{-\alpha_s + 2N\beta_s}{2N+1} && \text{(A.48)} \end{aligned}$$

For $t = 2, \ldots, N+1$

$$\begin{aligned} L_{t1} &= 2Re(V_{tt} D_{tt} W_{t1}) = && \text{(A.49)} \\ & 2Re\left[i(\alpha_t + i\beta_t)\frac{i-1}{2(2N+1)} \right] = && \text{(A.50)} \\ & \frac{-\alpha_t + \beta_t}{2N+1} && \text{(A.51)} \end{aligned}$$

and for $t = N+2, \ldots, 2N+1$

$$\begin{aligned} L_{t1} &= 2Re(V_{tt} D_{tt} W_{t1}) && \text{(A.52)} \\ &= 2Re\left[(\alpha_t - i\beta_t)\frac{-i-1}{2(2N+1)} \right] && \text{(A.53)} \\ &= \frac{-\alpha_t - \beta_t}{2N+1} && \text{(A.54)} \end{aligned}$$

For $t, s = 2, \ldots, N+1$ and $s \neq t$

$$L_{st} = 2Re(V_{ss} D_{ss} W_{st}) \quad (A.55)$$

$$= 2Re\left[i(\alpha_s + i\beta_s) \frac{i-1}{2(2N+1)} \right] \quad (A.56)$$

$$= \frac{-\alpha_s + \beta_s}{2N+1} \quad (A.57)$$

and, finally, for $s, t = N+2, \ldots, 2N+1$ and $s \neq t$, one gets:

$$L_{st} = 2Re(V_{ss} D_{ss} W_{st}) \quad (A.58)$$

$$= 2Re\left[(\alpha_s - i\beta_s) i \frac{i-1}{2(2N+1)} \right] = \quad (A.59)$$

$$\frac{-\alpha_s - \beta_s}{2N+1} \quad (A.60)$$

Summing up, we have here provided closed analytical expressions for all the entries of the Laplacian matrix, as a function of the assigned spectrum. The calculation has been carried out by assuming a specific form of the Laplacian eigenvectors, which enables for analytical progress to be made, and which represents a particular case of the general recipe here illustrated.

A.3 Positiveness of L

The aim of this section is to work out the algebraic steps needed to rewrite (5.46) in the simpler form given by (A.75) and (A.76).

Let us thus rewrite (5.46)

$$\begin{cases} 2N\alpha_t < \beta_t < -2N\alpha_t \\ \beta_t > -\frac{1-2N}{2N+1}\alpha_t - \frac{2}{2N+1}\sum_{k=2, k\neq t}^{N+1} \alpha_k \\ \beta_t < \frac{1-2N}{2N+1}\alpha_t + \frac{2}{2N+1}\sum_{k=2, k\neq t}^{N+1} \alpha_k \\ \alpha_t < \beta_t < -\alpha_t \\ \frac{\alpha_t}{2N} < \beta_t < -\frac{\alpha_t}{2N} \end{cases}$$

where the inequalities hold for $t = 2, \ldots, N+1$. Then the second and the third conditions of system (5.46) can be matched simultaneously provided:

$$\alpha_t < \frac{2}{2N-1} \sum_{k \neq t} \alpha_k \quad \forall t = 2, \ldots, N+1 \quad (A.61)$$

Remark that:

$$2N\alpha_t < \alpha_t < \frac{\alpha_t}{2N} \tag{A.62}$$

holds for arbitrary values of $\alpha_t < 0$ and N. Hence, system (5.46) simplify as follows:

$$\begin{cases} \frac{\alpha_t}{2N} < \beta_t < -\frac{\alpha}{2N} \\ \alpha_t < \frac{2}{2N-1} \sum_{k\neq t} \alpha_k \\ \beta_t > -\frac{1-2N}{2N+1}\alpha_t - \frac{2}{2N+1} \sum_{k=2,k\neq t}^{N+1} \alpha_k \\ \beta_t < \frac{1-2N}{2N+1}\alpha_t + \frac{2}{2N+1} \sum_{k=2,k\neq t}^{N+1} \alpha_k \end{cases} \tag{A.63}$$

for $t = 2, \ldots, N+1$.

Focus now on the conditions for β_t. We assume that the following condition holds:

$$\frac{1-2N}{2N+1}\alpha_t + \frac{2}{2N+1} \sum_{k=2,k\neq t}^{N+1} \alpha_k > -\frac{\alpha_t}{2N} \tag{A.64}$$

and we set to explore its consequences. Eq. (A.64) yields:

$$\alpha_t < \frac{4N}{4N^2 - 4N - 1} \sum_{k\neq t} \alpha_k = \frac{1}{N - 1 - \frac{1}{4N}} \sum_{k\neq t} \alpha_k \tag{A.65}$$

For $N > 1$, conditions (A.63) maps therefore in the following equivalent system:

$$\begin{cases} \frac{\alpha_t}{2N} < \beta_t < -\frac{\alpha_t}{2N} \\ \alpha_t < \frac{2}{2N-1} \sum_{k=2,k\neq t}^{N+1} \alpha_k \\ \alpha_t < \frac{1}{N-1-\frac{1}{4N}} \sum_{k\neq t} \alpha_k \end{cases} \tag{A.66}$$

Remark that:

$$\frac{1}{N - 1 - \frac{1}{4N}} \sum_{k=2,k\neq t}^{N+1} \alpha_k < \frac{2}{2N-1} \sum_{k=2,k\neq t}^{N+1} \alpha_k \tag{A.67}$$

due to the inequality

$$\frac{1}{N - 1 - \frac{1}{4N}} > \frac{2}{2N-1} \tag{A.68}$$

which holds for every $N > 1$. Hence, system (A.66) takes the form:

$$\begin{cases} \frac{\alpha_t}{2N} < \beta_t < -\frac{\alpha_t}{2N} \\ \alpha_t < \frac{1}{N-1-\frac{1}{4N}} \sum_{k\neq t} \alpha_k \end{cases} \tag{A.69}$$

System (A.69) has no solutions, under the working hypothesis that we have put forward to deriving it. In fact:

$$\alpha_t + \frac{1}{N-1-\frac{1}{4N}}\alpha_t < \frac{1}{N-1-\frac{1}{4N}}\sum_k \alpha_k \tag{A.70}$$

that is

$$\alpha_t < \frac{1}{N-\frac{1}{4N}}\sum_k \alpha_k = \frac{4N}{4N^2-1}\sum_k \alpha_k \tag{A.71}$$

and summing on every t we get

$$\sum_t \alpha_t < \frac{4N^2}{4N^2-1}\sum_k \alpha_k \tag{A.72}$$

which in turn implies $\frac{4N^2}{4N^2-1} < 1$, a condition that is obviously never met. We now go back to revise ansatz (A.64), and consider the alternative scenario:

$$\frac{1-2N}{2N+1}\alpha_t + \frac{2}{2N+1}\sum_{k=2,k\neq t}^{N+1}\alpha_k < -\frac{\alpha_t}{2N} \tag{A.73}$$

System (A.63) becomes

$$\begin{cases} \beta_t > -\frac{1-2N}{2N+1}\alpha_t - \frac{2}{2N+1}\sum_{k=2,k\neq t}^{N+1}\alpha_k \\ \beta_t < \frac{1-2N}{2N+1}\alpha_t + \frac{2}{2N+1}\sum_{k=2,k\neq t}^{N+1}\alpha_k \\ \alpha_t < \frac{2}{2N-1}\sum_{k=2,k\neq t}^{N+1}\alpha_k \\ \alpha_t > \frac{1}{N-1-\frac{1}{4N}}\sum_{k\neq t}\alpha_k \end{cases} \tag{A.74}$$

Following a path analogous to the one discussed above, we get:

$$\frac{4N}{4N^2-1}\sum_k \alpha_k < \alpha_t < \frac{2}{2N+1}\sum_k \alpha_k \tag{A.75}$$

and

$$\alpha_t - \frac{2}{2N+1}\sum_k \alpha_k < \beta_t < -\alpha_t + \frac{2}{2N+1}\sum_k \alpha_k \tag{A.76}$$

Appendix B

Details on the Master Stability Function on hypergraphs

B.1 Compute the MSF using MEGNO

To compute the MSF one has to solve Eq. (6.26); discarding the division into reaction and coupling part, one can rewrite the previous equation as

$$\frac{d\delta\mathbf{x}_i}{dt} = \sum_j \mathcal{J}_{ij}(t)\delta\mathbf{x}_j \,,$$

that is a time dependent ODE, often named *variational equation*. The latter should thus be solved together with the evolution of the reference trajectory

$$\frac{d\mathbf{x}_i}{dt} = \mathcal{F}(\mathbf{x}_i) \,,$$

where again we put in the function $\mathcal{F}$ the reaction and the coupling.

Then calling $\delta\mathbf{x}(t) = \delta\mathbf{x}(t; \delta\mathbf{x}_0)$ the solution of the variational equation with initial datum $\delta\mathbf{x}(0) = \delta\mathbf{x}_0$, the *M*ean *E*xponential *G*rowth factor by *N*earby *O*rbits, MEGNO [47, 48], can be defined as:

$$Y_{\mathbf{s}}(t) := \frac{2}{t}\int_0^t \frac{\dot{\delta}(\tau)}{\delta(\tau)}\tau \, d\tau \,, \tag{B.1}$$

where $[\delta(\tau)]^2 = ||\delta\mathbf{x}(\tau)||^2 = (\delta\mathbf{x}(\tau), \delta\mathbf{x}(\tau))$, i.e. the norm of the vector $\delta\mathbf{x}$, being $(\cdot, \cdot)$ the scalar product. We also emphasised that the MEGNO is being

computed with respect to the reference orbit $\mathbf{s}(t)$. A trivial computation gives:

$$\begin{aligned}\frac{d}{dt}\delta^2 &= 2\delta\dot{\delta} \\ &= (\frac{d}{dt}\delta\mathbf{x},\delta\mathbf{x}) + (\delta\mathbf{x},\frac{d}{dt}\delta\mathbf{x}) = (\mathcal{J}\delta\mathbf{x},\delta\mathbf{x}) + (\delta\mathbf{x},\mathcal{J}\delta\mathbf{x})\,, \quad \text{(B.2)}\end{aligned}$$

hence

$$\frac{\dot{\delta}(s)}{\delta(s)} = \frac{(\mathcal{H}\delta\mathbf{x},\delta\mathbf{x})}{\delta^2}\,, \quad \text{(B.3)}$$

where $\mathcal{H} = (\mathcal{J}^T + \mathcal{J})/2$ is the Hermitian part of $\mathcal{J}$.

Together with the MEGNO one usually defines also the *(time)–averaged MEGNO*:

$$\bar{Y}_{\mathbf{s}}(t) := \frac{1}{t}\int_0^t Y_{\mathbf{s}}(\tau)\,d\tau\,. \quad \text{(B.4)}$$

While $Y(t)$ could widely oscillate for large t and thus preventing from any effective use of it, it can be shown that the average-MEGNO is well behaved and allows to study the dynamics for long times. Indeed the main feature of average-MEGNO (and/or the MEGNO) is to allows to distinguish between regular orbits, for which $\bar{Y}(t) \to 0$, and irregular orbits, for which $\bar{Y}(t)$ grows unbounded, and more precisely $\bar{Y}(t) \sim \lambda t/2$ being λ the largest Lyapunov characteristic number (or maximal Lyapunov exponent) of the orbit $\mathbf{s}(t)$. Let us observe that for regular orbits MEGNO is able to differentiate between periodic ones, $Y(t) \to 0$, and quasi-periodic ones, $Y(t) \to 2$.

Let us observe that one can overcome the problem of the growth of δ in case of chaotic orbits using the following trick. Being $\delta\mathbf{x}$ a solution of the variational equation, one can introduce the "reduced vector" $\mathbf{w}$, $\mathbf{w} = \delta\mathbf{x}/\delta$, whose evolution is given by:

$$\dot{\mathbf{w}} = \mathcal{J}\mathbf{w} - (\mathcal{H}\mathbf{w},\mathbf{w})\,;$$

then it can easily proved that $||\mathbf{w}(t)|| = 1$, indeed

$$\begin{aligned}\frac{d}{dt}||\mathbf{w}||^2 &= (\frac{d}{dt}\mathbf{w},\mathbf{w}) + (\mathbf{w},\frac{d}{dt}\mathbf{w}) \\ &= (\mathcal{J}\mathbf{w},\mathbf{w}) - (\mathcal{H}\mathbf{w},\mathbf{w})||\mathbf{w}||^2 + (\mathbf{w},\mathcal{J}\mathbf{w}) - (\mathcal{H}\mathbf{w},\mathbf{w})||\mathbf{w}||^2 \\ &= 2(\mathcal{H}\mathbf{w},\mathbf{w})(1 - ||\mathbf{w}||^2) = 0\,,\end{aligned}$$

where we used the fact that $||\mathbf{w}(0)|| = 1$.

Appendix C

Publications

This research activity has led to several publications in international journals. These are summarized below.[1]

International Journals

1. **Nicoletti S.**, Zagli N., Fanelli D., Livi R., Carletti T., Innocenti G., "Non-normal amplification of stochastic quasicycles", *Physical Review E*, vol. 98, 032214, 2018.
2. **Nicoletti S.**, Fanelli D, Zagli N., Asllani M., Battiselli G., Carletti T., Chisci L., Innocenti G., Livi R., "Resilience for stochastic systems interacting via a quasi-degenerate network", *Chaos*, vol. 29, 083123, 2019.
3. Carletti T., **Nicoletti S.**, Fanelli D., "Dynamical systems on Hypergraphs", *Journal of Physics: Complexity*, vol. 1, 3, 2020.
4. **Nicoletti S.**, Carletti T, Fanelli D., Battistelli G., Chisci L., "Generating directed networks with prescribed Laplacian spectra", *Journal of Physics: Complexity*, vol. **0**, 000000, 2020.

[1] The author's bibliometric indices are the following: H-index = 3, total number of citations = 18 (source: Google Scholar on Month 2, 2021).

Bibliography

[1] A. V. A. Barrat, M. Barthélemy, *Dynamical Processes on Complex Networks*. Cambridge University Press, 2008.

[2] D. M. Abrams and S. H. Strogatz, "Chimera states for coupled oscillators," *Phys. Rev. Lett.*, vol. 93, p. 174102, Oct 2004.

[3] L. Adamic, "The small world web," *International Conference on Theory and Practice of Digital Libraries*, pp. 443–452, 1999.

[4] R. Albert, "Scale- free networks in cell biology," *J Cell Sci*, 10 2005.

[5] R. Albert and A.-L. Barabási, "Statistical mechanics of complex networks," *Reviews of modern physics*, vol. 74, no. 1, p. 47, 2002.

[6] R. Albert and A.-L. Barabási, "Statistical mechanics of complex networks," *Rev. Mod. Phys.*, vol. 74, pp. 47–97, Jan 2002.

[7] C. Altafini, "Consensus problems on networks with antagonistic interactions," *IEEE Transactions on Automatic Control*, vol. 58, no. 4, pp. 935–946, 2013.

[8] P. W. Anderson, "Absence of diffusion in certain random lattices," *Physical Review Letters*, vol. 109, p. 1492, 1958.

[9] R. M. Anderson and R. May, *Infection Diseases of Humans: Dynamics and Control*. Oxford University Press, 1991.

[10] I. Aranson and L. Kramer, "The world of the complex ginzburg-landau equation," *Reviews of Modern Physics*, vol. 74, p. 99, 2002.

[11] I. S. Aranson and L. Kramer, "The world of the complex ginzburg-landau equation," *Rev. Mod. Phys.*, vol. 74, pp. 99–143, Feb 2002.

[12] A. Arenas, A. Díaz-Guilera, J. Kurths, Y. Moreno, and C. Zhou, "Synchronization in complex networks," *Physics reports*, vol. 469, no. 3, pp. 93–153, 2008.

[13] M. Asllani, D. Busiello, T. Carletti, D. Fanelli, and G. Planchon, "Turing patterns in multiplex networks," *Physical Review E*, vol. 90, p. 042814, 2014.

[14] M. Asllani, T. Carletti, and D. Fanelli, "Tune the topology to create or destroy patterns," *Eur. Phys. J. B*, p. 89, 2016.

[15] M. Asllani, T. Biancalani, D. Fanelli, and A. McKane, "The linear noise approximation for reaction-diffusion systems on networks," *European Physical Journal B*, p. 473, 11 2013.

[16] M. Asllani, D. M. Busiello, T. Carletti, D. Fanelli, and G. Planchon, "Turing patterns in multiplex networks," *Phys. Rev. E*, vol. 90, p. 042814, Oct 2014.

[17] M. Asllani and T. Carletti, "Topological resilience in non-normal networked systems," *Phys. Rev. E*, vol. 97, p. 042302, Apr 2018.

[18] ——, "Universality of non-normality in real complex networks," 03 2018.

[19] M. Asllani, J. Challenger, F. Pavone, L. Sacconi, and D. Fanelli, "The theory of pattern formation on directed networks," *Nature communications*, vol. 5, p. 4517, 07 2014.

[20] M. Asllani, F. Di Patti, and D. Fanelli, "Stochastic turing patterns on a network," *Physical review. E, Statistical, nonlinear, and soft matter physics*, vol. 86, p. 046105, 10 2012.

[21] M. Asllani, R. Lambiotte, and T. Carletti, "Structure and dynamical behavior of non-normal networks," *Science Advances*, vol. 4, no. 12, 2018.

[22] M. Asslani, F. Di Patti, and D. Fanelli, "Stochastic turing patterns on a network," *Phys. Rev. E*, vol. 86, p. 046105, Oct 2012.

[23] P. Ball, *The self-made tapestry: Pattern formation in Nature*. Oxford University Press, 1999.

[24] A.-L. Barabási, *Network science*. Cambridge university press, 2016.

[25] A.-L. Barabási and R. Albert, "Emergence of scaling in random networks," *Science*, vol. 286, no. 5439, pp. 509–512, 1999.

[26] M. S. Bartlett, "Measles periodicity and community size," *Journal of the Royal Statistical Society. Series A (General)*, vol. 120, no. 1, pp. 48–70, 1957.

[27] A. R. Benson, D. F. Gleich, and J. Leskovec, "Higher-order organization of complex networks," *Science*, vol. 353, no. 6295, pp. 163–166, 2016.

[28] R. Benzi, A. Sutera, and A. Vulpiani, "The mechanism of stochastic resonance," *Journal of Physics A: Mathematical and General*, vol. 14, no. 11, pp. L453–L457, nov 1981.

[29] C. Berge, *Graphs and hypergraphs*, ser. North-Holland Pub. Co. American Elsevier Pub. Co, 1973.

[30] T. Biancalani, D. Fanelli, and F. Di Patti, "Stochastic turing patterns in the brusselator model," *Phys. Rev. E*, vol. 81, p. 046215, Apr 2010.

[31] T. Biancalani, F. Jafarpour, and N. Goldenfeld, "Giant amplification of noise in fluctuation-induced pattern formation," *Phys. Rev. Lett.*, vol. 118, p. 018101, Jan 2017.

[32] S. Bilal and R. Ramaswamy, "Synchronization and amplitude death in hypernetworks," *Phys. Rev. E*, vol. 89, p. 062923, Jun 2014.

[33] S. Boccaletti, V. Latora, Y. Moreno, M. Chavez, and D.-U. Hwang, "Complex networks: Structure and dynamics," *Physics Reports*, vol. 424, no. 4, pp. 175 – 308, 2006.

[34] ——, "Complex networks: Structure and dynamics," *Physics Reports*, vol. 424, no. 4-5, pp. 175–308, 2006.

[35] S. Boccaletti, A. Pisarchik, C. del Genio, and A. Amann, *Synchronization - From coupled systems to complex networks.* United Kingdom: Cambridge University Press, 3 2018.

[36] A. Bodó, G. Katona, and P. Simon, "Sis epidemic propagation on hypergraphs," *Bull. Math. Biol.*, vol. 78, no. 4, p. 713, 2016.

[37] P. Botti and R. Merris, "Almost all trees share a complete set of immanental polynomials," *J. Graph Theory*, vol. 17, 1993.

[38] P. C. Bressloff, "Metastable states and quasicycles in a stochastic wilson-cowan model of neuronal population dynamics," *Phys. Rev. E*, vol. 82, p. 051903, Nov 2010.

[39] J. Bronski and L. Deville, "Spectral theory for dynamics on graphs containing attractive and repulsive interactions," *SIAM Journal on Applied Mathematics*, vol. 74, 01 2014.

[40] T. Carletti, F. Battiston, G. Cencetti, and D. Fanelli, "Random walks on hypergraphs," *Physical Review E*, vol. 101, p. 022308, 2020.

[41] G. Cencetti, F. Bagnoli, G. Battistelli, L. Chisci, F. Di Patti, and D. Fanelli, "Topological stabilization for synchronized dynamics on networks," *The European Physical Journal B*, vol. 90, 01 2017.

[42] G. Cencetti, F. Bagnoli, G. Battistelli, L. Chisci, and D. Fanelli, "Spectral control for ecological stability," *The European Physical Journal B*, vol. 91, 01 2018.

[43] G. Cencetti, P. Clusella, and D. Fanelli, "Pattern invariance for reaction-diffusion systems on complex networks," *Scientific Reports*, vol. 8, 12 2018.

[44] J. Challenger, R. Burioni, and D. Fanelli, "Turing instabilities from a limit cycle," *Physical Review E*, vol. 92, 11 2014.

[45] W. Chen, D. Wang, J. Liu, T. Başar, K. Johansson, and L. Qiu, "On semidefiniteness of signed laplacians with application to microgrids," vol. 49, 12 2016, pp. 97–102.

[46] U. Chitra and B. J. Raphael, "Random walks on hypergraphs with edge-dependent vertex weights," *arXiv preprint arXiv:1905.08287*, 2019.

[47] P. Cincotta, C. Giordano, and C. Simó, "Phase space structure of multi-dimensional systems by mean of the mean exponential growth factor of nearby orbits," *Physica D*, vol. 182, p. 151, 2003.

[48] P. Cincotta and C. Simó, "Simple tools to study global dynamics in non-axisymmetric galactic potentials - i," *Astronomy and astrophysics*, vol. 147, p. 205, 2000.

[49] V. Colizza, R. Pastor-Satorras, and A. Vespignani, "Reaction-diffusion processes and metapopulation models in heterogeneous network," *Nature Phys*, vol. 3, 04 2007.

[50] A. Compere, A. Lemaître, and N. Delsate, "Detection by megno of the gravitational resonances between a rotating ellipsoid and a point mass satellite," *Celest. Mech and Dyn. Astron.*, vol. 112, 2012.

[51] O. T. Courtney and G. Bianconi, "Generalized network structures: The configuration model and the canonical ensemble of simplicial complexes," *Physical Review E*, vol. 93, no. 6, p. 062311, 2016.

[52] K. Z. Coyte, J. Schluter, and K. R. Foster, "The ecology of the microbiome: Networks, competition, and stability," *Science*, vol. 350, no. 6261, pp. 663–666, 2015.

[53] M. C. Cross and P. C. Hohenberg, "Pattern formation outside of equilibrium," *Rev. Mod. Phys.*, vol. 65, pp. 851–1112, Jul 1993.

[54] D. Cvetković, "Spectral recognition of graphs," *YUJOR. Yugoslav Journal of Operations Research*, vol. 22, 01 2012.

[55] C. J. D., J. Neuman, and W. van Drongelen, "Wilson–cowan equations for neocortical dynamics," *J. Math. Neurosci.*, vol. 6, p. 1, 2016.

[56] T. Dauxois, F. Di Patti, D. Fanelli, and A. J. McKane, "Enhanced stochastic oscillations in autocatalytic reactions," *Phys. Rev. E*, vol. 79, p. 036112, Mar 2009.

[57] G. F. de Arruda, G. Petri, and Y. Moreno, "Social contagion models on hypergraphs," *Phys. Rev. Research*, vol. 2, p. 023032, 2020.

[58] M. H. DeGroot, "Reaching a consensus," *Journal of the American Statistical Association*, vol. 69, no. 345, pp. 118–121, 1974.

[59] R. J. Deissler and K. Kaneko, "Velocity-dependent lyapunov exponents as a measure of chaos for open-flow systems," *Physics Letters A*, vol. 119, no. 8, pp. 397 – 402, 1987.

[60] K. Devriendt and P. Van Mieghem, "The simplex geometry of graphs," *Journal of Complex Networks*, vol. 7, no. 4, pp. 469–490, 2019.

[61] F. Di Patti, D. Fanelli, F. Miele, and T. Carletti, "Benjamin-feir instabilities on directed networks," *Chaos, Solitons & Fractals*, vol. 96, 07 2016.

[62] F. Di Patti, D. Fanelli, F. Miele, and T. Carletti, "Ginzburg-landau approximation for self-sustained oscillators weakly coupled on complex directed graphs," *Communications in Nonlinear Science and Numerical Simulation*, vol. 56, pp. 447 – 456, 2018.

[63] S. di Santo, P. Villegas, R. Burioni, and M. A. Muñoz, "Non-normality, reactivity, and intrinsic stochasticity in neural dynamics: a non-equilibrium potential approach," *Journal of Statistical Mechanics: Theory and Experiment*, vol. 2018, no. 7, p. 073402, jul 2018.

[64] K. P. E. and P. E., *Numerical Solution of Stochastic Differential Equations*. Springer, 1992.

[65] T. Elmhirst and M. Golubitsky, "Nilpotent hopf bifurcations in coupled cell systems," *Siam Journal on Applied Dynamical Systems - SIADS*, vol. 5, 01 2006.

[66] P. Erdös and A. Rényi, "On the evolution of random graphs," *Publ. Math. Inst. Hung. Acad. Sci.*, vol. 5, pp. 17–60, 1960.

[67] E. Estrada and J. A. Rodríguez-Velázquez, "Complex networks as hypergraphs," *arXiv preprint physics/0505137*, 2005.

[68] E. Estrada and G. Ross, "Centralities in simplicial complexes. applications to protein interaction networks," *J. Their. Biol.*, vol. 438, p. 46, 2018.

[69] M. Faloutsos, P. Faloutsos, and C. Faloutsos, "On power-law relationships of the internet topology," *ACM SIGCOMM Computer Communication Review*, vol. 29, 03 2003.

[70] D. Fanelli, F. Ginelli, R. Livi, N. Zagli, and C. Zankoc, "Noise-driven neuromorphic tuned amplifier," *Phys. Rev. E*, vol. 96, p. 062313, Dec 2017.

[71] G. Ferraz de Arruda, M. Tizzani, and Y. Moreno, "arxiv:2005.10891," *arXiv preprint*, 2020.

[72] W. Fleming and R. Rishel, *Deterministic and Stochastic Optimal Control*. Springer, 1975.

[73] C. Folke, "Resilience: The emergence of a perspective for social–ecological systems analyses," *Global Environmental Change*, vol. 16, no. 3, pp. 253 – 267, 2006.

[74] A. Forrow, F. G. Woodhouse, and J. Dunkel, "Functional control of network dynamics using designed laplacian spectra," *Phys. Rev. X*, vol. 8, p. 041043, Dec 2018.

[75] C. G. and C. A., *Data Science and Complex Networks: Real Case Studies with Python*. Oxford University Press, 2016.

[76] I. P. G. Nicolis, *Self-Organization in Nonequilibrium Systems: from Dissipative Structures to Order Through Fluctuations*. Wiley, 1977.

[77] L. V. Gambuzza, F. Di Patti, G. L., S. Lepri, M. Romance, R. Criado, M. Frasca, V. Latora, and S. Boccaletti, "The master stability function for synchronization in simplicial complexes," *arXiv preprint arXiv:2004.03913v1*, 2020.

[78] L. Gammaitoni, P. Hänggi, P. Jung, and F. Marchesoni, "Stochastic resonance," *Rev. Mod. Phys.*, vol. 70, pp. 223–287, Jan 1998.

[79] V. García-Morales and K. Krischer, "The complex ginzburg-landau equation: An introduction," *Contemporary Physics - CONTEMP PHYS*, vol. 53, pp. 79–95, 03 2012.

[80] C. W. Gardiner, *Handbook of Stochastic Methods*. Springer, 2004.

[81] G. Ghoshal, V. Zlatić, G. Caldarelli, and M. E. Newman, "Random hypergraphs and their applications," *Physical Review E*, vol. 79, no. 6, p. 066118, 2009.

[82] M. S. Goldman, "Memory without feedback in a neural network," *Neuron*, vol. 61, p. 621, 2009.

[83] K. Goździewski, E. Bois, and A. Maciejewski, "Global dynamics of the gliese 876 planetary system," *Mon. Not. R. Astron. Soc.*, vol. 332, p. 839, 2002.

[84] D. S. Grebenkov and B.-T. Nguyen, "Geometrical structure of laplacian eigenfunctions," *SIAM Review*, vol. 55, p. 601, 2013.

[85] J. Grilli, G. Barabás, M. J. Michalska-Smith, and S. Allesina, "Higher-order interactions stabilize dynamics in competitive network models," *Nature*, vol. 548, no. 7666, p. 210, 2017.

[86] R. Grimshaw, *Nonlinear Ordinary Differential Equations*. Routledge, 2017.

[87] L. Gunderson, C. Allen, and C. Holling, "Foundation of ecological resilience," *Bibliovault OAI Repository, the University of Chicago Press*, 01 2010.

[88] L. H., S. L. Z., B. A. M. P., B. D., and D. J., *Molecular Cell Biology*. New York: W. H. Freeman, 2000.

[89] T. F. H. Risken, *The Fokker-Planck equation*. Springer, 1996.

[90] L. Halbeisen and N. Hungerbühler, "Reconstruction of weighted graphs by their spectrum," *European Journal of Combinatorics*, vol. 21, no. 5, pp. 641 – 650, 2000.

[91] L. G. Harrison, *Kinetic theory of living pattern*. Cambridge University Press, 1993.

[92] S. Hata and H. Nakao, "Localization of laplacian eigenvectors on random networks," *Scientific Reports*, vol. 7, 12 2017.

[93] S. Hata, H. Nakao, and A. Mikhailov, "Dispersal-induced destabilization of metapopulations and oscillatory turing patterns in ecological networks," *Scientific reports*, vol. 4, p. 3585, 01 2014.

[94] G. Hennequin, T. P. Vogels, and W. Gerstner, "Non-normal amplification in random balanced neuronal networks," *Phys. Rev. E*, vol. 86, p. 011909, Jul 2012.

[95] J. O. Hirschfelder and P. R. Certain, "Degenerate rs perturbation theory," *The Journal of Chemical Physics*, vol. 60, no. 3, pp. 1118–1137, 1974.

[96] E. E. Holmes, M. A. Lewis, J. E. Banks, and R. R. Veit, "Partial differential equations in ecology: Spatial interactions and population dynamics," *Ecology*, vol. 75, no. 1, pp. 17–29, 1994.

[97] R. Hoyle, *Pattern Formation: An Introduction to Methods*. Cambridge University Press, 2006.

[98] L. Huang, Q. Chen, Y.-C. Lai, and L. M. Pecora, "Generic behavior of master-stability functions in coupled nonlinear dynamical systems," *Physical Review E*, vol. 80, p. 036204, 2009.

[99] C. Hubaux, A. Libert, N. Delsate, and T. Carletti, "Influence of earth's shadowing effects on space debris stability," *Advances in Space Research*, vol. 51, no. 1, p. 25, 2013.

[100] L. Hufnagel, D. Brockmann, and T. Geisel, "Forecast and control of epidemics in a globalized world," *Proceedings of the National Academy of Sciences*, vol. 101, no. 42, pp. 15 124–15 129, 2004.

[101] I. Iacopini, G. Petri, A. Barrat, and V. Latora, "Simplicial models of social contagion," *Nature communications*, vol. 10, no. 1, p. 2485, 2019.

[102] M. Ipsen and A. S. Mikhailov, "Evolutionary reconstruction of networks," *Phys. Rev. E*, vol. 66, p. 046109, Oct 2002.

[103] A. K. Jiotsa, A. Politi, and A. Torcini, "Convective lyapunov spectra," *Journal of Physics A: Mathematical and Theoretical*, vol. 46, no. 25, p. 254013, jun 2013.

[104] J. Jost and R. Mulas, "Hypergraph laplace operators for chemical reaction networks," *Advances in Mathematics*, vol. 351, p. 870, 2019.

[105] E. Kandel, S. J., and J. T., *Principles of Neural Science*. McGraw-Hill, 2000.

[106] D.-H. Kim and A. E. Motter, "Ensemble averageability in network spectra," *Phys. Rev. Lett.*, vol. 98, p. 248701, Jun 2007.

[107] N. Kouvaris, S. Hata, and A. Diaz-Guilera, "Pattern formation in multiplex networks," *Scientific Reports*, vol. 5, p. 10840, 2015.

[108] ——, "Pattern formation in multiplex networks," *Scientific Reports*, vol. 5, p. 10840, 06 2015.

[109] A. Krawiecki, "Chaotic synchronization on complex hypergraphs," *Chaos, Solitons and Fractals*, vol. 65, p. 44, 2014.

[110] Y. Kuramoto, "Self-entrainment of a population of coupled non-linear oscillators," *Int. Symp. Math. Prob. Theor. Phys.*, vol. 39, pp. 420–422, 1975.

[111] ——, *Chemical oscillations, waves, and turbulence*. Springer- Verlag, New York, 1984.

[112] L. J. L. and S. H., "A gallavotti–cohen-type symmetry in the large deviation functional for stochastic dynamics," *J. Stat. Phys.*, vol. 95, p. 333, 1999.

[113] R. Lambiotte, M. Rosvall, and I. Scholtes, "From networks to optimal higher-order models of complex systems," *Nat. Phys.*, vol. 15, p. 313, 2019.

[114] G. T. Landi, T. Tomé, and M. J. de Oliveira, "Entropy production in linear langevin systems," *Journal of Physics A: Mathematical and Theoretical*, vol. 46, no. 39, p. 395001, sep 2013.

[115] ——, "Entropy production in linear langevin systems," *Journal of Physics A: Mathematical and Theoretical*, vol. 46, no. 39, p. 395001, sep 2013.

[116] V. Latora, V. Nicosia, and G. Russo, *Complex networks: principles, methods and applications*. Cambridge University Press, 2017.

[117] S. Lepri, A. Politi, and A. Torcini, "Chronotopic lyapunov analysis. i. a detailed characterization of 1d systems," *Journal of Statistical Physics*, vol. 82, pp. 1429–1452, 03 1996.

[118] ——, "Chronotopic lyapunov analysis: Ii. toward a unified approach," *Journal of Statistical Physics*, vol. 88, pp. 31–45, 01 1997.

[119] A.-S. Libert, C. Hubaux, and T. Carletti, "The global symplectic integrator: an efficient tool for stability studies of dynamical systems. application to the kozai resonance in the restricted three-body problem," *Monthly Notices of the Royal Astronomy Society*, vol. 414, p. 659, 2011.

[120] L.-D. Lord, P. Expert, H. Fernandes, G. Petri, T. Van Hartevelt, F. Vaccarino, G. Deco, F. Turkheimer, and M. Kringelbach, "Insights into brain architectures from the homological scaffolds of functional connectivity networks," *Front. Syst. Neurosci.*, vol. 10, p. 85, 2016.

[121] E. N. Lorenz, "Deterministic nonperiodic flow," *J. Atmos. Sci.*, vol. 20, p. 130, 1963.

[122] M. Lucas, G. Cencetti, and F. Battiston, "A multi-order laplacian framework for the stability of higher-order synchronization," *arXiv preprint arXiv: 2003.09734v1*, 2020.

[123] M. Lucas, D. Fanelli, T. Carletti, and J. Petit, "Desynchronization induced by time-varying network," *EPL (Europhysics Letters)*, vol. 121, p. 50008, 03 2018.

[124] J. Macia, Francesc Posas and R. V. Solé, "Distributed computation: the new wave of synthetic biology devices," *Trends Biotechnol.*, vol. 30, p. 342, 2012.

[125] R. M. May, "Will a large complex system be stable?" *Nature*, vol. 238, no. 5364, p. 413, 1972.

[126] P. N. McGraw and M. Menzinger, "Laplacian spectra as a diagnostic tool for network structure and dynamics," *Phys. Rev. E*, vol. 77, p. 031102, 2008.

[127] A. J. McKane and T. J. Newman, "Predator-prey cycles from resonant amplification of demographic stochasticity," *Phys. Rev. Lett.*, vol. 94, p. 218102, Jun 2005.

[128] B. D. McKay, "On the spectral characterisation of trees," *Ars Combinatoria*, vol. 3, 1977.

[129] H. Meinhardt, *Models of biological pattern formation.* Academic Press, 1982.

[130] P. Menck, J. Heitzig, N. Marwan, and J. Kurths, "How basin stability complements the linear-stability paradigm," *Nature Physics*, vol. 9, no. 2, pp. 89–92, Feb. 2013.

[131] A. E. Motter, "Bounding network spectra for network design," *New Journal of Physics*, vol. 9, no. 6, pp. 182–182, jun 2007.

[132] R. Mulas, C. Kuehn, and J. Jost, "Coupled dynamics on hypergraphs: Master stability of steady states and synchronization," *arXiv preprint arXiv: 2003.13775v1*, 2020.

[133] R. Muolo, M. Asllani, D. Fanelli, P. Maini, and T. Carletti, "Patterns of non-normality in networked systems," *Journal of Theoretical Biology*, vol. 480, 07 2019.

[134] M. K. Murphy BK, "Balanced amplification: a new mechanism of selective amplification of neural activity patterns," *Neuron.*, vol. 61(4), pp. 635–648.

[135] J. D. Murray, *Mathematical biology II: Spatial models and biomedical applications.* Springer-Verlag, 2001.

[136] ——, *Mathematical Biology.* Springer, New York, 2003.

[137] J. D. Murray, E. A. Stanley, and D. L. Brown, "On the spatial spread of rabies among foxes," *Proceedings of the Royal Society of London. Series B, Biological Sciences*, vol. 229, no. 1255, pp. 111–150, 1986.

[138] H. Nakao, "Complex ginzburg-landau equation on networks and its non-uniform dynamics," *The European Physical Journal Special Topics*, vol. 223, pp. 2411–2421, 10 2014.

[139] H. Nakao and A. Mikhailov, "Turing patterns in network-organized activator-inhibitor systems," *Nature Physics*, vol. 6, pp. 544–550, 05 2010.

[140] H. Nakao and A. S. Mikhailov, "Turing patterns in network-organized activator-inhibitor systems," *Nature Physics*, vol. 6, p. 544, 2010.

[141] E. Negahbani, D. A. Steyn-Ross, M. L. Steyn-Ross, W. M. T., and S. J. W., "Excitatory and inhibitory interactions in localized populations of model neurons," *J. Math. Neurosci.*, vol. 5, p. 9, 2015.

[142] M. G. Neubert and H. Caswell, "Alternatives to resilience for measuring the responses of ecological systems to perturbations," *Ecology*, vol. 78, no. 3, pp. 653–665, 1997.

[143] ——, "Alternatives to resilience for measuring the responses of ecological systems to perturbations," *Ecology*, vol. 78, no. 3, pp. 653–665, 1997.

[144] M. G. Neubert, H. Caswell, and J. Murray, "Transient dynamics and pattern formation: reactivity is necessary for turing instabilities," *Mathematical Biosciences*, vol. 175, no. 1, pp. 1 – 11, 2002.

[145] M. E. J. Newman, "The structure of scientific collaboration networks," *Proceedings of the National Academy of Sciences*, vol. 98, no. 2, pp. 404–409, 2001.

[146] ——, *Networks: An Introduction*. Oxford University Press, 2010.

[147] M. E. Newman, *Networks: An Introduction*. Oxford: Oxford University Press, 2010.

[148] S. Nicoletti, T. Carletti, D. Fanelli, G. Battistelli, and L. Chisci, "Generating directed networks with prescribed laplacian spectra," 2020.

[149] S. Nicoletti, D. Fanelli, N. Zagli, M. Asllani, G. Battistelli, T. Carletti, L. Chisci, G. Innocenti, and R. Livi, "Resilience for stochastic systems interacting via a quasi-degenerate network," *Chaos: An Interdisciplinary Journal of Nonlinear Science*, vol. 29, no. 8, p. 083123, 2019.

[150] S. Nicoletti, N. Zagli, D. Fanelli, R. Livi, T. Carletti, and G. Innocenti, "Non-normal amplification of stochastic quasicycles," *Phys. Rev. E*, vol. 98, p. 032214, Sep 2018.

[151] G. Nicolis and I. Prigogine, *Self-organization in nonequiibrium systems: From dissipative structures to order through fluctuations*. J. Wiley and Sons, 1977.

[152] H. G. Othmer and L. E. Scriven, "Instability and dynamic pattern in cellular networks," *J. Theor. Biol.*, vol. 32, p. 507, 1971.

[153] H. Othmer and L. Scriven, "Instability and dynamic pattern in cellular networks," *Journal of Theoretical Biology*, vol. 32, no. 3, pp. 507 – 537, 1971.

[154] ——, "Non-linear aspects of dynamic pattern in cellular networks," *Journal of Theoretical Biology*, vol. 43, no. 1, pp. 83 – 112, 1974.

[155] F. Padró and J. Diaz-Lopez, "Spectral reconstruction of complex networks," *Physica A: Statistical Mechanics and its Applications*, vol. 387, pp. 6436–6442, 11 2008.

[156] M. J. Panaggio and D. M. Abrams, "Chimera states: coexistence of coherence and incoherence in networks of coupled oscillators," *Nonlinearity*, vol. 28, no. 3, pp. R67–R87, feb 2015.

[157] R. Pastor-Satorras and A. Vespignani, *Evolution and structure of the Internet: A statistical physics approach.* Cambridge University Press, 2007.

[158] A. Patania, G. Petri, and F. Vaccarino, "The shape of collaborations," *EPJ Data Sci.*, vol. 6, p. 18, 2017.

[159] L. M. Pecora and T. L. Carroll, "Master stability functions for synchronized coupled systems," *Phys. Rev. Lett.*, vol. 80, pp. 2109–2112, Mar 1998.

[160] L. M. Pecora, T. L. Carroll, G. A. Johnson, D. J. Mar, and J. F. Heagy, "Fundamentals of synchronization in chaotic systems, concepts, and applications," *Chaos: An Interdisciplinary Journal of Nonlinear Science*, vol. 7, no. 4, pp. 520–543, 1997.

[161] G. Petri and A. Barrat, "Simplicial activity driven model," *Physical Review Letters*, vol. 121, no. 22, p. 228301, 2018.

[162] G. Petri, P. Expert, F. Turkheimer, R. Carhart-Harris, D. Nutt, P. J. Hellyer, and F. Vaccarino, "Homological scaffolds of brain functional networks," *Journal of The Royal Society Interface*, vol. 11, no. 101, p. 20140873, 2014.

[163] A. Pikovsky, M. Rosenblum, and J. Kurths, *Synchronization: a universal concept in nonlinear sciences.* Cambridge University Press, Cambridge, UK, 2003, vol. 12.

[164] I. Prigogine and R. Lefever, "Symmetry breaking instabilities in dissipative systems. ii," *The Journal of Chemical Physics*, vol. 48, no. 4, pp. 1695–1700, 1968.

[165] W. H. R. and C. J. D., "Excitatory and inhibitory interactions in localized populations of model neurons," *Biophys. J.*, vol. 12, p. 1, 1972.

[166] B. Rink and J. Sanders, "Amplified hopf bifurcations in feed-forward networks," *SIAM Journal on Applied Dynamical Systems*, vol. 12, 11 2012.

[167] J. J. Sakurai and J. J. Napolitano, *Modern Quantum Mechanics*. Pearson Education Ltd., 2013.

[168] E. Schöll, "Synchronization patterns and chimera states in complex networks: Interplay of topology and dynamics," *The European Physical Journal Special Topics*, vol. 225, pp. 891–919, 09 2016.

[169] F. Sorrentino, "Synchronization of hypernetworks of coupled dynamical systems," *New Journal of Physics*, vol. 14, no. 3, p. 033035, mar 2012.

[170] S. H. Strogatz, *Sync: The Emerging Science of Spontaneous Order*. Penguin, 2004.

[171] ——, *Nonlinear Dynamics and Chaos*. Westview Press, 2015.

[172] S. Strogatz, "From kuramoto to crawford: Exploring the onset of synchronization in populations of coupled oscillators," *Physica D: Nonlinear Phenomena*, vol. 143, pp. 1–20, 09 2000.

[173] ——, "Strogatz, s.h.: Exploring complex networks. nature 410, 268," *Nature*, vol. 410, pp. 268–76, 04 2001.

[174] J. Stuart and R. DiPrima, "The eckhaus and benjamin-feir resonance mechanisms," *Proc R Soc Lond A*, vol. 362, p. 27, 1978.

[175] T. Tomé, "Entropy production in nonequilibrium systems described by a Fokker-Planck equation," *Brazilian Journal of Physics*, vol. 36, pp. 1285 – 1289, 12 2006.

[176] L. Trefethen and M. Embree, *Spectra and Pseudospectra: The Behavior of Nonnormal Matrices and Operators*, 01 2005.

[177] L. N. Trefethen, A. E. Trefethen, S. C. Reddy, and T. A. Driscoll, "Hydrodynamic stability without eigenvalues," *Science*, vol. 261, no. 5121, pp. 578–584, 1993.

[178] A. M. Turing, *The chemical basis of morphogenesis*. Philosophical Transactions of the Royal Society of London B: Biological Sciences, 1952, vol. 237.

[179] G. R. V. Latora, V. Nicosia, *Complex networks: principles, methods and applications*. Cambridge University Press, 2017.

[180] S. Valk, N. Delsate, A. Lemaître, and T. Carletti, "Global dynamics of high area-to-mass ratios geo space debris by means of the megno indicator," *Advances in Space Research*, vol. 43, p. 1509, 2009.

[181] A. van Harten, "On the validity of the ginzburg-landau equation," *J. Nonlinear Sci.*, vol. 1, pp. 397–422, 1991.

[182] N. G. van Kampen, *Stochastic Processes in Physics and Chemistry*. Elsevier, 2007.

[183] A. Wagner and D. A. Fell, "The small world inside large metabolic networks," *Proceedings of the Royal Society of London. Series B: Biological Sciences*, vol. 268, no. 1478, pp. 1803–1810, 2001.

[184] E. Wallace, M. Benayoun, W. van Drongelen, and J. D. Cowan, "Emergent oscillations in networks of stochastic spiking neurons," *PLOS ONE*, vol. 6, no. 5, pp. 1–16, 05 2011.

[185] D. Watts and H. S. Strogatz, "Collective dynamics of 'small world' networks," *Nature*, vol. 393, pp. 440–442, 01 1998.

[186] H. Wilson and J. Cowan, "A mathematical theory of the functional dynamics of cortical and thalamic nervous tissue," *Kybernetik*, vol. 13, pp. 55–80, 10 1973.

[187] C. Zankoc, D. Fanelli, F. Ginelli, and R. Livi, "Intertangled stochastic motifs in networks of excitatory-inhibitory units," *Phys. Rev. E*, vol. 96, p. 022308, Aug 2017.

[188] ——, "Desynchronization and pattern formation in a noisy feed-forward oscillator network," *Phys. Rev. E*, vol. 99, p. 012303, Jan 2019.

Acknowledgments

Tre anni che sembrano molti di più. Questo dottorato è stata un'esperienza di vita bellissima, fatta di lavoro, legami e scoperte che porterò sempre con me.

Il primo ringraziamento lo dedico a Duccio, colonna portante del CSDC, un punto di riferimento per tutto il dipartimento (e oltre), persona brillante e geniale. Sempre presente, sempre attento, non mi hai mai lasciata sola. Ripenso con nostalgia alle prime chiaccherate di fronte alla lavagna, ai calcoli svolti insieme. Grazie perchè ho vissuto questo dottorato con serenità per merito tuo. Sei stato il miglior tutor che potessi desiderare, umanamente e professionalmente. Sono orgogliosa di aver lavorato con te.

Grazie Teo, perchè ho potuto sempre contare su di te. Sei stato fondamentale per me e così lo sono stati i tuoi consigli mai banali, la tua supervisione costante, la tua gentilezza.

Grazie a Luigi, Giorgio e Giacomo, per il supporto, le discussioni e le infinite revisioni agli articoli.

Grazie Giovanna, un po' mamma, un po' amica, un po' collega. Sono stati tre anni di confidenze e risate. Grazie perchè mi hai spronata sempre e i tuoi consigli sono stati preziosi. Mi mancheranno le nostre chiaccherate delle 8 di fronte al caffè.

Grazie Gloria, sempre disponibile, amica di infinità bontà. Per avermi sopportata nel tentativo (vano) di cambiarti look (non mi sono arresa). Sei un tesoro.

Grazie Fra, consigliera di arredamento e cucina, i tuoi racconti di vita indiavolata la mattina sono stati memorabili.

Grazie Leo, perchè in questi tre anni mi hai fatto vivere come in una serie tv, tu Anthony, io Charlotte (ma anche Mrs. Maisel). Sei una delle persone più sensibili e intelligenti che conosca, sii felice.

Grazie Lorenzo, nonostante le tue cuffie (*non c'è comportazione*), grazie Ihusan per avermi fatto parlare in inglese, grazie Chicchi perchè sei troppo simpatico. Grazie Vale, dolcissima e sempre pronta ad ascoltarmi. Grazie Maxime, per il bellissimo viaggio a Salina che abbiamo condiviso.

Grazie Giulia, di te conserverò sempre il ricordo di Namur, di Bruxelles, di Grease visto insieme. Grazie perchè mi hai fatta sentire meno sola.

Grazie Niccolò, per avermi aiutata i primi mesi del dottorato. Spero di rivederti presto, manchi a tutti.

Grazie al mio grande amore, Filippo. Mio amico, mio complice. Mi

hai aiutata a crescere e siamo cresciuti insieme. Questa esperienza la devo anche, e soprattutto, a te. Grazie a Carla e Raffaello, uniti da una vita, perché senza di voi non avrei avuto Lui.

Grazie alla mia famiglia. A mamma, una roccia, a papà, che ha superato lo scoglio più grande ed è cambiato come mai avrei pensato che potesse fare, a Olga, a cui sono indissolubilmente legata. Alla mia nonna, un pezzo del mio cuore, e a zio, altro degno erede della vecchia Roccia, grazie perchè le sei vicino.